Using Airborne Hyperspectral Imagery to Estimate Chlorophyll a and Phycocyanin in Three Central Indiana Mesotrophic to Eutrophic Reservoirs

Rebecca Elizabeth Sengpiel

Submitted to the faculty of the University Graduate School
in partial fulfillment of the requirements
for the degree
Master of Science
in the Department of Earth Sciences,
Indiana University

August 2007

Accepted by the Faculty of Indiana University, in partial fulfillment of the requirements for the degree of Master of Science

Lin Li, Ph.D., Chair

Lenore P. Tedesco, Ph.D.

Master's Thesis

Committee

Jeffrey S. Wilson, Ph.D.

Acknowledgements

I wish to thank my committee members for allowing me the opportunity to accomplish this goal. Furthermore, I would like to thank all of the graduate students and faculty in the Department of Earth Sciences, IUPUI and the staff of CEES who participated in the September 6 and 7, 2005 sampling excursion and who assisted in the lab analyses.

I also want to wish to thank the Veolia Water Indianapolis, LLC White River Laboratories for all of their assistance with sample analyses; the University of Nebraska CALMIT laboratory for acquiring the AISA imagery; IndyParks and Eagle Creek Park for dock space and launch access; and Kent Duckwell for launch access to Geist and Morse Reservoirs.

And last, but not least, I would like to thank my husband, my family and friends, and University of the Pacific Geology Professors for all of their help, support and inspiration.

This project was funded by the Indiana Department of Natural Resources LARE Grant and Veolia Water Company LLC, Central Indiana Water Resources Partnership.

Abstract

Rebecca Elizabeth Sengpiel

USING AIRBORNE HYPERSPECTRAL IMAGERY TO ESTIMATE CHLOROPHYLL A AND PHYCOCYANIN IN THREE CENTRAL INDIANA MESOTROPHIC TO EUTROPHIC RESERVOIRS

This thesis presents the results of an analysis of predicting phytoplankton pigment concentrations (chlorophyll *a* and phycocyanin) from remotely sensed imagery. Hyperspectral airborne and hand-held reflectance spectra were acquired on three reservoirs (Geist, Morse and Eagle Creek) in Central Indiana, USA. Concurrent with the reflectance acquisition, *in situ* samples were collected and analyzed in laboratories to quantify the pigment concentration and other water quality parameters. The resultant concentration was then linked to Airborne Imaging Spectrometer for Applications (AISA) reflectance spectra for the sampling stations to develop predictive models. AISA reflectance spectra were extracted from the imagery which had been processed for radiometric calibration and geometric correction. Several previously published algorithms were examined for the estimation of pigment concentration from the spectra. High coefficients of determination were achieved for predicting chlorophyll *a* in two of the three reservoirs (Geist $R^2 = 0.712$, Morse $R^2 = 0.895$ and Eagle Creek Reservoir $R^2 = 0.392$). This situation was similar for PC prediction, where two of the three reservoirs had high coefficients of determination between pigment concentration and reflectance (Geist $R^2 = 0.805$, Morse $R^2 = 0.878$ and Eagle Creek Reservoir $R^2 = 0.316$). The results of this study show that reflectance spectra collected with an airborne hyperspectral imager are statistically significant, $p < 0.03$, in predicting chlorophyll *a* and phycocyanin pigment concentration in all three reservoirs in this study without the consideration of other parameters. The algorithms were then applied to the AISA image to generate high spatial resolution (1 m^2) maps of Chlorophyll *a* and Phycocyanin distribution for each reservoir.

Lin Li, Ph.D., Chair

Table of Contents

List of Tables

List of Figures

1.0 INTRODUCTION

Adverse Effects of Cyanobacteria in Limnitic Ecosystems

Cyanobacterial blooms are one of most important issues concerning environmental agencies, water authorities and public health organizations because harmful algal blooms can cause environmental problems ranging from degradation of drinking water quality and economic values to threatening human and animal health (Backer, 2002; Carmichael, 2001; Hallegraeff, 1993).

Ecological Degradation

Cyanobacteria can have detrimental effects on reservoir ecology when their population growth results in bloom formation. Ecological effects of a cyanobacterial bloom include changes in phytoplankton community structure, changes in fish community structure and lake anoxia. Cyanobacteria have several competitive advantages that allow them to out compete than other phytoplankton, resulting in a decrease of phytoplankton diversity. For example, in a natural system, Cyanobacteria will out compete diatoms (Chrysophyta) and green algae (Chlorophyta) for nutrients and light, allowing cyanobacteria to replace formerly dominant phytoplankton species in a water body when the conditions are right (Backer, 2002).

As cyanobacterial blooms form mats or scums on the surface of the water, the penetration of light to lower levels in the water column decreases. This can lead to a high degree of shading, reducing the light level below the bloom. Prolonged light reduction below the bloom causes conditions at which other photosynthetic organisms cannot survive, reducing ecological diversity of the water body (Backer, 2002).

The collapse of a cyanobacterial bloom can have a harmful effect by reducing the dissolved oxygen of a lake or reservoir. The collapse of a bloom provides a large amount of

organic matter for decomposition, consuming dissolved oxygen in the water. The lower concentration of dissolved oxygen in the water can be lethal to fish and invertebrate species (Backer, 2002). The constant supply of organic matter from decaying blooms can cause a long term reduction in dissolved oxygen concentrations in the water shifting fish populations from those that need higher dissolved oxygen levels and live in cooler bottom waters (e.g. Bass and Perch,) to those that do not (e.g. Carp or Shad).

Aesthetic Degradation

Aesthetic degradation can occur from cyanobacterial blooms because of the formation of surface scums that contribute to undesirable odor and taste to drinking water and fish. Cyanobacterial blooms are not always visible on the surface of a water body, but at high cell concentrations the water clarity is impaired (Backer, 2002). Gas vesicles, present in some species, allow vertical position adjustment within the water column permitting cyanobacteria to form unsightly surface scums (Chorus & Bartram, 1999).

Cyanobacterial blooms can impart a musty and earthy taste to water and to organisms that live in the water. These odors or flavors can be caused by the common metabolic by-products for cyanobacteria, Geosmin and 2-methylisoborneol (MIB) (Chorus & Bartram, 1999). Many of the cyanobacterial genera that are known to produce odor compounds are also known to include toxin forming species. However, there is no evidence of a correlation between toxin production and the production of taste and odor producing compounds making them a poor indicator of potentially harmful cyanobacteria (Chorus & Bartram, 1999).

Human Health Effects

Human and animal consumption or contact with toxins produced by cyanobacteria can cause adverse health effects. The toxicity of a cyanobacterial bloom is a function of the

type toxin, the amount of toxin in the bloom, and the age, sex, type and amount of toxin consumed by the animal or human (Carmichael, 2001). Several genera of cyanobacteria capable of producing toxins are found in Indianapolis' reservoirs (e.g. *Anabaena, Aphanizomenon, Cylindrospermopsis,* and *Microcystis).*

Introduction of the Study

Objective of the Research

The reliable mapping of cyanobacteria concentrations is important in Central Indiana, and other locations where blooms of cyanobacteria such as *Anabaena, Aphanizomenon* or *Pseudanabaena* occur almost annually in drinking water reservoirs. If data about the spatial distribution of cyanobacterial blooms were available to water quality authorities or management agencies, the information could be used to facilitate timely and informed management decisions.

The primary objective of this research is to examine the capability of hyperspectral remote sensing techniques to map the spatial distribution and concentration of chlorophyll *a* and phycocyanin in three central Indiana reservoirs, and to assess the characteristics of each reservoir, which influence the effectiveness of these techniques. A secondary objective is to determine the best algorithm for mapping water quality parameters with hyperspectral imagery of optically complex reservoirs in Central Indiana.

Significance of the Research

This study tests methods of cyanobacterial and chlorophyll a detection which will improve upon the current method of quantification in shallow, turbid inland waters. Remote sensing has been used in a number of applications in water quality monitoring and management as it is cost effective and time efficient method for mapping cyanobacteria blooms (Jupp, et al., 1994; Richardson, 1996; Kallio, et al., 2003). The reservoirs studied in

this research have low secchi disk measurements and high suspended sediment concentrations, making pigment detection more difficult and creating an ideal situation for testing the robustness of the pigment prediction algorithms. With the development of robust algorithms, they can be applied to a time-series of remote sensing imagery, providing an efficient way to track bloom development and collapse. Furthermore, results of this research may be extendable to other Midwestern meso-eutrophic to eutrophic reservoirs, providing information for other water resource managers who may be considering this type of water management tool.

Overview of Study

Airborne hyperspectral imagery was recorded over three central Indiana reservoirs. Concurrent with image acquisition, field hyperspectral data and water quality data were gathered, allowing comparison between airborne imagery and ground truth data. Regression analyses between pigment concentration and spectral band ratios, and band combinations yielded promising results for the success of this water resource tool. These equations were applied to the airborne hyperspectral imagery to create high resolution maps of pigment concentrations.

Overview of Research Directly Related to the Problem

A large volume of literature exists on using remote sensing for mapping chlorophyll *a*, an indicator of algal concentration and a key parameter for assessment of water quality (Schalles, et al., 1998). Because of their photosynthetic pigments, cyanobacteria can be detected using various remote sensing platforms. Cyanobacteria create energy through photosynthesis via several pigments: chlorophyll *a* (Chl a), phycocyanin (PC), allophycocyanin, phycoerythrin, beta-carotene, and others (Richardson, 1996; Rowan,

1989). Remote sensing systems can detect changes in electromagnetic energy due to the absorption of Chl a in blue and red electromagnetic wavelengths.

Algorithms developed for remotely sensed field data, which predict Chl a concentration using the red absorption trough and near-infrared reflectance feature, have produced estimates with a high correlation to *in situ* pigment values as a proxy for phytoplankton concentration (e.g Gitelson, 1992; Mittenzwey, et al., 1992; Dekker, 1993; Yacobi, et al., 1995; Schalles, et al., 1998; Gons, 1999; Gitelson, et al., 2000). These algorithms have been extended successfully to airborne and satellite imagery (both hyperspectral and multispectral) for predicting Chl a concentration (e.g. Millie, et al., 1992; Dekker, et al., 1992; Dekker, 1993; Jupp, et al., 1994; Kallio, et al., 2001; Gons, et al., 2002; Kallio, et al., 2003). The detection of chlorophyll *a* from airborne and satellite platforms allows the assessment of this water quality parameter over a much broader area when compared to traditional field sampling approaches.

Several recent studies have investigated the relationship between hyperspectral water reflectance, both airborne and field platforms, and taxon-specific algal accessory pigments such as phycocyanin. The presence and concentration of phycocyanin is used as a proxy for the concentration and distribution cyanobacteria (Dekker, 1993; Schalles & Yacobi, 2000; Mertes, et al., 2004; Vincent, et al., 2004; Simis, et al., 2005; Simis, et al., 2007). Phycocyanin absorbs strongly at approximately 620 nm, though the maximum absorption varies with species (Rowan, 1989). Both this absorption trough and other spectral characteristics have been used to quantify phycocyanin. Phycocyanin has been estimated from field spectra using single bands, band combinations and band ratios (Dekker, 1993; Gitelson, et al., 1995; Schalles & Yacobi, 2000; Simis, et al., 2005). Only in a few studies has phycocyanin been the target investigated with airborne and satellite imagery (Millie, et al.,

1992; Dekker, 1993; Jupp, et al., 1994; Richardson, et al., 1994; Vincent, et al., 2004). Using airborne hyperspectral sensors and Landsat TM/ EMT+, phycocyanin distribution has been mapped and quantified using single band, band combinations and band ratio algorithms (Millie, et al., 1992; Dekker, 1993; Vincent, et al., 2004).

2.0 BACKGROUND

A Brief Overview of Cyanobacteria

Cyanobacteria Systematics

Biologists observe and compare characteristics of organisms so they can be identified reliably and sorted into recognizably distinct groups. The goal for such groupings is to understand how all organisms relate to one another by way of evolutionary descent (Chorus & Bartram, 1999). However, the systematics of microbial organisms has been difficult to determine and new discoveries are changing past classifications. For example, cyanobacteria were often referred to as Blue-green algae because of their superficial resemblance to algae, and ecological role as a primary producer. Even though cyanobacteria and algae both obtain energy through photosynthesis, evolutionary they are only distantly related. Cyanobacteria are prokaryotic, lacking internal organelles, a discrete nucleus and the histone proteins while algae are eukaryotic.

Cyanobacterial Ecological Diversity

The majority of cyanobacteria are aerobic photoautotrophs, requiring only water, carbon dioxide, inorganic substances and light for survival (Chorus & Bartram, 1999). Though photosynthesis is their principal mode of energy metabolism, some species are able to live during long periods of complete darkness. Cyanobacteria can be found in almost every conceivable habitat, but are most prominently found in limnic and marine environments. Cyanobacteria thrive in water that is salty or fresh, in extreme cold and hot temperatures, and in environments where few other phytoplankton can exist. For example, salt-tolerant cyanobacterial species grow at combined salt concentrations as high as 3 - 4 molar mass (Chorus & Bartram, 1999). The success of cyanobacteria in such diverse modern habitats is attributed to their long evolutionary history. The changing metal

composition and low oxygen of early environments may have influenced the evolution of metal-utilizing proteins and the tolerance of low oxygen conditions that cyanobacteria exhibit today (Whitton & Potts, 2000).

Cyanobacteria also form diverse symbiotic associations with many of the major phyla of animals and plants. The hypothesis for the endosymbiotic origin of chloroplasts is one possible symbiotic relationship with important implications. The endosymbiotic theory proposes that chloroplasts, which are responsible for photosynthesis in eukaryotes (algae and higher plants), evolved from an endosymbiotic relationship with cyanobacteria. The evolutionary formation of a photosynthetic eukaryote can be explained by a cyanobacteria being engulfed and co-developed by a host (Chorus & Bartram, 1999).

Cyanobacterial Morphology

Cyanobacteria are morphologically diverse with unicellular, colonial or filamentous forms. Colonies may form into filaments, sheets or even hollow balls. In some cases, filamentous colonies have the ability to differentiate cells into different roles. In some groups, cells may be differentiated into heterocysts, capable of nitrogen fixation, and akinetes, enabling survival under unfavorable conditions (Chorus & Bartram, 1999). Cyanobacteria have several other adaptations that allow them to out-compete other organisms for resources. With the accessory pigments such as phycocyanin, they are able to effectively use a region of the light spectrum between the absorption peaks of Chl a and the carotenoids for photosynthetic metabolism. Another adaptation is the phycobiliprotein synthesis (phycocyanins, phycocerytherins, allophycocyanins and phycoerytherocyanins) within a cyanobacterium is particularly sensitive to environmental influences, especially light quality, allowing the ratio between phycocyanin and phycoerythrin to change (Chorus & Bartram, 1999). Thus, depending on the habitat, cyanobacteria are capable of producing

the accessory pigment needed to absorb light most effectively. Cyanobacteria also have the ability to store nutrients when they are in excess, allowing them to survive during nutrient limited conditions. Nitrogen fixation is another modification that makes cyanobacteria unique. Heterocyst-forming species are able to fix nitrogen gas from the atmosphere or water into ammonia to use for biological processes, allowing cyanobacteria to flourish in nitrogen limited conditions. Finally, many species of cyanobacteria possess gas-filled cytoplasmic inclusions that enable buoyancy regulation. These vesicles enable them to optimize their vertical position in the water column finding a suitable niche for survival and growth.

Bloom Formation

Under the right environmental conditions, cyanobacteria can experience high rates of growth resulting in formation of large blooms (Backer, 2002). Several factors can affect the formation of a cyanobacterial bloom. One of the factors is the duration of light and the light intensity. If cyanobacteria are exposed intermittently to high light intensity, an intensity approximately less than half of what would be at the surface of a lake, they can grow at a near maximum rate (Chorus & Bartram, 1999). Cyanobacteria which form surface blooms seem to have a higher tolerance for high light intensities than other phytoplankton. This is possibly due to their higher carotenoid production which protects the cells from photo-oxidation (Chorus & Bartram, 1999). While they are tolerant of high light intensities, cyanobacteria do not require it for bloom formation, in fact they often form more blooms under low light intensities. This occurs because at low light intensities cyanobacteria are able to harvest different wavelengths of light and have a higher growth rate than other phytoplankton. Therefore, as blooms develop and the water becomes more turbid, due to high phytoplankton density, cyanobacteria can out-compete other species and become dominant.

Another factor affecting bloom formation is the growth rate and stability of cyanobacteria species. Interestingly, the growth rate of cyanobacteria is usually much lower than that of many other algal species. Generally, cyanobacteria double at 0.3 - 1.4 doublings per day, while some types of green algae can have growth rates of up to 1.3 - 2.3 doublings per day (Chorus & Bartram, 1999). These slow growth rates indicate that cyanobacteria require long water retention times to enable bloom formation. However, once they have been established, slow growth rates are compensated by the high stability of the population. Cyanobacteria have few natural enemies, so they are not grazed to the same extent as other algae (Chorus & Bartram, 1999), resulting in a large, stable, population of cyanobacteria.

Occurrences of algal blooms have globally increased due to several factors, including eutrophication (Carmichael, 2001). Eutrophication is a natural lake aging process when lakes become more productive. This productivity can be manifested in the formation of cyanobacterial blooms. Anthropogenic inputs to a lake or reservoir will accelerate eutrophication by adding large concentrations of plant nutrients to the water. It was previously assumed that cyanobacteria required high phosphorus and nitrogen concentrations, because of their common development in eutrophic lakes. However, experimental data have shown that cyanobacteria can thrive under low nutrient conditions because of their high nutrient affinity and high storage capacity, meaning they can out-compete other organisms under conditions of phosphorus or nitrogen limitation (Chorus & Bartram, 1999). Nevertheless, *Microcystis*, a genus of cyanobacteria, has been regularly documented in Lake Erie as a result of anthropogenic activities (Makarewicz, 1993).

Photosynthetic Pigments of Phytoplankton

Photosynthesis begins when light is absorbed by an accessory pigment. This pigment can be a chlorophyll, carotenoid or biliprotein depending on the type of organism. A wide variety of different accessory complexes are found in different photosynthetic systems, allowing the phytoplankton to increase the wavelengths of light absorbed. Photosynthesis occurs in two stages: in the first phase, the energy absorbed by photosynthetic pigments is used to excite molecules within the cells which are then converted into Adenosine Triphosphate (ATP) and Nicotinamide adenine dinucleotide phosphate (NADPH). During the second phase, ATP and NADPH are used to convert captured carbon dioxide and water into carbohydrates with oxygen being a byproduct. There are three types of photosynthetic pigments that can be found in photosynthetic phytoplankton: chlorophylls, carotenoids and biliproteins. The roles of chlorophylls and biliproteins in the light harvesting process are well known. However, the role of the carotenoids is less clear. They may have two functions, to aid in the harvesting of energy for photosynthesis and the prevention of chlorophyll destruction by oxygen (Rowan, 1989).

Chlorophylls

There are several kinds of chlorophylls found in phytoplankton, the most important of which is Chl a. It is not surprising that chlorophyll *a* is the essential molecule for harvesting electromagnetic energy because almost all plants, algae, and photosynthetic cyanobacteria contain it as a large percentage of their photosynthetic pigments. The basic structure of chlorophylls is an organic porphyrin ring with a chelated Mg^{+} ion in the middle and a long organic phytol tail. Chlorophylls *a*, *b*, and *d* are more similar to each other than chlorophyll *c*. Chlorophylls *a* and *b* differ in the side chain of the molecule, while chlorophyll *a* and *d* are very similar with only a slightly different porphyrin ring.

Chlorophyll *a* is the primary photosynthetic pigment, while forms *b*, *c* and *d* act as accessory pigments. Accessory pigments aid in photosynthesis by absorbing energy in other areas of the electromagnetic spectrum, increasing the thermochemical energy produced. While chlorophyll *a* is found in all algae and some photosynthetic bacteria, chlorophyll *b* is found mostly in green algae. Chlorophyll *c* is found in Cryptophyta, Dinophyta, Chrysophyta and a few other classes of algae. Rhodophyta and at least one class of Cyanophyta contain chlorophyll *d*.

Carotenoids

Unlike other photosynthetic pigments, the carotenoids are numerous with over 600 known types. Carotenoids are classified as either carotenes or xanthophylls depending upon the presence of oxygen in the molecule. Carotenoids function in the photosynthetic process either as an accessory pigment or as protection from photo-oxidation. Some examples of carotenoids are beta-carotene, lycopene and lutein. The majority of carotenoids are structured as organic molecules with two cyclic ends linked by a chain, though some lack the cyclic ends. Carotenoids range in color from pale yellow to deep red. There are a large range of carotenoids found in Cyanophyta, but a given species only contains seven or eight types; the most common of which is myxoxanthophyll (Rowan, 1989).

Biliproteins

There are four major types of biliproteins: phycocyanin, phycoerythrin, allphycocyanin and phycoerytherocyanins. These light harvesting pigments are found in Cyanophyta, Rhodophyta and Cryptophyta. The four types of biliproteins are formed by groups of joined proteins which contain one or more phycobilins. There are four types of phycobilins: phycourobilin, phycoerythrobilin, phycobiliviolin, and phycocyanobilin. The

number and type of phycobilins within the biliproteins, as well as the bonds between the phycobilins will alter the absorbance of the accessory pigment. Cryptophyta species will contain the biliproteins phycocyanin and phycoerythrin and Rhodophyta species may contain phycocyanin, phycoerythrin and allophycocyanin (Rowan, 1989). However, all four of the biliproteins can be found in different species of Cyanophyta.

A Brief Introduction of Cyanobacterial Toxins

Not all cyanobacteria species have the ability to produce toxins and those species that can, will not exclusively do so (i.e. toxic and non-toxic blooms of the same species can both be found). Cyanobacterial toxins are chemically and toxicologically diverse and appear to be more hazardous to terrestrial mammals than to aquatic biota (Chorus & Bartram, 1999). Humans are exposed to these toxins from drinking and recreational water supplies containing toxic cyanobacteria. These toxins affect humans by direct contact or uptake of the toxins through swallowing or aspiration (Backer, 2002). There are three molecular types of cyanobacterial toxins: cyclic peptides, alkaloids or lipopolysaccharides (LPS). Cyanobacterial toxins are often categorized according to the type of toxin, which are most commonly either hepatotoxins or neurotoxins.

Hepatotoxins

Hepatotoxins cause the functioning cells of the liver to shrink, allowing blood to seep into the liver tissue causing damage, shock and liver failure (Carmichael, 1994). Hepatotoxins usually remain contained within the cyanobacterial cells and are only released in substantial amounts when the cell is disrupted or destroyed. These toxins have serious implications for persistence and exposure to humans in surface water bodies because of their high chemical stability and water solubility (Chorus & Bartram, 1999). One type of hepatotoxin is Microcystis; it is a cyclic peptide that contains seven amino acids

(Backer, 2002). Toxicity is often reported as LD_{50}, which is an abbreviation for Lethal Dose, 50%, the dose of toxin that is required to kill half the members of a tested population. The LD_{50} of pure Mycrocystin toxins ranges from 45 - 1000 μg/kg (Backer, 2002). However, within a natural system, the toxicity may be different due to environmental factors such as temperature or pH. A survey of several cyanobacterial blooms from Lake Kasumigaura, Japan, found the LD_{50} of the blooms to mice ranged from 76 to 556 mg/kg of body weight (Shirai, et al., 1991). Cyanobacteria may also produce the hepatotoxin Nodularin, a five amino acid cyclic peptide. A study of a cyanobacterial bloom in New Zealand yielded the LD_{50} of 60 μg/kg of weight for this type of toxin (Carmichael, 1988). Cylindrospermopsin is another type of hepatotoxin which is produced by some cyanobacteria species. This cyclic alkaloid toxin primarily affects the liver, although it can cause considerable damage to other major organs. Cylindrospermopsin has an LD_{50} (in mice) of 200 μg/kg making it a relatively potent cyanobacterial toxin (Chorus & Bartram, 1999). Because these hepatotoxins affect the liver cells by inhibiting the protein phosphatases, non-lethal doses of these toxins may promote the development of carcinogenic alterations in humans, enhancing tumor growth (Carmichael, 1994).

Neurotoxins

Neurotoxins disrupt the signaling between the brain and muscles by inhibiting neuron communication in several ways, all of which may lead to death by paralysis of respiratory muscles (Carmichael, 1994). Examples of neurotoxins produced by cyanobacteria are anatoxin-a, anatoxin-a(s), saxitoxin and neosaxitoxin. Anatoxin-a, an alkaloid type toxin, mimics acetylcholine which stimulates muscles to contract, however unlike acetylcholine, the toxin cannot be degraded by any enzyme in human cells allowing it to remain and overstimulate muscles, causing paralysis (Carmichael, 1994). The pure form of this toxin has an LD_{50} 250 μg/kg (Backer, 2002). Anatoxin-a(s) inhibits the enzyme that

degrades acetylcholine (aceylcholinesterase) allowing the over stimulation of muscles. The LD_{50} of this toxin is 40 μg/kg (Backer, 2002). Saxitoxin and neosaxitoxin block the flow of ions in a neuron preventing the release of acetylcholine, disrupting intercellular communication (Carmichael, 2001). In the case of these toxins, the muscles become paralyzed because of the loss of communication.

Other Cyanobacterial Toxins

Cyanobacteria have also been linked to gastrointestinal disturbances and respiratory reactions. Though it is unknown whether these problems are caused by hepatotoxins, neurotoxins or possibly LPS (Carmichael, 2001). LPS are molecules consisting of lipids and polysaccharides. These molecules are a key component of the cell wall of all gram-negative bacteria. Though cyanobacterial LPS are considerably less potent than LPS from pathogenic gram-negative bacteria, they can cause allergic responses in human and animal tissues (Chorus & Bartram, 1999). Additionally, some species of cyanobacteria have been known to create dermatotoxic alkaloids like aplysiatoxins or debromoaplysiatoxins. The toxins produced by cyanobacteria such as *Lyngbya*, *Oscillatoria* and *Schizothrix* cause severe dermatitis and promote tumor production through physical contact (Chorus & Bartram, 1999).

Nature of Electromagnetic Radiation and light

Wave Model/Particle Theory

The creation, propagation and interaction of electromagnetic energy can be described with two theories: the wave theory and the particle theory. With the wave theory, electromagnetic energy is generally described as a self-propagating wave in space with fluctuating electric and magnetic fields. The electromagnetic energy has a discrete

wavelength (λ) and frequency (ν). The relationship between these characteristics is based on the following equation:

$$c = \lambda * \nu \qquad (1.0)$$

where "c" is the speed of light in a vacuum (3.0×10^8 m/s). In the particle theory, electromagnetic energy exists of discrete packets of energy, called photons. Each photon has a specific energy at a certain wavelength or frequency. These relationships are based on the following equation,

$$\xi = h*\nu = h*c/\lambda \qquad (1.1)$$

where "h" is Planck's Constant ($6.625 * 10^{-34}$ J), and ξ is the specific energy of the photon. By this equation, photons with smaller wavelengths have more energy than those with longer wavelengths. In this paper, it is important to think of the light emanating from a water body as a flux of photons (N), or the number of photons arriving at an area per unit time. The energy flux produced (Φ) by the photons at each discrete wavelength is a product of the individual energy of each photon and the number of photons per unit area and time (Bukata, et al., 1995). This can be expressed in the equation:

$$\Phi = h* \nu* N \qquad (1.2)$$

The change in the photon flux, N, emanating from a water body is directly caused by the characteristics of the water body as the photons interact with water molecules, phytoplankton, etc. (Bukata, et al., 1995). Therefore, the energy flux reflected by the water and received later by a remote sensing platform is a function of the characteristics of the water body.

Remote Sensing of Water Quality

Radiance, Irradiance and Reflectance

Radiance and irradiance are terms which help describe the flux of photons. While both terms refer to a measurement of radiant flux, or the number of photons at a particular site, they refer to slightly different portions of the total number of photons. Radiance is a concept of radiant intensity, the number of photons incident at a point per unit solid angle. It is sometimes easier to think of radiant intensity in reverse. For example a flashlight emits a certain number of photons from a single point, the bulb, outwards radially. The infinitesimal cone of photons outgoing from the flashlight is the radiant intensity. When considering a surface, whether it be water or land, radiant intensity emanating or incident upon each point on that surface must be considered. This concept is radiance, or the radiant flux exiting perpendicularly through an area, every point on a surface, at a certain angle. However, what is not included in radiance is aspect by which light will impinge on a surface from all directions. Irradiance includes all of the radiant flux impinging upon a point. One way to visualize this is shown in Figure 1.

Figure 1- Drawing of Radiance and Irradiance

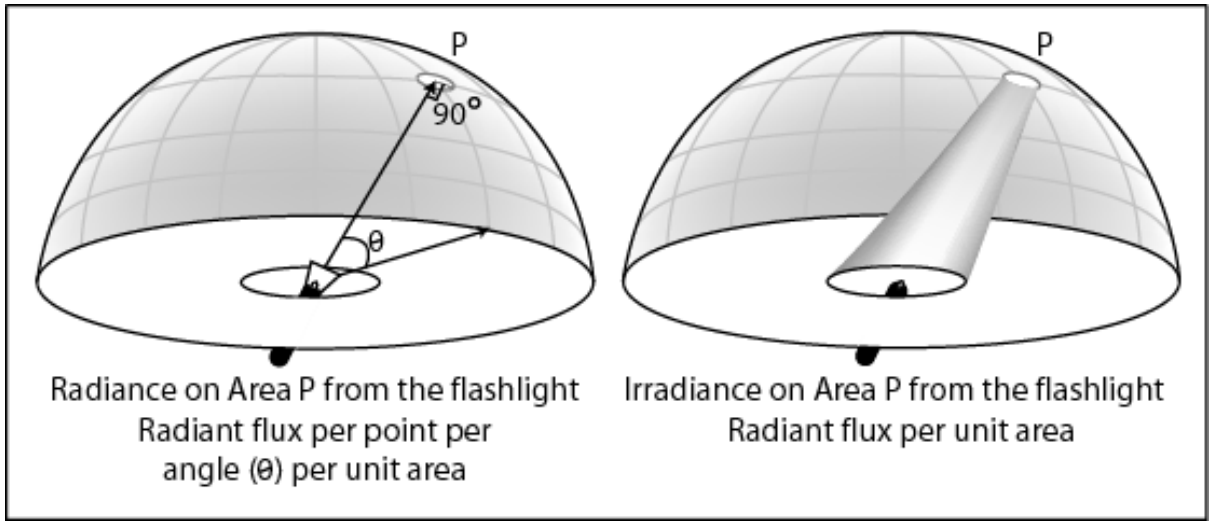

For example, consider a flashlight located within a larger hemisphere, with the top of the flashlight on, the light is directed at one location in the hemisphere, dependent upon the direction and angle the flashlight is pointing. If the cap were removed, the light is able to propagate in all directions and angles of the hemisphere, hitting at several angles and directions. The first situation, with the cap on, is radiance, the second situation is irradiance. With remote sensing, downwelling irradiance (E_d) and upwelling irradiance (E_u) is often measured. Downwelling irradiance is the irradiance at a point due to downwelling light and is recorded by an upward-looking radiometer with a cosine collector. Upwelling irradiance is the irradiance at a point due to a stream of light moving upwards from that point; this is usually measured with a downward-looking radiometer with a cosine collector. The ratio of upwelling irradiance to the downwelling irradiance is reflectance, or in a water body, it is also known as subsurface volume reflectance (R).

$$R = E_u / E_d \tag{1.3}$$

Energy-Matter Interactions

As electromagnetic energy propagates through a medium, it will likely interact with molecules and particles which may change its speed, wavelength, intensity or spectral distribution. One way energy can be changed is refraction. As electromagnetic energy travels trough media of different densities, i.e. from air to water, it is refracted. Refraction, or the bending of light, occurs because as electromagnetic energy enters a substance with a different density it slows down causing its wavelength to change.

Another affect any medium, such as the atmosphere, can cause is scattering. There are three identified types of scattering, Rayleigh, Mie and Non-selective. Rayleigh scattering occurs when the diameter of the object is a lot smaller than the incident radiation, i.e. scattering by oxygen molecules. The degree of scattering varies as a function of the ratio of

the particle diameter to the wavelength of the radiation, along with many other factors including polarization and angle. Mie scattering occurs when the particle size is approximately equal to the wavelength of electromagnetic energy. The amount of Mie scattering is often greater than Rayleigh scattering, and more of the longer wavelengths are scattered. Non-selective scattering occurs with large particles, and as the name suggests, it scatters all wavelengths equally.

Electromagnetic energy can also be absorbed by objects in its path. Absorption is the process by which radiant energy is taken up and converted into another form. Most often, the amount of absorption varies with the wavelength of the light, leading to the appearance of color. This is the process by which phytoplankton pigments in water bodies can be detected.

Lastly, electromagnetic energy can be reflected by an object. Absorption is the process by which the direction of energy is the changed, often back in the direction the wave originated. Reflection can be specular, where the angle of incidence is similar to the angle of exitance, i.e. calm water, or diffuse.

Extraterrestrial Solar Radiation

For outdoor remote sensing applications, the downwelling irradiance is most likely supplied by solar radiation. Energy leaves the sun as electromagnetic radiation or as corpuscular radiation. More than 95% of the solar radiation falls between the region of 0.29 to 2.4 μm (Bukata, et al., 1995). The electromagnetic energy emitted by the sun is not always constant. The variations are caused by transient, non-stationary temperature variations called sunspots. However, most of the change in electromagnetic energy reaching the Earth occurs in the longer x-ray and microwave, wavelength emissions. There is also variation in the amount of energy received due to seasonal variations in the elliptical

orbit of the Earth. A standard value of 1367 watts/m^2 has been adopted as the total extraterrestrial irradiance received by the Earth; this value varies by only 1 watt/m^2 over the 11 year solar cycle (Bukata,et al., 1995). This standard value is useful for satellite remote systems, because it is the downwelling irradiance at the sensor.

Remote Sensing Above Water

Light Paths

With water remote sensing, the various paths that the electromagnetic energy can take before it reaches the remote sensing platform must be considered. It is useful for conceptualizing the process, to make the following simplistic divisions of the light path, though in reality, they are not as distinct (Figure 2).

Figure 2- Simple Drawing of Light Paths

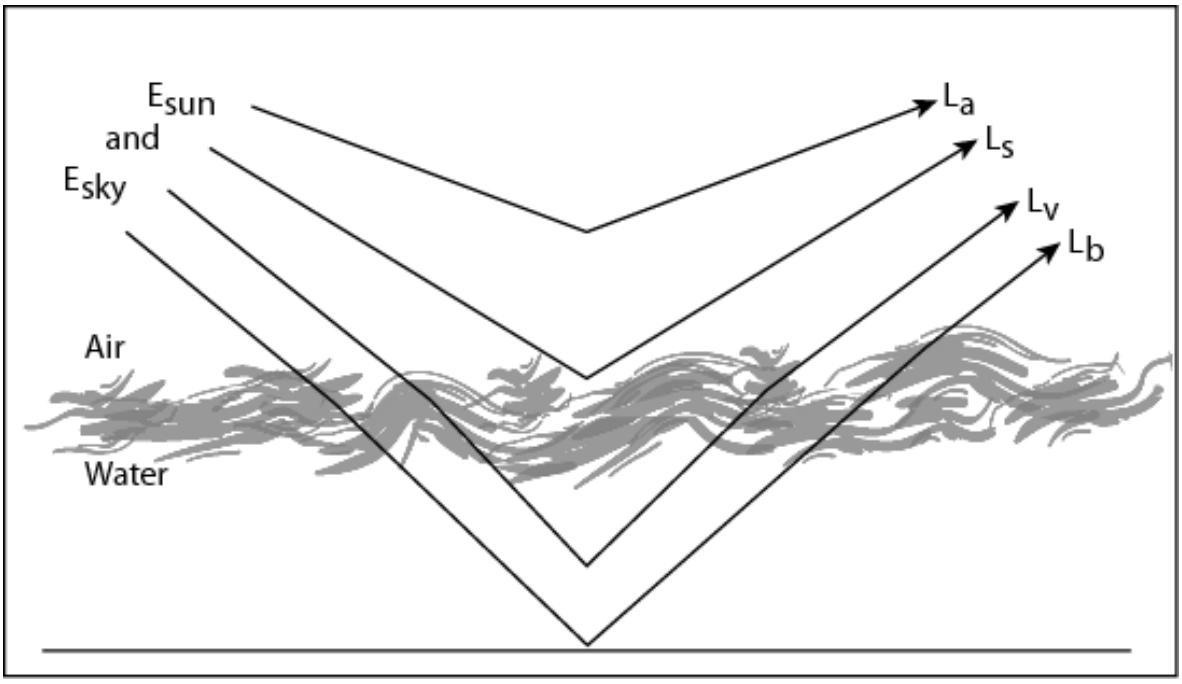

As 1367 watts/m^2 of energy from the sun heads to the surface, E_{sun}, some of it will interact with the atmosphere, giving the electromagnetic energy source E_{sky}. E_{sky} is the downwelling

irradiance from the sun that has been diffusely scattered by the atmosphere. The upwelling radiance, as there is often no cosine collector, recorded by the sensor can originate from four sources. The first is L_a, which is the portion of radiance that results from downwelling irradiance returning the sensor before reaching the water surface, representing the response of the atmosphere. L_s, is radiance that is a result of reflection from the water surface. L_v represents the response from the volume of the water column as the energy enters the water column and re-emerges. Finally, L_b is the portion of radiance that is a result of the light penetrating the air-water interface, reaching the bottom of the water body and re-emerging. Therefore, the total radiance received at the sensor (L) is a sum of all of the radiant flux on each path (Equation 1.4):

$$L = L_a + L_s + L_v + L_b \tag{1.4}$$

For the detection of photosynthetic pigments, the L_v component is the most important because it represents the aquatic absorption and scattering processes impacting the photo flux from the water column.

Considerations for Airborne Remote Sensing

For those who conduct remote sensing for water quality purposes, the desire is to remove the other radiance components to obtain the response solely of L_v. In some cases, L_b can be eliminated because the depth of water is enough where no light would reach the bottom. The radiance component from the surface of the water, L_s, is sometimes accounted for with the use of a surface reflection algorithm (Bukata, et al., 1995). However, it is often the case that it is most difficult to account for the atmospheric component because it is comprised of spatially and temporarily variable components. It is often easier to think of water quality remote sensors as viewing one attenuating medium, water, through another attenuating medium, the atmosphere. With field platforms, the thickness of atmosphere

between the sensor and the target is much smaller. The smaller thickness means there are fewer particles and molecules to absorb and scatter light, making the L_a component smaller. With airborne and satellite platforms, the water is viewed through a much greater thickness of atmosphere, so L_a component is much larger and more variable making it difficult to estimate the effects. In most cases, even the most complex atmospheric correction algorithms cannot account for all of the variability.

3.0 Review of Remote Sensing of Inland Waters

Spectral Characteristics of Inland Waters

Case I vs. Case II

In the field of remote sensing, water bodies have been divided into two categories based on their spectral characteristics. These divisions, first introduced by Morel and Prieur in 1977, are Case I and Case II. Case I waters are those with a high concentration of Chl a relative to scattering by other constituents (Morel & Prieur, 1977). This definition has been generalized to refer to waters where all of the optical properties are determined by the concentration of phytoplankton and their associated pigments. Examples of these types of waters would be oceanic waters or clear inland water systems. Case II waters are classified as those with optical properties influenced by phytoplankton and dominated by the presence of inorganic particulate matter and dissolved organic matter (Morel & Prieur, 1977; Pozdnyakov, et al., 2005). Most inland and estuarine waters fall into the second category. The accuracy of quantifying a water quality parameter by remote sensing relies on how optically active that parameter is and whether other parameters interfere with its recorded reflectance (Liu, et al., 2003). Therefore, Case I waters, with lower amounts of other optically active constituents, are considered to be spectrally simple compared to Case II waters.

Approximate Absorption Maxima of Pigments Found in Cyanobacteria

Organisms in the Cyanophyta phylum contain biliproteins within a structure called the phycobilisome. As mentioned in earlier sections, Cyanophyta can possibly contain the photosynthetic pigments chlorophyll *a*, chlorophyll *d*, many different carotenoids, phycocyanin, phycoerythrin, allphycocyanin and phycoerytherocyanins. Chlorophyll has two absorption maxima, one in the shorter wavelengths (blue light) and one in longer

wavelengths (red light). The maxima for chlorophyll *a* are approximately 430nm and 665 nm, while chlorophyll *d* absorbs maximally at approximately 448 nm and 690 nm (Rowan, 1989). Phycoerythrin in cyanobacterial species can exhibit two absorption maximums at approximately 559 nm and 569 nm at a neutral pH (Rowan, 1989). Phycocyanin, at a neutral pH, exhibits an absorption maximum of approximately 620 nm. Allophycocyanin absorbs maximally at approximately 615 and 650 nm (Rowan, 1989). The absorption maximum for phycoerytherocyanin, at a neutral pH, is approximately 573 nm, 590 nm and 630 nm (Rowan, 1989).

Sample of Above Water Reflectance Spectra

The average airborne hyperspectral reflectance from Geist Reservoir, a Case II water, measured with an Airborne Imaging Spectrometer for Applications (AISA) is presented in Figure 3. The AISA reflectance curve demonstrates typical above water spectral characteristics of productive inland waters.

Figure 3- Average Airborne Hyperspectral Reflectance Spectra from Geist Reservoir

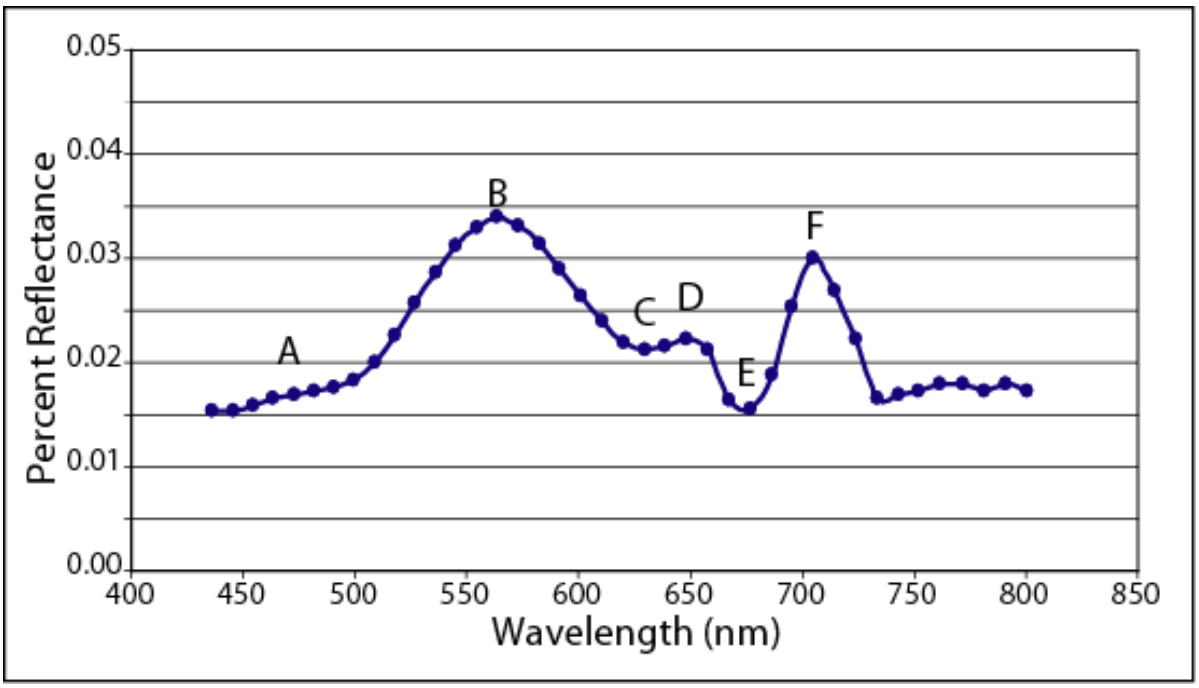

The absorption in the lower wavelengths (A) is likely due to a combination of Chl a, carotenoids and dissolved organic matter (Rowan, 1989; Rundquist, et al., 1996; Gitelson, et al., 1999; Schalles & Yacobi, 2000; Vincent, et al., 2004). The green peak (B) is present at the position of maximum reflectance caused by minimum absorption of algal pigments and scattering by non-organic particles and phytoplankton cell walls (Dekker, 1993; Rundquist, et al., 1996; Gitelson, et al., 2000; Schalles & Yacobi, 2000). A trough at 628 nm (C) represents the absorption maximum of PC (Rowan, 1989; Dekker, 1993; Richardson, 1996; Gitelson, et al., 1999; Schalles & Yacobi, 2000). At 650 nm, a small peak (D) represents a region of reduced pigment absorption and possibly fluorescence due to the PC (Rowan, 1989; Schalles & Yacobi, 2000). The second absorption peak of Chl a and cell wall scattering competitively influence the spectra causing a trough at 675 nm (E) (Rundquist, Han, et al., 1996; Gitelson, et al., 2000). This trough is followed by a peak at 704 nm (F) which is caused by the interaction of scattering by suspended matter, including algal cells, and

absorption due to water and Chl a (Gitelson, et al., 1995; Gitelson, et al., 2000; Schalles & Yacobi, 2000). Beyond this peak the spectra is strongly influenced by the absorption of water, causing low reflectance.

Optical Properties of Natural Waters

Inherent and Apparent Optical Properties

Once incoming photons have passed through the air-water boundary, they will undergo attenuation in the water body. A spectrometer measures the amount of attenuation as a function of reflectance, by measuring the apparent optical properties of the water body. These measurements are called apparent properties because they are a function of the inherent optical properties and the illumination characteristics when they were measured. Inherent optical properties are a consequence of the water body itself, including the organic and inorganic constituents. These optical properties are termed the attenuation coefficient, the absorption coefficient, the scattering coefficient, the backscattering probability, and the volume scattering function (Gordon, et al., 1975). These inherent optical properties at each wavelength (λ) are related to the apparent measurable subsurface (0^-) reflectance, $R(0^-, \lambda)$, with this simplified equation:

$$R(0^-, \lambda) = E_u(0^-, \lambda) / E_d(0^-, \lambda) = f * b_b/(a + b_b) \quad (1.1)$$

Where E_u and E_d are the subsurface upwelling and downwelling irradiance, "a" is the total absorption coefficient, b_b is the total backscattering coefficient and *f* is a factor that is dependent upon the light field (Gordon, et al., 1975; Kirk, 1984; Morel & Gentili, 1991; Jupp, et al., 1994; Gons, 1999; Hakvoort, et al., 2002; Vos, Hakvoort, et al., 2003; Simis, et al., 2005). The total absorption and backscattering coefficients of a water body can be expressed as a function of their constituents of the water (Dekker, 1993; Jupp, et al., 1994; Gons, 1999; Hakvoort, et al., 2002; Vos, et al., 2003; Simis, et al., 2005). For example, if the

following constituents: chlorophyll *a* (Chl a), total suspended matter (TSM) and color dissolved organic matter (CDOM) are present in a volume of water, the total absorption (a) and backscattering (b_b) would be:

$$a = a_w + a^*_{chl\ a}\,\text{Chl a} + a^*_{TSM}\,\text{TSM} + a^*_{CDOM}\,\text{CDOM} \quad (1.2)$$

$$b_b = b_{b,w} + b^*_{b,chl\ a}\,\text{Chl a} + b^*_{b,TSM}\,\text{TSM} + b^*_{b,CDOM}\,\text{CDOM} \quad (1.3)$$

Where a^*_x or $b^*_{b,x}$ indicate the specific absorption or backscattering coefficient of the constituent and the subscript "w" indicates absorption and backscattering due to the water.

Upwelling Radiance

The upwelling radiance from the air-water interface can be measured by above water remote sensing platforms and converted to above-water (0) reflectance for each wavelength with the equation:

$$R(0,\lambda) = L_u/L_d \quad (1.4)$$

Where L_u is the upwelling radiance measured at the sensor and L_d is the downwelling radiance measured at the sensor. To relate the subsurface reflectance to the upwelling radiance, the downwelling direct and diffuse irradiance and the transmission of the photons through the air-water interface need to be considered. This relationship can be seen in the following equation (Bukata, et al., 1995):

$$R(0^-,\lambda) = Q^*(L_u - f_1{*}E_{sky} - f_2{*}E_{sun})/(T^*(f_3{*}E_{sky} - f_4{*}E_{sun})) \quad (1.5)$$

Where "Q" is a factor to convert from upwelling irradiance below the water surface to upwelling radiance below the water surface, f_1 and f_2 are the ratios of upwelling radiance

entering the field-of-view of the remote sensing device to downwelling sky and sun irradiance respectively, "T" is the transmission of radiance through the air-water interface (which includes a factor for the index of refraction), and f_3 and f_4 are fractions representing the amount of downwelling sky and sun irradiance that is transmitted into the water respectively. Because above-water reflectance is a function of the inherent properties of the water, it allows the study of subsurface water quality parameters from surface spectral reflectance measurements.

Empirical, Semi-Empirical and Bio-optical/Analytical Models

Morel and Gordon (1980) introduced three different approaches that can be used to quantify water quality characteristics from remotely sensed data. The first approach is an empirical one, where statistical relationships are found between spectral values and measured water parameters (Morel & Gordon, 1980). This method is similar to the semi-empirical method, where statistical relationships are sought between spectral characteristics, but the relationships are made with specific spectral characteristics whose source is more or less understood (Morel & Gordon, 1980). Additionally, the third type of model is a bio-optical or analytical one, from now on referred to as bio-optical, where the inherent and apparent optical properties are used to model the reflectance spectra to predict constituent concentration (Morel & Gordon, 1980).

Empirical and Semi-empirical Models

Empirical and semi-empirical models can involve relationships between single bands, band combinations or band ratios and water quality constituents. These types of models require that *in situ* water quality data be taken concurrently with remote sensing data acquisition; otherwise models developed will have no reference for concentration of the water quality constituent and cannot account for temporal variability of that parameter

(Hakvoort, et al., 2002; Liu, et al., 2003). Empirical and semi-empirical models involve a regressed relationship that can be linear, exponential or polynomial. It is quite common to use linear relationships to relate spectral data to water quality data. The format of the linear semi-empirical model is:

$$y = a*x + b \qquad (2.0)$$

where "y" is the water quality constituent, "x" is a single band, band combination or band ratio and "a" and "b" are regression coefficients. Linear semi-empirical models have been used to relate parameters such as phytoplankton pigment concentration (i.e. Chl a, PC, carotenoids and pheophytin a), dissolved organic carbon, total phosphorous, secchi disk depth, total suspended sediment and turbidity to field, airborne or satellite spectral data (Gitelson, 1992; Millie, et al., 1992; Dekker, et al., 1992; Dekker, 1993; Gitelson, 1993; Gitelson, et al., 1995; Yacobi, et al., 1995; Fraser, 1998; Kuster, et al., 1998; Schalles, et al., 1998; Kallio, et al., 2001; Matthews, et al., 2001; Kallio, et al., 2003; Vincent, et al., 2004; Simis, et al., 2005; Zimba & Gitelson, 2006). In some cases, linear regression models do not fit because of the exponential nature of the relationship between the constituent and reflectance. This occurs because the correlations are based on the scattering properties of the water constituents; an increase in scattering increases the multiple scattering giving an exponential increase (Dekker, et al., 1992). Additionally, at high reflectance values, sensors are relatively insensitive to change, leading to a non-linear relationship (Liu, et al., 2003). Because of the non-linearity at high concentrations, a few studies have used exponential or polynomial models to explain the relationship between water constituents such as Chl a, PC and spectral reflectance (Dekker, et al., 1992; Mittenzwey, et al., 1992; Schalles & Yacobi, 2000; Wang, et al., 2005). The formats for exponential and polynomial empirical or semi-empirical models are:

2.1 $y = a^{xb}$

2.2 $y = a*x^2 + b*x + c$

where y represents the water quality constituent, x is a single band, band combination or band ratio and "a", "b" and "c" are constants. Another technique used to increase the success of an empirical or semi-empirical model is to transform the data before it is put into the model. Log transformations of water constituents and spectra and derivative transformations of spectra have been performed to increase the success of semi-empirical models (Fraser, 1998; Rundquist, et al., 1996; Kallio, et al., 2001; Dall'Olmo, Gitelson, et al., 2005). Regardless of their success, semi-empirical models are often site specific and cannot be transferred to other locations without modification of the constants (Fraser, 1998; Liu, et al., 2003).

Bio-optical/Analytical models

Bio-optical models relate the optical return from a natural water body to the biological and other aquatic components using the subsurface reflectance model developed by Gordon et al. (1975). Using measured inherent and apparent optical properties of water quality constituents, subsurface reflectance is used to create a bio-optical model which can then simulate subsurface reflectance at any range of water quality constituent concentrations (Brando & Dekker, 2003). The inversion of a bio-optical model allows the calculation of constituent concentrations from subsurface reflectance. This method is advantageous because it does not require concurrent ground truth sampling once absorption and backscattering coefficients for each component are available (Hakvoort, et al., 2002). Bio-optical models have been used to estimate constituents such as pigment concentrations (Chl a), total suspended matter, dissolved organic matter, secchi disk depth and turbidity from either field, airborne or satellite spectra (Dekker, et al., 1992; Dekker, 1993; Jupp, et al., 1994; Hoogenbloom, et al., 1998; Gons, 1999; Gons, et al., 2002; Hakvoort, et al., 2002;

Brando & Dekker, 2003; Pozdnyakov, et al., 2005; Simis, et al., 2005). The disadvantage to this type of water quality modeling is that it is far more 'equation' intensive and may take more time to estimate water quality parameters than a more simple semi-empirical model.

Choice of Remote Sensing Systems for Inland Waters

Field-based Systems

Successful remote sensing depends upon many factors, one of which is an educated decision, based on the scope of the project, about the type of remote sensing system needed. Field-based spectroradiometers are commonly used for remote sensing projects because they are comparatively inexpensive, portable, and have a high spectral resolution suitable for most water quality monitoring needs. Besides being an instrument used to collect the main data set, field-based spectroradiometers are often used to collect secondary data sets which are used to calibrate other airborne or satellite data. Field-based spectroradiometers such as Spectralon, SpectraColorimeter, PR 650 and Ocean Optics ST1000 have been used for remote sensing of phytoplankton pigments and other water quality parameters (Hoogenbloom, et al., 1998; Gons, 1999; Jupp, et al., 1994; Gitelson, et al., 2000; Schalles & Yacobi, 2000).

Airborne Systems

The use of airborne systems for the remotes sensing of water quality parameters has been limited due to its high cost and low flexibility (Hakvoort, et al., 2002). Airborne remote sensing platforms have several advantages and disadvantages. First, airborne spectrometers have an advantage over field-based platforms in that they can capture large areas very quickly providing information on spatial variability (Dekker, et al., 1992). Additionally, airborne platforms have the advantage of higher spatial and spectral resolutions than satellite systems, making them an ideal way to image small inland water

bodies (Mertes, et al., 2004). Furthermore, the channels of airborne sensors are often programmable and the spatial resolution is flexible, allowing the user to define the spectral regions they would like to detect and the spatial resolution which would be best for their study. However, airborne data have the disadvantage of lower spectral resolution than field spectroradiometers and the need for atmospheric aerosol calibration. Airborne based platforms such as CAMS, PMI, CAESAR, CASI, AISA and EPS-A have been used for remote sensing of phytoplankton pigments and other water quality parameters, a selection of instruments and their associated parameters as used in water quality remote sensing studies is provided in Table 1.

Table 1- Summary of Airborne Sensor Characteristics used in Water Quality Applications

Sensor	Spatial Resolution	Spectral Resolution	Spectral Range	Parameters Estimated	Reference
CAMS (Calibrated Airborne Multispectral Scanner)	2.5 m	30nm - 70nm	450 - 900 nm	Chl a, PC	Millie, et al., 1992
PMI (Programmable Multispectral Imager)	4 m	2.6 - 300nm programm-able	430 - 805 nm	Chl a, TSM, Secchi disk	Dekker, et al., 1992
CASEAR (CCD Airborne Experimental Scanner for Applications in Remote Sensing)	4 m	10 - 30nm programm-able	40 - 1050 nm	Chl a, TSM, Secchi disk	Dekker, et al., 1992
CASI (Compact Airborne Spectrographic Imager)	Not Reported	1.8 nm	380 - 895 nm	Turbidity, Chl a, PC	Dekker, 1993; Jupp, et al., 1994
Spectron Engineering SE590 spectroradiometer (fitted with 1˚ optical lens for airborne applications)	20 m	10 nm	358 - 1107 nm	Chl a	Fraser, 1998
AISA (Airborne Imaging Spectrometer For Applications)	1 m	5 - 8 nm programm-able	450 - 800 nm	Chl a,	Kuster, et al., 1998; Kallio, et al., 2001; Kallio, et al., 2003
EPS-A	3 m	"hyper-spectral"	450 - 750 nm*	Chl a, TSM, DOM	Hakvoort, et al., 2002

***Indicates estimated from publication data**

Satellite Systems

The limited spatial resolution of most current satellite systems limits their applicability for remote sensing of smaller inland water bodies. However, in cases where the target is large enough there has been success with the detection of water quality constituents from satellite-borne platforms. Sea-viewing Wide-Field-of-View (SeaWiFS) sensor has been used for the detection of Chl a, dissolved organic matter and total suspended matter in a few inland water studies (Vos, et al., 2003; Dall'Olmo, et al., 2005; Pozdnyakov, et al., 2005). Vos et al. (2003) found that the most common problem with the SeaWiFS data is the lack of images of good quality due to cloud cover. The Hyperion sensor on the EOS-1 satellite, LANDSAT TM 5 and ETM+7 satellites, Medium Resolution Imaging Spectrometer (MERIS), Moderate Resolution Imaging Spectometer (MODIS) and Satellite Pour l'Observation de la Terre (SPOT) have all been used in the study of water quality constituents in inland waters. A selection of satellite-based sensors used in water quality remote sensing is provided in Table 2.

Table 2- Summary of Satellite Sensor Characteristics used in Water Quality Applications

Sensor	Spatial Resolution	Spectral Resolution	Spectral Range	Reference
Hyperion	30 m	220 bands	357 - 2576 nm	Brando & Dekker, 2003; Wang, et al., 2005
LANDSAT TM (5,7)	30 m (band 6 is 120m)	7 bands	450 nm - 12.5 µm	Dekker, et al., 1992; Yacobi, et al., 1995; Vincent, et al., 2004
MERIS	300 m	15 bands	400 - 1050 nm	Gons, et al., 2002; Giardino, et al., 2005
MODIS	250 m to 1000 m (depending on the band)	36 bands	400 - 1440 nm	Dall'Olmo, et al., 2005; Pozdnyakov, et al., 2005
SeaWiFS	1.1 km	8 bands	402 - 885 nm	Vos, et al., 2003; Dall'Olmo, et al., 2005; Pozdnyakov, et al., 2005)
SPOT 2	10 m to 20 m	4 bands	500 - 890 nm	Dekker, et al., 1992

Water Quality Parameters Commonly Quantified

Turbidity and Secchi Disk Depth

Water clarity is affected by many water quality parameters. Without looking at specific constituents, two measurements, turbidity and secchi disk depth, measure the general water clarity. Turbidity is a cloudiness or haziness of water caused by individual particles including all of the inorganic and organic particles within chemically "pure" water. Turbidity is measured in Nephelometric Turbidity Units (NTU) or Formazin Nephelometric Units (FNU) based on how well the particles scatter light. Particles of differing size but the same concentration will scatter light differently causing differences in turbidity concentrations by similar suspended solid concentrations. Studies which used airborne and satellite based spectroradiometers to model turbidity concentrations based their relationships between NTU or FNU and spectral reflectance include Jupp, et al. (1994), Fraser (1998), Kuster, et al. (1998), Kallio, et al. (2001) and Vincent, et al. (2004).

Secchi disk depth is measured by lowering a white and black object into water and tracking the depth at which the object becomes invisible. Despite the subjective nature of its measurement, the simplicity, convenience and the long history of use has made this parameter a common part of water quality studies. Secchi depth is related to optical parameters such as the attenuation coefficient and scattering albedo and can provide a quantitative estimate of inherent and apparent optical properties (Bukata, Jermoe, Kondratyev, & Pozdnyakov, 1995). Due to the many useful qualities, secchi disk depth measurements have been used to study water quality and have been related to field and airborne data in several studies including Dekker, et al. (1992), Kuster, et al. (1998), Kallio, et al. (2001) and Kallio, et al. (2003)

Total Suspended Solids (Seston, Tripton)

Total Suspended Solids (TSS), also known as Seston or Total Suspended Matter (TSM), refers to all of the inorganic and organic matter suspended within the water column. Tripton comprises a portion of TSS, but refers to only the inorganics within the water. TSS cause strong backscattering of the incident radiation making it detectable with remote sensing systems (Liu, et al., 2003). Kallio et al. (2001) used an AISA sensor to estimate several water quality parameters in oligotrophic to eutrophic lakes in Finland; one of these parameters was TSS. Using the reflectance from the NIR portion of the spectrum ($R_{705 - 714}$) they were able to achieve and R^2 of 0.85 between reflectance and TSS concentration. Many other studies have had success estimating TSS concentrations for remotely sensed field, airborne and satellite data including Dekker, Malthus, Wijnen, & Seyhan (1992), Dekker (1993), Kuster, et al. (1998), Hakvoort, et al. (2002), Vos, et al. (2003), Pozdnyakov, et al. (2005) and Wang, et al. (2005).

Phytoplankton pigments are often the parameter of primary concern for water quality studies. Because of the strong scattering characteristics of TSS, several studies have investigated the effect of TSS concentrations on Chl a reflectance signatures. Suspended sediments are optically diverse and will scatter and absorb light differently according to physical and chemical characteristics (Schalles, et al., 2001). Quibell (1991) was one of the first studies to investigate the additive effects of suspended sediment concentrations on Chl a reflectance signatures. This study found that the reflectance peak at 550 nm was shifted towards the longer wavelengths, depending upon the amount of sediment. The positions of reflectance peaks and troughs from approximately 600 - 720 nm were not shifted, but increased in value (Quibell, 1991). While Quibell (1991) found that increasing sediment concentration appeared to have an equal additive affect in the Red and NIR wavelengths, Han, et al. (1994) reported different results. While studying the effects of sediment inputs

on the spectral reflectance from phytoplankton dominated by cyanobacteria, Han, Rundquist, Liu, Fraser, & Schalles (1994) found that the increasing sediment concentration had unequal effect at differing wavelengths. Both Han, et al. (1994) and Schalles, et al. (2001) found the ratio of near infrared to red reflectance is unaffected by increasing sediment concentration or type and can be used to effectively estimate Chl a concentration in turbid waters.

Colored Dissolved Organic Matter

Colored dissolved organic matter (CDOM) is also referred to as yellow substances, aquatic humus, gilvin and gelbstoff. CDOM is caused by the deterioration of organic detritus in the water. This dissolved component absorbs light in the blue area of the spectrum imparting a yellow color to the water (Dekker, et al., 1992; Markager & Vincent, 2000). The absorbance of CDOM overlaps the blue absorption maximum of Chl a, affecting the amount of light available for photosynthesis. The absorbance exponentially decreases as wavelength increases (Dekker, et al., 1992; Markager & Vincent, 2000). Ratios for Chl a estimation which relate reflectance in the blue area of the spectrum to pigment concentration do not predict well in inland waters because of the absorption of CDOM (Gons, et al., 2002). Many studies have quantified this water quality parameter in inland waters with the use of remote sensing systems (Kallio, et al., 2001; Hakvoort, et al., 2002; Brando & Dekker, 2003; Pozdnyakov, et al., 2005).

Chlorophyll a

Studies Which Quantify the Parameter

Chl a concentration is commonly used as a proxy for phytoplankton concentration in ocean and lake water. Because of the link between phytoplankton concentrations and primary productivity, indicating trophic status, Chl a concentrations have been quantified

from remote sensing data in a wide variety of studies. Analytical models have had success modeling Chl a concentration from field based, airborne and satellite remote sensing data in a wide variety of lakes with differing trophic status (Dekker, et al., 1992; Dekker, 1993; Jupp, et al., 1994; Hoogenbloom, et al., 1998; Gons, 1999; Gons, et al., 2002; Hakvoort, et al., 2002; Brando & Dekker, 2003; Vos, et al., 2003; Pozdnyakov, et al., 2005; Simis, et al., 2005). Field-based studies commonly achieve high relationships, R^2 = 0.73 - 0.99, between semi-empirical reflectance algorithms and Chl a concentrations (Gitelson, 1992; Mittenzwey, et al., 1992; Gitelson, 1993; Gitelson, et al., 1994; Gitelson, et al., 1995; Rundquist, et al., 1996; Schalles, et al., 1998; Gitelson, et al., 2000; Schalles & Yacobi, 2000; Zimba & Gitelson, 2006). For airborne semi-empirical reflectance algorithms, the relationship is also high, R^2 = 0.68 - 0.98 (Dekker, et al., 1992; Dekker, 1993; Millie, et al., 1992; Fraser, 1998; Kuster, et al., 1998; Matthews, et al., 2001; Kallio, et al., 2001; Kallio, et al., 2003). Chlorophyll concentrations have also been estimated from satellite remote sensing systems with reasonable success since the 1970s (Bukata, et al., 1995). Satellite based studies of inland waters have achieved high R^2 values, ranging from 0.90 - 0.98, between semi-empirical reflectance algorithms and Chl a concentration in (Dekker, et al., 1992; Yacobi, et al., 1995; Dall'Olmo, et al., 2005; Wang, et al., 2005).

Semi-Empirical Algorithms Used To Quantify Chl a

There are several different semi-empirical algorithms used to estimate Chl a concentration from remotely sensed spectra. Historically, this estimation was only done in Case I waters (Morel & Prieur, 1977). One commonly used algorithm for spectrally simple waters is the blue/green ratio (Gitelson, et al., 1994; Matthews, et al., 2001). The algorithm uses the reflectance in the blue portion of the spectrum, which is highly sensitive to Chl a absorption and the green wavelengths where Chl a absorption is minimal. However, algorithms that worked to estimate Chl a concentration in Case I waters are not necessarily

suitable for Case II waters because of the presence of other optically active constituents (Gitelson, 1993; Gitelson, et al., 1994; Schalles, et al., 2001). It was shown by Gitelson, et al. (1994) that the correlation between the blue/green reflectance ratio R_{440}/R_{550} (R^2) is lower than 0.37 for a productive Case II lake in Israel. To improve estimating Chl a in Case II waters, several other algorithms using the NIR portion (~700 nm) of the spectrum were developed. One of these algorithms is the NIR/Red ratio based on the observation that the NIR portion of the spectrum has maximum reflectance due to the Chl a scattering, while the red wavelengths has a Chl a absorption maximum Because of the low absorbance of CDOM in longer wavelength regions (Dekker, et al., 1992; Markager & Vincent, 2000) and the insensitivity of this ratio to sediment concentration or sediment type (Han, et al., 1994; Schalles, et al., 2001) the NIR/RED ratio can be used to effectively estimate Chl a concentration in Case II waters. This ratio algorithm has been used to estimate Chl a in Case II waters, ranging from oligotrophic to eutrophic, from all three remote sensing platform types (Dekker, et al., 1992; Dekker, 1993; Gitelson, 1992; Gitelson, 1993; Gitelson, et al., 1994; Yacobi, et al., 1995; Rundquist, et al., 1996; Kuster, et al., 1998; Schalles, et al., 1998; Gitelson, et al., 2000; Kallio, et al., 2001; Kallio, et al., 2003). Other algorithms which use the spectral feature at the NIR band include the position of this reflectance peak (Gitelson, 1992; Gitelson, 1993; Gitelson, et al., 2000; Schalles & Yacobi, 2000), the sum of the reflectance below the peak (Gitelson, et al., 1994; Schalles, et al., 1998; Gitelson, et al., 2000) and the height of the peak from a reference line (Yacobi, et al., 1995; Schalles, et al., 1998; Gitelson, et al., 2000). Other algorithms relate the fluorescence of Chl a to *in situ* Chl a concentration (Gitelson, et al., 1994; Matthews, et al., 2001). However, accuracies of the algorithms are limited by the efficiency of different phytoplankton to fluoresce and the reduced light intensity available for fluorescence (Gitelson, et al., 1994).

Phycocyanin

More recently, the focus of remote sensing of water quality has switched from estimation of phytoplankton concentration through the use of the pigment Chl a to identification of algal populations through the use of taxonomically significant accessory pigments such as PC (Richardson, 1996) as it is indicative of cyanobacterial concentration (Mertes, et al., 2004; Simis, et al., 2005). This shift has come about by the advent of hyperspectral remote sensing systems which have the capability to differentiate accessory pigments. Only a few studies have explored the relationship between PC absorption and remote sensing data. Studies such as Jupp, et al. (1994) and Richardson, Buisson, Liu, & Ambrosia (1994), airborne spectral data were used to detect the presence of PC as a proxy for cyanobacterial presence but not quantify the amount of pigment. In a study done by Millie, et al. (1992), log transformed PC concentration was correlated to the reflectance of a single CASI band centered at 615 nm, and the low squared correlation ($R^2 = 0.35$) was attributed to variability of pigment extraction (Millie, et al., 1992). Dekker (1993) investigated a relationship between field-based and airborne subsurface reflectance, and found that the band combination $0.5(R_{600}+R_{648})-R_{624}$ could be used for estimating PC concentration in oligotrophic to eutrophic lakes in the Netherlands. The problem of extraction variability was also cited by Schalles & Yacobi (2000) as a cause for low correlations when they estimated pigment concentrations from field reflectance data from Carter Lake in Nebraska. In their study, Schalles & Yacobi (2000) found that a relationship between PC concentration and the ratio of reflectance, R_{650}/R_{625}, yielded an R^2 of 0.612. It was also noticed that the concentration of PC was highly inversely correlated to green peak position due to the erosion of the right side of the reflectance peak from PC absorption (Schalles & Yacobi, 2000). The first successful attempt to detect PC from LANDSAT TM data was achieved by Vincent, et al. (2004). By developing two different band combination

algorithms, an $R^2 > 0.73$ could be achieved for LANDSAT 5 TM and LANDSAT 7 TM data in Lake Erie (Vincent, et al., 2004). Most recently, a semi-analytical model of subsurface PC reflectance was developed by Simis, et al. (2005). The model developed uses a ratio of the subsurface spectral reflectance at 620 nm and 704 nm as well as the absorption by PC and backscattering to predict PC concentration. Under the assumptions that CDOM had no absorption affect in the area of the spectrum of concern and that the backscattering component could be retrieved from a single band in the NIR, R^2 correlation of 0.94 was achieved between pigment concentration and field-based subsurface reflectance from lakes in the Netherlands (Simis, et al., 2005).

4.0 Review of Image Processing

Geometric Rectification

Georeferencing

Remote sensing images collected by aircraft platforms will inherently have various geometric distortions as the three-dimensional surface of the Earth is represented as a two-dimensional image (Jensen, 1996; Du, et al., 2002). Additionally, other distortions can arise from such things as the perspective of the sensor optics, the motion of the scanning system, and the platform altitude, attitude, and velocity. Because of this distortion, the images must be corrected before they can be mosaicked and used to extract water quality information for this study. Georeferencing is one step in the process to minimize the distortions caused during the image collection process. This involves identification of Ground Control Points (GCPs) on both the image and a base image with a known datum. The selection of GCPs is very important for geometric correction, and, if selected correctly, the derived relation between the images will be of high quality (Du, et al., 2002). Once the GCPs have been identified, different warping techniques are available to relate the images to each other. One of these techniques is polynomial warping. Polynomial equations are used to fit the coordinates of one image to the other using least-squares regressions (Jensen, 1996). After the GCPs have been selected and related together, software is then used to resample, or re-draw, the image such that its spatial location and orientation best matches that defined by the selected GCPs. There are three common resampling techniques: nearest neighbor, bilinear, and cubic convolution. Nearest neighbor resampling uses the nearest pixel without any interpolation to create the warped image, bilinear resampling calculates a linear interpolation between four pixels to resample the warped image and cubic convolution uses the nearest 16 pixels to approximate data value of a pixel, using cubic polynomials to resample the image (ITT Visual Information Solutions, 2004). Because of the common use

of the polynomial warping and the smoothness that a cubic convolution wrap creates, both of these methods were included in the image processing of this study.

Mosaicking

Mosaicking is used to create a large image from two or more adjacent of overlapping images. Two problems are likely to be encountered during a mosaicking process: first, the images may not be properly corrected for geometric distortions and second is edge effects. With improperly correct images, the only solution to this problem is to warp and resample the image again with new GCPs, ideally creating a new georectified image with a better match to the image to which it is to be mosaicked. The second problem, edge effects, is the brightening at the image edge as a result of the increased path length of the signal due to the field of view of the sensor (Matthews, et al., 2001). These effects are non-systematic distortions which are not removed with geometric or standard radiometric rectification. To aid in the elimination of the seams from image mosaics, the image edges can be feathered. Feathering is a technique which blends the edge of a top image with the bottom image based on a specified blending distance. The distance specified is used to create a linear ramp that averages the two images across that distance (ITT Visual Information Solutions, 2004). The feathering method was used in this study to minimize any edge effects, by averaging of the pixel values with those in the adjacent image, creating a seamless mosaic.

Radiometric Rectification

Absolute Radiometric Rectification

In an ideal situation, the photon flux recorded by a remote sensing platform would closely resemble that which is actually leaving the feature of interest. However, this often does not occur because of distortions caused by atmospheric scattering and the remote sensing system itself. Absolute radiometric correction must be done to relate the digital

numbers recorded at the sensor to those leaving the surface of the Earth (Du, et al., 2002). Previous work suggests that the removal of atmospheric path radiance is essential to retrieval parameters from aerial data (Matthews, et al., 2001). While sensor distortions can be accounted for with the application of calibration coefficients, atmospheric correction must be achieved by predicting the photon flux that interacts with the atmosphere. One method for approximating atmospheric path radiance involves using radiative transfer models. Unfortunately, the parameters (e.g. atmospheric absorption and scattering and sensor-target illumination geometry) of the atmospheric characteristics that these models require are often costly and impractical to measure (Eckhardt, et al., 1990; Yang & Lo, 2000; Cohen, et al., 2001). Additionally, these atmospheric scattering and absorption parameters are difficult to measure accurately even when they are measured at the same time as the image is recorded (Du, et al., 2002). Because of these reasons, in-situ spectral data were used in the current study to provide a reference of at surface reflectance, as an alternative to more complex atmospheric correction methods based on radiative transfer models. Thus, the retrieval of the spectral signatures of the features associated with this study could be accomplished.

Relative Radiometric Rectification

Spectral data acquired by remote sensing systems at different times are influenced by changing atmospheric conditions, sensor calibration, sensor geometry, illumination conditions and data processing procedures (Schott, et al., 1988; Eckhardt, et al., 1990; Hall, et al., 1991; Coppin & Bauer, 1994; Yang & Lo, 2000). The idea behind absolute calibration is that multiple images take under different illumination and atmospheric conditions will inherently be normalized to each other because they represent the spectral response from the surface. However, it is often the case that absolute normalization techniques will not account for all of the variability between image acquisitions making comparisons between

different images inaccurate (Heo & FitzHugh, 2000; Cohen, et al., 2001). Relative radiometric normalization is a technique that is used to make it appear as though all of the images were taken with the same sensor, at the same geometry and same illumination conditions. The relative radiometric normalization technique alters the digital count values of one or more images based on the digital counts of a reference image. The fundamental idea behind relative radiometric normalization is that linearity exists between the radiance reaching an airborne or satellite sensor, at any wavelength, and the reflectivity of the target (Schott, et al., 1988). This linearity can be expressed as:

$$L = a*r + k_2 \qquad (2.3)$$

Where "L" is the radiance recorded at the sensor, "r" is the targets reflectivity, "a" is a constant representing the upwelling and downwelling radiance and atmospheric transmission, and k_2 is the path radiance. Assuming the target has the same reflectivity, r, in both images, the atmospheric and calibration differences between scenes are linearly related because the data values recorded by each sensor are linearly related to the target's reflectivity (Schott, et al., 1988; Caselles & Lopez Garcia, 1989; Hall, et al., 1991). Normalization methods include the Gaussian method, histogram matching, the deterministic method and simple regression. The simple regression is widely recommended as the best of the methods (Heo & FitzHugh, 2000). With the simple regression method, the linearity between the two images is expressed by the following equation which is applied to each band of the image:

$$R_{1,x} = a * R_{2,x} + b \qquad (2.4)$$

Where R_1 is the radiance from a pixel in the reference image of band "x", R_2 = radiance from a pixel in the image of band "x" to be normalized and "a" and "b" are empirical parameters. By calculating the average gain ("a") and offset ("b") for multiple pairs of control points for

each band, the images can be normalized to each other. The simple regression normalization technique has been used by researchers in various remote sensing studies to normalize multiple images (Schott, et al., 1988; Caselles & Lopez Garcia, 1989; Hall, et al., 1991; Coppin & Bauer, 1994; Elvidge, et al.., 1995; Heo & FitzHugh, 2000; Yang & Lo, 2000; Du, et al., 2001; Du, et al., 2002; Teillet, et al., 2006). As with GCPs, the selection of the radiometric control points is critical to a successful normalization between images (Du, et al., 2002; Olthof, et al., 2005). Several suggestions, summarized by Heo & FitzHugh (2000), have been made to ensure good radiometric control points. It is best to choose flat targets with approximately the same elevation (so changes in the sun angle will not affect the spectral response), select a wide range of brightness values and select pixels with minimal amounts of vegetation (since their spectral signature is temporally variable).

To ensure the successful application of the "simple regression" normalization technique, two issues must be addressed. First, this technique requires that the control points selected are devoid of statistical outliers (Elvidge, et al., 1995), and, second, bias must be avoided when selecting control points (Du, et al., 2002). There are several techniques available to aid in the selection of statistically average features. One techniques proposed by Schott, et al. (1988) uses a NIR/Red ratio and band thresholding to identify and black out vegetation and water pixels leaving only urban, rock and soil pixels. From the pixels identified as urban, gains and offsets are calculated to match the standard deviations and the means of the selected pseudo invariant feature (PIFs) in each image. Another technique was developed by Hall, et al. (1991), in which dark and bright pixels were selected independently from each image and used for the normalization. The dark pixels were commonly deep water pixels, while the bright pixels were dry land features. Another technique to aid in the selection of radiometric control points is the by using scattergrams to identify data sets with no-change (Elvidge, et al., 1995). By looking at scattergrams

between each band in the image to be normalized and each band in the reference image, pixels that are invariant can be identified. Pixels which fall within the "no-change" areas of the scattergrams are then selected and used to calculate the gains and offsets for the normalization of each band (Elvidge, et al., 1995). To reduce bias due to the selection of control points by the user, Du, et al. (2001) and Du, et al. (2002) suggested using PCA analyses to calculate gain and offset values between images. This technique is unique because it does not rely on the user to select the control point pairs, creating objective and repeatable results (Du, et al., 2001; Du, et al., 2002).

Radiometric normalization is not only necessary for the calibration of images for change-detection studies, but also used to create seamless mosaics of single-date images (Cohen, et al., 2001; Olthof, et al., 2005). Single-date images are temporally variable, just on a smaller scale than images typically used in long term change-detection studies. To minimize error across the final mosaic, the center swath is often chosen as a normalization reference for the adjacent overlapping images (Olthof, et al., 2005). Furthermore, as relative radiometric normalization adjusts the properties of one image to another, if the reference data for the radiometric adjustment is field reflectance data, the atmospheric path radiance can be removed (Du, et al., 2002).

5.0 Problem Statement

The Objective of the Research

The primary objective of this research is to estimate spatial distribution and concentration of Chl a and PC in three central Indiana optically complex reservoirs using remote sensing techniques. This research enhances the understanding of situations in which these techniques can be used to detect and map cyanobacterial concentration in inland water bodies.

Justification of the Problem Statement

This study utilizes the spectral characteristics of Chl a and PC, cyanobacterial photosynthetic pigments, to estimate cyanobacterial densities. While Chl a estimation techniques for airborne imagery have been used before, they have not been applied to imagery of meso-eutrophic to eutrophic reservoirs in Indiana. Nor have common Chl a estimation algorithms such as reference line height or sum of the NIR reflectance peak been applied to AISA imagery. Additionally, since estimation of PC from remote sensing data is a relatively recent development, PC estimation algorithms have not been applied to imagery collected with an AISA sensor or to imagery collected in small inland reservoirs. Algorithms found during the literature review were applied to AISA imagery to predict the distribution and abundance of cyanobacterial photosynthetic pigments as a proxy for in-vitro measurements of extracted pigments. Linear regression techniques and standard error analysis was used to determine the algorithms which estimate pigment concentrations most accurately from the collected AISA imagery.

Why the Answer is Useful

The adverse affects caused by cyanobacteria blooms, i.e. degradation of lakes and reservoirs, aesthetic problems, changes in the taste of treated drinking water and potential toxicity, are well known. While cyanobacteria blooms in Indianapolis drinking water reservoirs have been intensively investigated, water resource managers lack a tool capable of providing information about the spatial distribution and composition of blooms. Monitoring of cyanobacteria blooms and the conditions that foster bloom formation via *in-situ* water sampling is both time and labor intensive, and often limited to infrequent collections at a small number of stations within a lake or reservoir. This study is useful because it tests a method of cyanobacterial detection which may improve upon the current method of quantification in central Indianapolis reservoirs because remote sensing provides a faster, more efficient method for mapping cyanobacteria blooms (Jupp, et al., 1994; Richardson, 1996; Kallio, et al., 2003). The development of this technique provides another tool for water resource managers to use in monitoring cyanobacterial blooms.

6.0 Materials and Methods

Study Sites

All three of the reservoirs (Figure 4), are located in central Indiana which borders on the edge of the climatic influence of the Great Lakes, where cooler Canadian air combines with the Gulf tropical air to create a continental humid climate (Sturm, et al., 1991).

Figure 4- Location of Study Sites

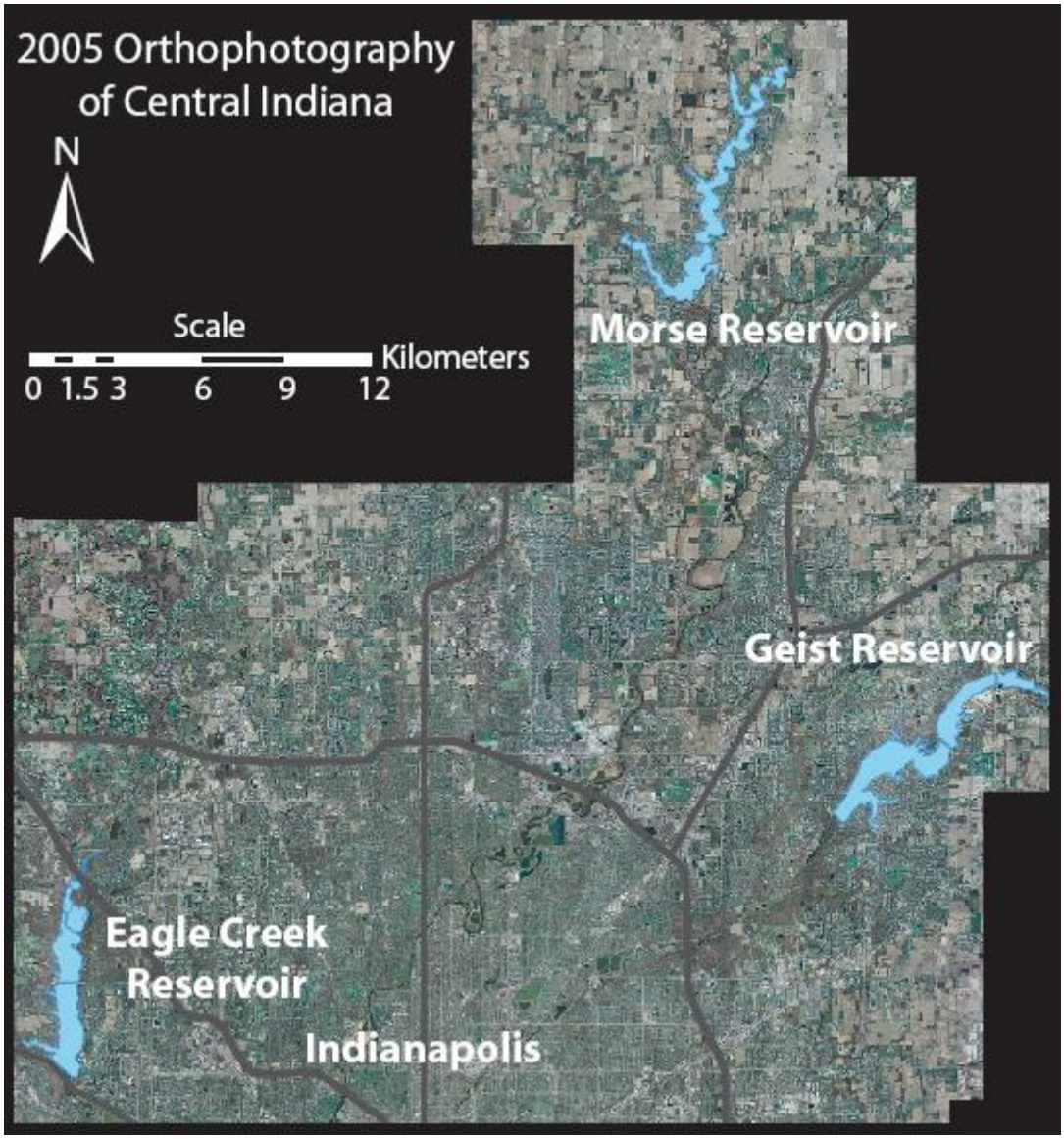

The annual precipitation of central Indiana is distributed evenly throughout the year (Tedesco, et al., 2003). Due to warm stable conditions in the reservoirs, and the input of soil nutrients from surrounding lands, algal blooms occur almost every year from May to September. As part of a routine lake monitoring programs, the Indiana Department of Environmental Management has classified the three reservoir's trophic status as within the Mesotrophic to Eutrophic range (Indiana Department of Environmental Managment, 2002; Indiana Department of Environmental Managment, 2004; Indiana Department of Environmental Management, 2006). The trophic status of these reservoirs indicates that they have medium to high nutrient supplies which could contribute to cyanobacterial growth. With low Secchi disk measurements, less than 1.0 m, and high TSS concentrations, greater than 10 mg/L, all three reservoirs can be functionally defined as Case II waters since the reflectance spectra are strongly affected by suspended sediments as well as phytoplankton pigments (Morel & Prieur, 1977).

Geist Reservoir

Geist Reservoir is a small (area of 7.5 km^2), shallow (mean depth 3.2 m), reservoir located in central Indiana, northeast of Indianapolis. A main component of the Indianapolis drinking water system, the reservoir was constructed in 1944 to regulate the flow into Fall Creek. Geist Reservoir is fed by Fall Creek Watershed, which encompasses a 588 km^2 area above Geist Dam (Tedesco, et al., 2005). USGS Stream Gage (#03351500) data from Fall Creek (1941 - 2003) showed a median daily instantaneous flow of 2.6 m^3/s into the reservoir, indicating that the estimated residence time, based on this inflow rate, is 55 days. In 2000, the Fall Creek Watershed land use was dominated by agriculture (58.3%)(Tedesco, et al., 2003).

Morse Reservoir

Morse Reservoir was constructed in 1956 to regulate the flow of Cicero Creek. Morse Reservoir is located north of Indianapolis in Hamilton County and is a small (area of 6 km^2), shallow (mean depth of 4.7 m) reservoir with the estimated watershed size above the catchment of 590 km^2 (Tedesco, et al., 2005). USGS Stream Gage (#03349510) data from Cicero Creek (2004 - 2006), shows that the estimated median daily instantaneous flow into Morse Reservoir is 1.0 m^3/s; the estimated residence time based on this data is 70 days. A high percentage of agricultural land use in Cicero Creek Watershed, 76.9% in 2000 (Tedesco, et al., 2003), contributes to the nutrient loading into Morse Reservoir.

Eagle Creek Reservoir

Eagle Creek Reservoir was originally constructed in 1967, in the northwest corner of Marion County, for flood control purposes. Eagle Creek Reservoir is a small (area of 5.0 km^2), shallow reservoir (mean depth of 4.2 m) with an estimated reservoir volume of 20,900,000 m^3 (Tedesco, et al., 2005). The reservoir is fed by Eagle Creek Watershed, which encompasses a 420 km^2 area above the Eagle Creek Dam. A water balance budget, using the USGS Stream Gage data (#03353200, 1957 - 2003) to estimate median daily flow, indicates a residence time of 56 days for Eagle Creek Reservoir (Pascual, Rafits, Filippelli, & Tedesco, 2006). Over half of the land in the watershed, 60.1% (Tedesco, et al., 2005), is used for agricultural land use. Nutrients from these sources and other inputs have led to high nutrient concentrations in the reservoir.

Sample Acquisition and Field Spectroscopy

Water Samples

Physical and chemical surface water data were taken at several sample stations on each reservoir (see following section for details). The water samples taken were measured

for pigment concentration (Chl a and PC), total suspended solids, orthophosphorus and suspended organic matter content. Additional measurements of the water quality characteristics (alkalinity, total hardness, dissolved organic carbon, total organic carbon, chloride, sulfate, total phosphorus, NH_4-N, nitrate, nitrite, total and dissolved silica, calcium, magnesium, potassium, sodium, MIB/Geosmin and Turbidity (NTU)), were performed by the Veolia Water Indianapolis, LLC. laboratories using the EPA and American Public Health Association Standard Methods. Parameters such as temperature, conductivity, pH, dissolved oxygen, total dissolved solids and salinity were measured using a YSI 600 XLM Multi-Parameter Sonde. Secchi disk depth was also measured at each station on each reservoir. These water samples were used to quantitatively relate reflectance and water quality parameters, allowing the development of algorithms which estimate concentration from remotely sensed data.

Field Spectroscopy

Ground truth samples and field reflectance spectra were collected at multiple sites on all three reservoirs on September 7th, 2005. Field spectral reflectance was measured with the fiber-optical head at approximately a height of 1 m above the water surface and positioned at nadir viewing direction. At each site, both the upwelling radiance of water, L_u, and the downwelling radiance, L_d, were measured. The downwelling radiance was measured from a Spectralon reference panel assumed to be a Lambertian, perfectly diffuse, reflector (Labsphere Inc., North Sutton, NH). Each upwelling radiance spectrum measured from the water surface was calibrated to reflectance by dividing with the downwelling radiance, equation 2.5:

$$R = L_u / L_d \qquad (2.5)$$

Measured reflectance at each site was the average of 20 consecutive upwelling radiance readings in order to reduce noise. The spatial coordinates of each site on the reservoir was recorded using a Trimble Pro-XRS (Trimble Navagation, Inc., Sunnyvale, CA) global positional system (GPS).

For Geist Reservoir, samples were collected at 27 sites throughout the reservoir (Figure 5). The spectroradiometer used for Geist Reservoir was an ASD FieldSpec ultraviolet/visible and near-infrared (UV/VNIR) spectroradiometer (Analytical Devices, Inc., Boulder, CO, USA). This ASD FieldSpec model recorded a continuous spectrum across 701 bands in the region of 348 - 1074 nm.

Field data was measured on Morse Reservoir at 28 sites (Figure 6). The field spectral reflectance was recorded with an ASD FieldSpec ultraviolet/visible and near-infrared (UV/VNIR) spectroradiometer (Analytical Devices, Inc., Boulder, CO, USA). This ASD FieldSpec model recorded a continuous spectrum across 2,153 bands in the region of 350 - 2500 nm.

Field data was measured at 32 sites on Eagle Creek Reservoir (Figure 7). The field spectral reflectance was recorded with an Ocean Optics USB2000 visible and near infrared (V/NIR) spectroradiometer (Ocean Optics, Inc., Dunedin, FL, USA). This spectroradiometer recorded a continuous spectrum across 340 to 1020 nm in 2,049 bands. Unfortunately, due to an error in calibration, the data collected by this sensor was unusable for this study.

Figure 5- Sample Locations of Geist Reservoir

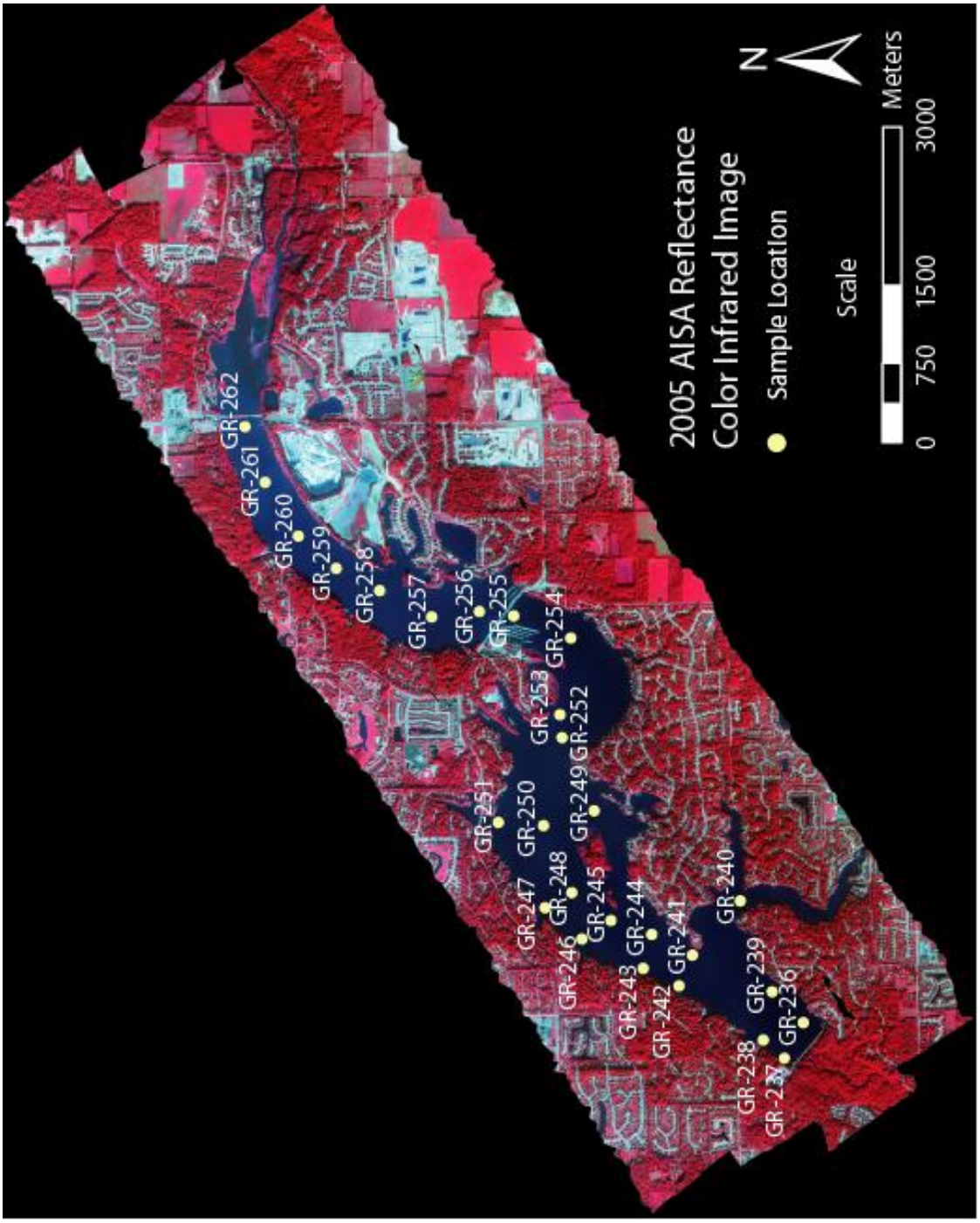

Figure 6- Sample Locations of Morse Reservoir

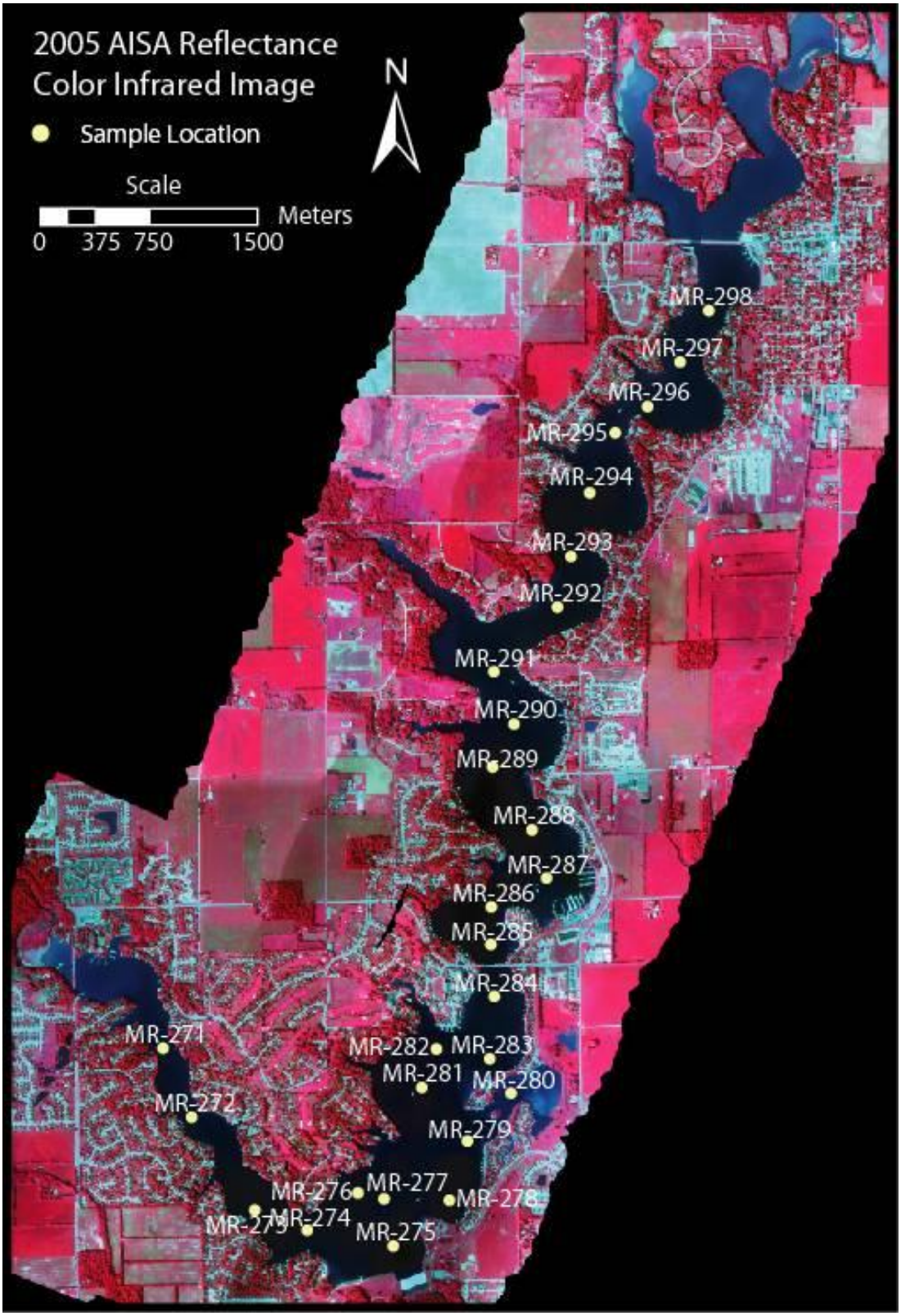

Figure 7- Sample Locations of Eagle Creek Reservoir

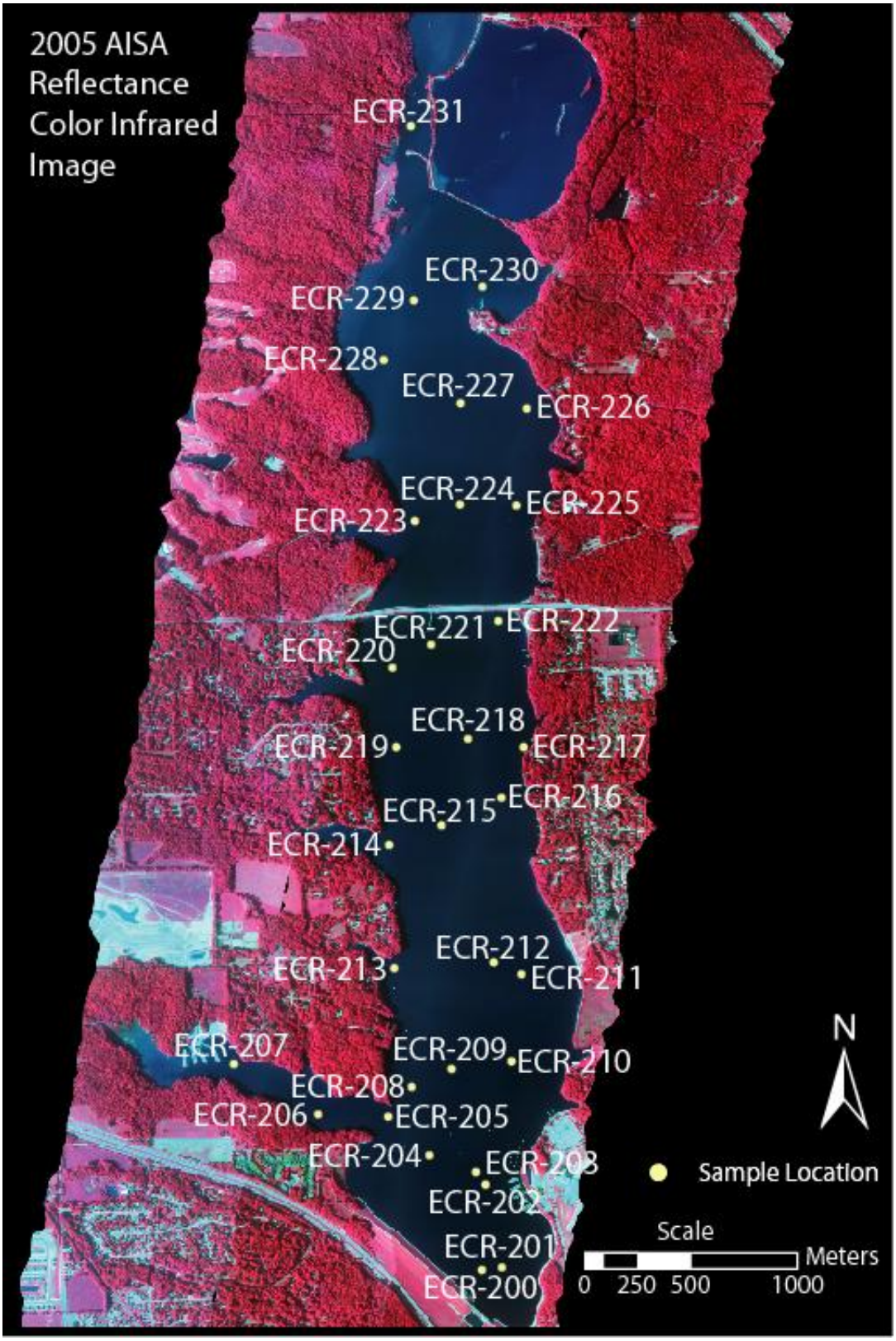

Airborne Hyperspectral Imagery

Concurrent with field sampling, an airborne imaging spectrometer for applications sensor (AISA), model "AISA-Eagle" (Spectral Imaging Ltd., Oulu, Finland), was used to acquire hyperspectral imagery of the reservoirs. This sensor was fitted onboard a Piper-Saratoga airplane; the research aircraft of the Center for Advanced Land Management Information Technologies at the University of Nebraska-Lincoln. The AISA-Eagle sensor is a pushbroom imager with a charge coupled device CCD sensor. This airborne sensor has a programmable set-up, allowing the collection of data in up to 512 discrete channels through the spectral range of 400 - 1000 nm. The AISA sensor provided by CALMIT is calibrated 2 - 3 times per year using a NIST traceable uniform light source and integrating sphere (Perk, et al., 2006). To account for the majority of the geometric distortion that occurs during image collection, a GPS unit (6 satellites minimum) collects x, y, and z data of the aircraft. To provide both radiance and at-sensor reflectance products, downwelling irradiance is measured at the same time as image acquisition by using a spectroradiometer pointing upward through the aircraft hull.

For this study, the AISA-Eagle was set to collect the images with 62 bands in the spectral region of approximately 392 - 982 nm with a bandwith of 7 - 8 nm (Table 3). The instantaneous field of view (IFOV), of the AISA sensor, across the track is 1 mrad, resulting in 1 m wide pixels and 1000 m wide swath from an altitude of 1000 m. The entirety of Geist, Morse and Eagle Creek Reservoirs were covered with four, five and three swaths respectively (Figure 8, 9 and 10). The timing of the swath acquisitions for each reservoir can be seen in Table 4.

Table 3- AISA Channels, Mean Range, Center and Channel Width used in this Study

Band Number	Mean Range (nm)			Wavelength Center (nm)	Channel Width (nm)
1	388.01	-	396.77	392.39	8.76
2	396.77	-	405.53	401.15	8.76
3	405.53	-	414.29	409.91	8.76
4	414.29	-	423.05	418.67	8.76
5	423.04	-	431.80	427.42	8.76
6	431.77	-	440.68	436.22	8.91
7	440.71	-	449.75	445.23	9.04
8	449.75	-	458.79	454.27	9.04
9	458.79	-	467.83	463.31	9.04
10	467.83	-	476.87	472.35	9.04
11	476.87	-	485.91	481.39	9.04
12	485.90	-	494.94	490.42	9.04
13	494.94	-	503.98	499.46	9.04
14	503.98	-	513.02	508.50	9.04
15	513.02	-	522.06	517.54	9.04
16	522.06	-	531.10	526.58	9.04
17	531.09	-	540.13	535.61	9.04
18	540.11	-	549.23	544.67	9.12
19	549.25	-	558.53	553.89	9.28
20	558.53	-	567.81	563.17	9.28
21	567.81	-	577.09	572.45	9.28
22	577.09	-	586.48	581.78	9.39
23	586.48	-	595.88	591.18	9.40
24	595.88	-	605.28	600.58	9.40
25	605.28	-	614.68	609.98	9.40
26	614.69	-	624.09	619.39	9.40
27	624.09	-	633.49	628.79	9.40
28	633.49	-	642.89	638.19	9.40
29	642.89	-	652.29	647.59	9.40
30	652.29	-	661.69	656.99	9.40
31	661.69	-	671.09	666.39	9.40
32	671.10	-	680.50	675.80	9.40
33	680.50	-	689.90	685.20	9.40
34	689.89	-	699.30	694.60	9.41
35	699.31	-	708.74	704.02	9.43
36	708.74	-	718.17	713.45	9.43
37	718.17	-	727.60	722.88	9.43
38	727.59	-	737.02	732.31	9.43
39	737.02	-	746.45	741.74	9.43
40	746.44	-	755.97	751.20	9.53
41	755.98	-	765.59	760.79	9.61
42	765.60	-	775.21	770.40	9.61
43	775.21	-	784.82	780.01	9.61
44	784.81	-	794.42	789.62	9.61

Band Number	Mean Range (nm)			Wavelength Center (nm)	Channel Width (nm)
45	794.42	-	804.03	799.23	9.61
46	813.65	-	832.85	823.25	19.20
47	832.85	-	842.43	837.64	9.58
48	842.43	-	852.01	847.22	9.58
49	852.01	-	861.59	856.80	9.58
50	861.59	-	871.17	866.38	9.58
51	871.17	-	880.75	875.96	9.58
52	880.76	-	890.34	885.55	9.58
53	890.34	-	899.92	895.13	9.58
54	899.92	-	909.50	904.71	9.58
55	909.49	-	919.10	914.30	9.61
56	919.10	-	928.73	923.92	9.63
57	928.73	-	938.36	933.55	9.63
58	938.36	-	947.99	943.18	9.63
59	947.98	-	957.61	952.80	9.63
60	957.61	-	967.24	962.43	9.63
61	967.23	-	976.86	972.05	9.63
62	976.86	-	986.49	981.68	9.63

Table 4- Acquisition Times of AISA Data

Reservoir Swath	Time Acquisition Started (GMT)	Time Acquisition Started (Eastern, non-military)
Geist 1 - 1	21:37:19.0156	5:37:19.0156
Geist 1 - 2	21:43:14.7031	5:43:14.7031
Geist 1 - 3	21:48:14.7031	5:48:14.7031
Geist 1 - 4	21:53:40.2031	5:53:40.2031
Morse 1 - 1	20:29:48.8125	4:29:48.8125
Morse 1 - 2	20:35:27.2031	4:35:27.2031
Morse 1 - 3	20:41:17.6094	4:41:17.6094
Morse 1 - 4	20:47:44.3125	4:47:44.3125
Morse 1 - 5	20:53:48.7031	4:53:48.7031
Eagle Creek 1 - 1	21:15:10.2031	5:15:10.2031
Eagle Creek 1 - 2	21:20:50.8125	5:20:50.8125
Eagle Creek 1 - 3	21:27:2.1094	5:27:2.1094

AISA Radiance and Reflectance Products

While both the radiance and at-sensor reflectance products were provided, only the radiance product was used. This was done because the downwelling irradiance would be accounted for with calibration to the field data; there may have been loss of radiometric resolution during conversion to reflectance; and upon visual comparison it appeared as though the radiance product contained less noise than the reflectance product.

Furthermore, the at sensor reflectance product still needed geometric and atmospheric path radiance calibration.

Water Sample Analysis and Image Processing

Chlorophyll a Extraction

Sample pretreatment consisted of filtering 150 - 200 mL on to a 47 mm, 0.45 micron pore size acetate filters using a filtration manifold. Filters were then placed into a 15 mL falcon tube and kept in a dark freezer (-9 °C) until analysis. Filtration and freezing occurred within 8 hours of sample collection. Samples were frozen for no longer than 3 months. Extracted Chl a was analyzed according to EPA Method 445.0 (EPA, 1997). Prior to pigment quantification, filters were dissolved in 10 mL of 90% buffered acetone and allowed to extract in a dark freezer (-9 °C) for at least 24 hours and no longer than 48 hours. Pheophytin corrected Chl a was measured fluormetrically using a TD - 700 Fluorometer (Turner Designs, Inc.) equipped with a Daylight White Lamp and Chlorophyll Optical Kit (340 - 500 nm excitation filter and emission filer > 665 nm) and calibrated with Chl-a from Spinach standard (Sigma-Aldrich 10865). All steps in the Chl a extraction process were performed under subdued light conditions. A summary of the Chl a data can be seen in Table 5.

Table 5- Summary of Measured Chl a Concentration Data

Reservoir	Chl a Range µg/L	Chl a Average µg/L	Chl a Standard Deviation µg/L	Error Range between Duplicates %	Error Average between Duplicates %	Samples Removed Due to Error >30%
Geist	34.7 - 118.9	71.4	25.8	0 - 39	9	1
Morse	18.0 - 168.6	59.3	44.3	0 - 30	8	1
Eagle Creek	21.6 - 107.1	51.8	24.1	0 - 67	8	1

Phycocyanin Extraction

150 to 200 ml of sample was filtered through a Millipore 47mm glass fiber filter and placed in a dark freezer (-9 °C) until analysis. Filtration and freezing occurred within 8 hours of sample collection. Samples were frozen for no longer than 3 months. PC was extracted according to Sarada, et al. (1999). Prior to analysis, filters were transferred to a 50 mL polycarbonate centrifuge tube and suspended in 15 mL of 50 mM phosphate buffer. Filters were initially broken up using a stainless steel spatula and exposed to two grind and centrifuge cycles. Samples were centrifuged at 5 °C, 27,200 x g for 25 minutes using a Beckman J2 - 21M centrifuge. Extracted samples were analyzed for phycocyanin concentrations fluorometrically using a TD - 700 Fluorometer (Turner Designs, Inc.) equipped with a Cool White Mercury Vapor Lamp and a Phycocyanin Optical Kit (630 nm excitation and 660 nm emission filters) and calibrated using C-phycocyanin from *Spirulina sp*. (Sigma-Aldrich P6161). All steps in the PC extraction process were performed under subdued light conditions. A summary of the PC data can be seen in Table 6.

Table 6- Summary of Measured PC Concentration Data

Reservoir	PC Range µg/L	PC Average µg/L	PC Standard Deviation µg/L	Error Range between Duplicates %	Error Average between Duplicates %	Samples Removed Due to Error >30%
Geist	25.2 - 185.1	95.0	42.8	0 - 21	7	0
Morse	2.2 - 135.1	45.8	41.2	0 - 89	18	6
Eagle Creek	24.1 - 130.0	78.9	25.8	0 - 32	7	3

Image Preprocessing

Georectification

Each swath of AISA imagery of each reservoir was georectified to a 2003 aerial photograph of Marion and Hamilton counties in Indiana with the projection of Universal Transverse Mercator (UTM) Zone 16 North, WGS-1983 Datum. GGCPs, usually man-made

features, were manually selected between the image swaths and the aerial photograph. After a number of GGCPs have been selected, the total root mean square error (RMSE), between the predicted warp and location on the image, for each point is listed. Because of the high spatial resolution of the images, it is not uncommon for the warp to be off by one or two pixels in some locations, 1 - 2 m, therefore the GGCPs were selected until the RMSE within three to four pixels. The number of GGCPs and the average RMSE for each swath are listed in Table 7. The error of Eagle Creek Reservoir is likely to be higher because there were fewer man-made features surrounding the reservoir to choose as GGCPs. Images of the swath coverage for each reservoir can be seen in Figure 8, 9 and 10.

Table 7- Number and RMSE of the GCPs Selected for Each AISA Swath

AISA Swath	Number of GGCPs	RMSE
Geist 1 - 1	54	2.01
Geist 1 - 2	71	2.29
Geist 1 - 3	97	2.89
Geist 1 - 4	69	2.66
Morse 2 - 1	47	3.10
Morse 2 - 2	275	2.24
Morse 2 - 3	232	1.88
Morse 2 - 4	192	1.88
Morse 2 - 5	102	1.28
Eagle Creek 3 - 1	60	3.27
Eagle Creek 3 - 2	51	3.04
Eagle Creek 3 - 3	48	2.95

Figure 8- Swath Coverage of Geist Reservoir

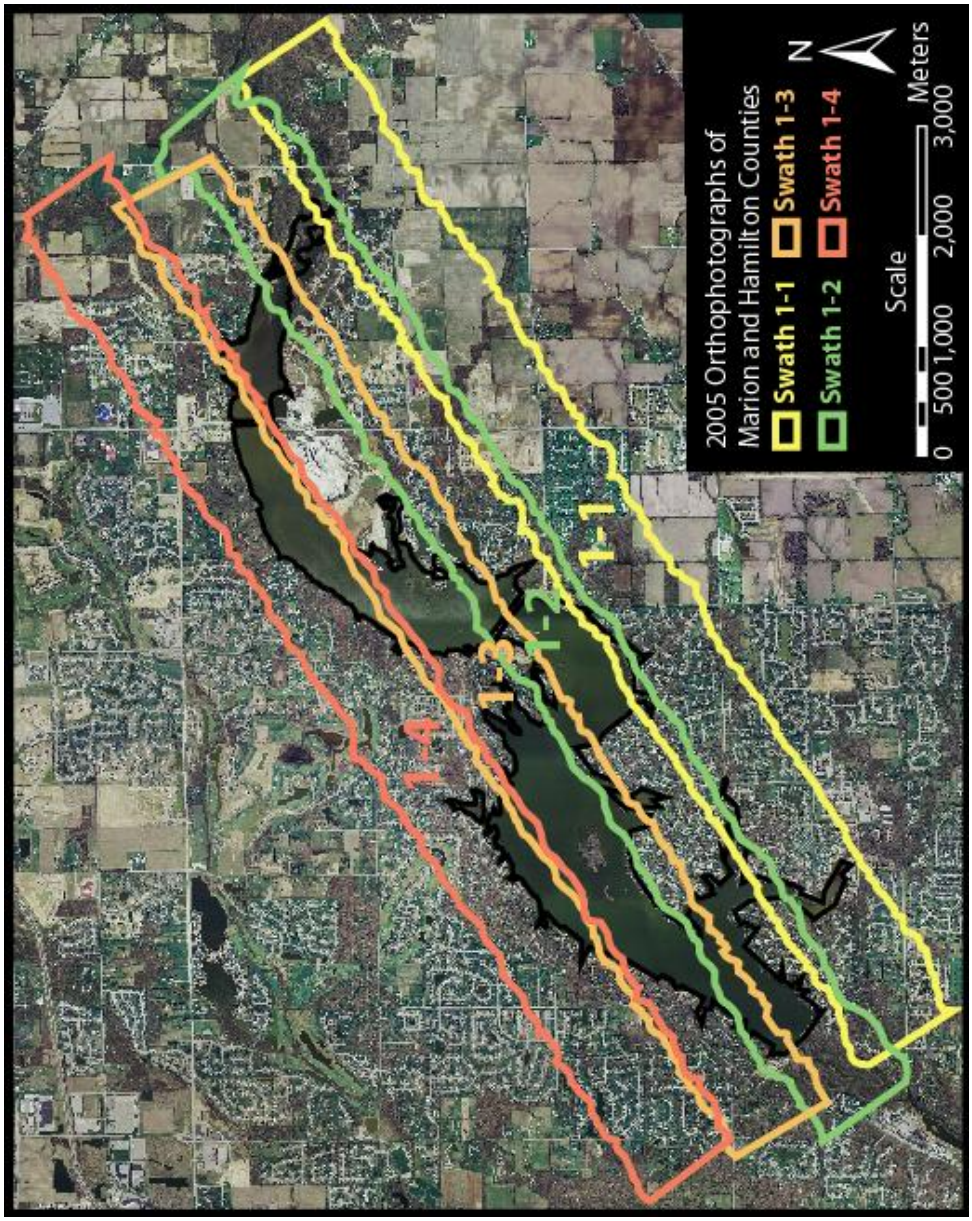

Figure 9- Swath Coverage of Morse Reservoir

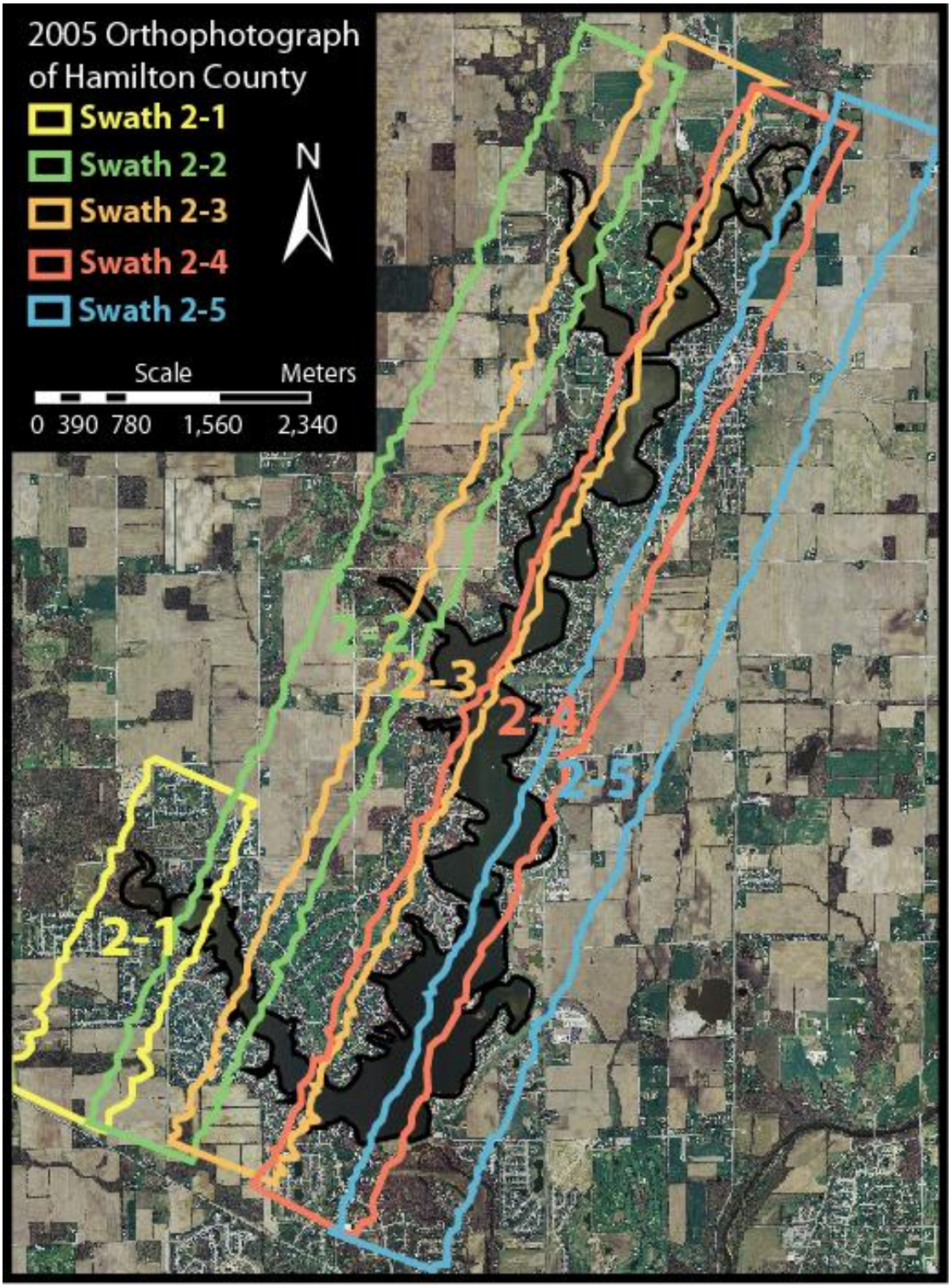

Figure 10- Swath Coverage of Eagle Creek Reservoir

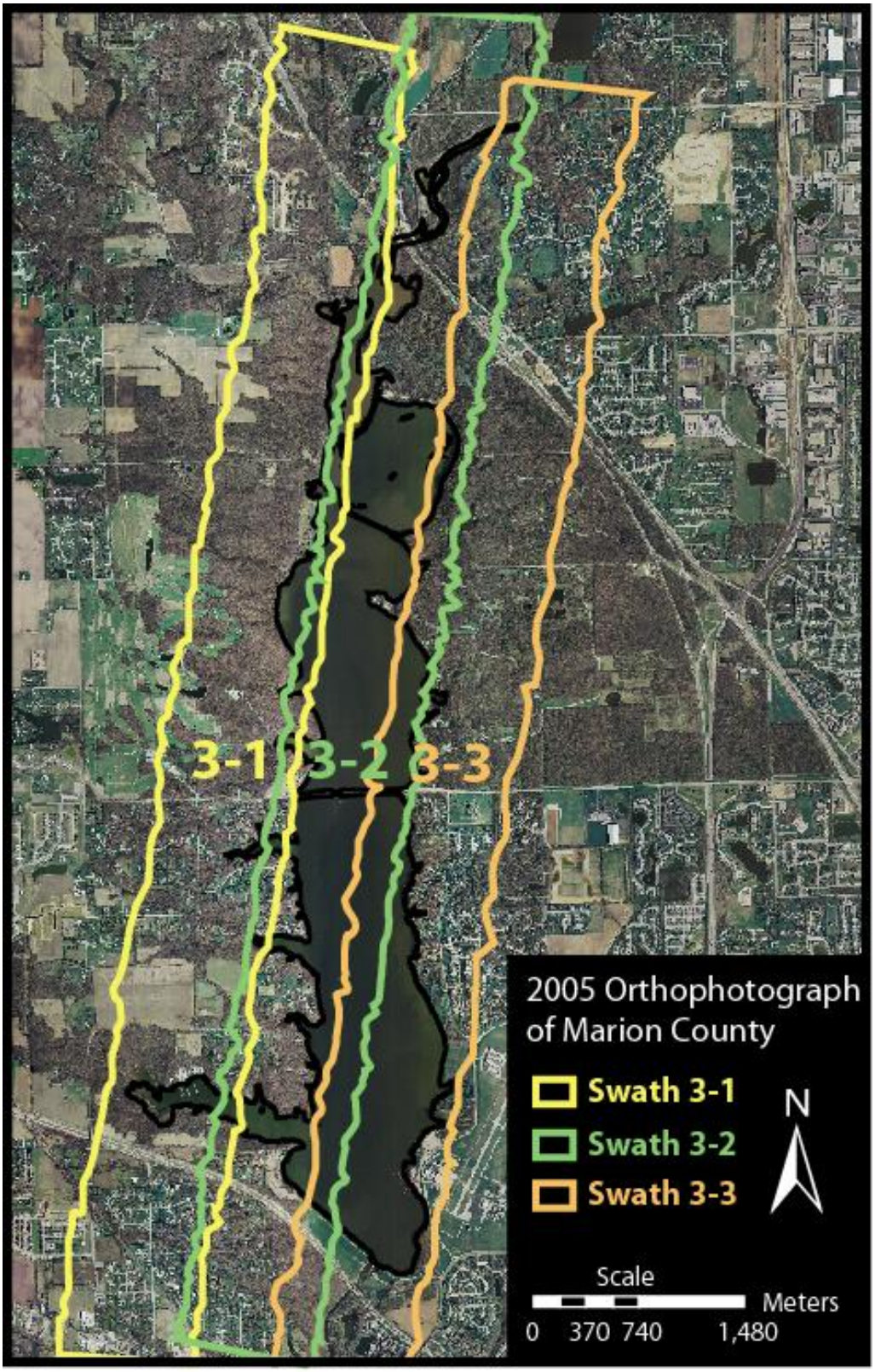

Normalization

Empirical Line Calibration technique in ENVI was used for image normalization. Empirical Line Calibration is a linear regression technique which forces spectral data to match a selected reference. While various techniques are available for the selection of radiometric control points, in this study, random pixels were chosen by the user following the suggestions of Heo & FitzHugh (2000). Points were selected from the overlapping area of both swaths and the linear regression was calculated and applied to each band of the data according to equation 2.4. Several issues were considered during the normalization process, including cross-track illumination, the selection of the radiometric control point pixels and the selection of the reference swath.

Cross-track Illumination

Due to significant illumination differences across the length of each swath, one linear regression per swath was not able to account for all of the radiometric differences between the reference and normalized swath, yielding visible differences between the two swaths. To account for the radiometric differences along the length of the swath, cross-track illumination correction was needed. Unfortunately, the cross-track illumination correction provided by ENVI consistently over compensated for the illumination differences creating results which were visibly erroneous. This prompted the need for the development of a different technique for normalization. In this technique, each swath which was to be normalized to the reference was split into sections that corresponded to changes in illumination (Table 8). Each piece was then normalized, using the Empirical Line Calibration function, separately to the reference swath to account for radiometric changes. The pieces of the swath were then mosaicked back together, giving an assurance of success when the mosaics matched seamlessly.

Radiometric Control Points

Each piece was normalized to the reference swath with more than 50 radiometric control points (often 100 control points) depending on the size of the piece. There are two ways to calculate the linear regression between the control points depending on when in the process the numbers are averaged; both methods will give the same numbers. Due to the method of point selection, the average of the pixel differences, R_1 and R_2 of Equation 2.4, were used to calculate the gain and offset for the image section rather than calculating all of the linear regression equations and then taking the average gain and offset. This method was found to be superior because the processing time was reduced.

Reference Swath

For each reservoir, the central swath with the greatest amount of water pixels in the image for each reservoir was chosen as the reference swath to reduce error that can occur as normalization is propagated across scenes (Olthof, et al., 2005). See Table 8 for the reference and normalized swaths.

Table 8- AISA Normalization Information

AISA Swath	Sections Swath was split into	Swath Normalized to
Geist 1 - 1	2	1 - 2 (after 1-2 was normalized)
Geist 1 - 2	3	1 - 3
Geist 1 - 3	Reference Swath	-
Geist 1 - 4	6	1 - 3
Morse 2 - 1	Not split	2 - 2 (after 2 - 2 was normalized)
Morse 2 - 2	3	2 - 3 (after 2 - 3 was normalized)
Morse 2 - 3	6	2 - 4
Morse 2 - 4	Reference Swath	-
Morse 2 - 5	4	2 - 4
Eagle Creek 3 - 1	4	3 - 2
Eagle Creek 3 - 2	Reference Swath	-
Eagle Creek 3 - 3	3	3 - 2

Comparison of Normalization Data

To show the success of the normalization, and the need for normalization between swaths, a pre- and post-normalization comparison is shown for each reservoir swath in

Table 9. The comparisons were made by selecting 10 random points within the overlapping area of the swaths for three bands of the image; the average value is reported in the table. The bands chosen for the comparison were those that were most often used in algorithm development (R_{628}, R_{675} and R_{704}). It can be seen that, on average, the error between the swaths is reduced to a value of at least 22 data numbers.

Table 9- AISA Data Normalization Statistics

AISA Swath	Swath Normalized to	Average Radiometric Error Between Swaths					
		628 nm		675 nm		704 nm	
		Pre	Post	Pre	Post	Pre	Post
Geist 1 - 1	1 - 2	90.7	5.4	85.6	5.9	98.0	5.7
Geist 1 - 2	1 - 3	82.9	5.6	57.0	6.0	70.8	10.2
Geist 1 - 3	-	-	-	-	-	-	-
Geist 1 - 4	1 - 3	116.7	7.2	94.8	5.9	112.3	11.1
Morse 1 - 1	1 - 2	142.9	18.1	113.3	19.5	205.5	19.3
Morse 1 - 2	1 - 3	147.3	18.6	123.6	21.9	159.1	20.8
Morse 1 - 3	1 - 4	35.0	7.0	30.9	9.1	44.9	13.6
Morse 1 - 4	-	-	-	-	-	-	-
Morse 1 - 5	1 - 4	116.8	10.4	96.3	11.3	104.2	13.6
Eagle Creek 1 - 1	1 - 2	116.7	7.2	94.8	5.9	122.3	11.1
Eagle Creek 1 - 2	-	-	-	-	-	-	-
Eagle Creek 1 - 3	1 - 2	82.9	5.6	57.0	6.0	70.8	10.2

Mosaicking

The swaths were mosaicked together using ENVI 4.2 mosaicking tool. In the overlapping area between each swath, a cutline was drawn for the mosaic. A cutline allows the user to define the mosaic edge of the image, instead of using the image edge (Figure 11).

Figure 11- Schematic of ENVI Cutline Function

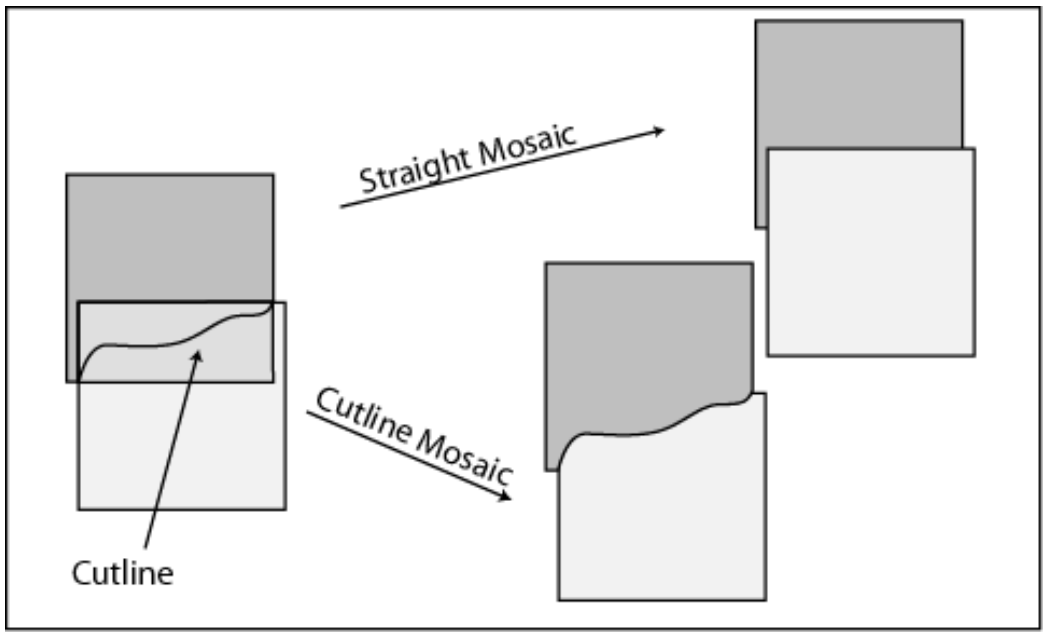

The cutlines were drawn in the locations which minimized the difference between the swaths. Because the radiometric values between the swaths of each reservoir were similar, minimal feathering distances were needed to create a seamless mosaic.

Atmospheric Calibration

Empirical Line Calibration

After mosaicking, both Geist and Morse Reservoirs were calibrated to remove atmospheric effects. This was done by using Empirical Line Calibration method in ENVI where the field spectra from all sampling sites were used as the reference radiometric control points and AISA radiance spectra as the control points to be calibrated. By doing this, the AISA image is converted from radiance into reflectance and the affects of the atmosphere between the sensor and the ground are ideally removed, but most likely significantly minimized.

FLAASH

Because field reflectance spectra were not available for Eagle Creek Reservoir a different method of atmospheric correction was needed. One such atmospheric correction technique is the Fast Line-of-sight Atmospheric Analysis of Spectral Hypercubes (FLAASH) module. FLAASH incorporates the MODTRAN4 radiation transfer code for atmospheric correction:

$$L = A*\rho/(1-\rho_e S)+B*\rho_e/(1-\rho_e S) +L_a \quad (2.6)$$

Where L is the at sensor radiance, ρ accounts for surface pixel reflectance, ρ_e is an average surface pixel reflectance for the surrounding pixels, S is a parameter for the spherical albedo of the atmosphere, L_a is the radiance backscattered by the atmosphere and "A" and "B" are coefficients that depend upon atmospheric and viewing geometry (Adler-Golend, et al., 1999). While FLAASH was the preferred method to use, it was not appropriate because of the small spectral scale and spectral signatures needed to identify cyanobacteria in this study. It seems that FLAASH can correctly account for atmospheric effects and extract a spectral signature that is similar to ground truth data over the entire spectral range from 400 nm to 2,000 nm (Adler-Golend, et al., 1999). However, when hyperspectral data is needed on spectral range of only from 400 nm to 800 nm the atmospheric correction cannot account for all of the variables, and the spectral signatures achieved with FLAASH appear very different from the water spectra retrieved from the water pixels in the other reservoirs, to the point where commonly used algorithms could not be utilized. Furthermore, FLAASH seems to have been developed for the calibration of satellite and airborne data which were not dominated by water pixels, aiding in the extraction of coherent spectra from land surfaces not water surfaces. Additionally, because of the spectral range the data was collected over, the absorption due to water vapor could only be

calculated from the image from the spectral range of 770 - 870 nm, while the 1050 - 1210 nm range is recommended to more accurately solve the radiative transfer equations (ITT Visual Information Services, 2006).

Eagle Creek Calibration

Because of the inadequacy of the FLAASH application for this study to calibrate the imagery of Eagle Creek Reservoir, the gain and offset values of the calibrations for Geist were used for each band. While it is not an ideal way to calibrate the imagery, it was decided that this was acceptable based on the similarities between the reservoirs. Because of the small difference between the acquisition times, similar elevations and proximity of the reservoirs it can reasonably be assumed that the sun angle and atmospheric conditions are similar between the reservoirs. Unfortunately this assumption cannot be verified with the current data.

Masking

To generate the maps of Chl a and PC, all of the land pixels were masked out. Masking was done to aid the user in visualizing the pigment concentration trends within the reservoir, eliminating extraneous data. This was accomplished by using a band threshold to identify and eliminate all but the water pixels. Basically, a band threshold tells the computer to look at the spectral signatures of all of the pixels in the image and select the ones that conform to certain criteria decided by the user. To facilitate the threshold in removing land pixels with similar spectral signatures to water pixels (i.e. shadowed pixels) and other water pixels outside the reservoir (i.e. pools and retention ponds), an outline of the reservoir was combined with the band threshold. The outline and band thresholding were combined in such a way that the reservoir's outlines were almost exclusively decided by the spectral signatures of the pixel. The number of water surface pixels in each

reservoir, which also includes some of the pixels from the inflow creeks, can be seen in Table 10.

Table 10- Number of Water Pixels Retrieved from AISA Data for Each Reservoir

Reservoir	Number of Water Pixels
Geist	93,599,169
Morse	84,872,190
Eagle Creek	5,536,020

7.0 Algorithm Analysis

From each atmospherically calibrated image, the reflectance, averaged over a 3 x 3 pixel area, was extracted at each sample location and used for algorithm assessment. An average of the pixels around each sample site was extracted to account for any shift in the boat position during sampling and any error in GPS measurement. Estimated pigment concentrations were extracted from the AISA imagery by using 1) algorithms developed to estimate Chl a and PC from airborne data and 2) algorithms developed for hand held spectroradiometers data in eutrophic-oligotrophic lakes to estimate Chl a and PC. The calculated water quality variables were acquired by applying the following regression equations to each algorithm:

2.7	$C_i = a * x + b$
2.8	$C_i = a * \ln x + b$
2.9	$C_i = a * x^2 + b * x + d$
3.0	$C_i = a * e^{b*x}$
3.1	$C_i = a * x^b$

Where C_i is the concentration of parameter "i", "x" is an independent variable (single band or band combination) and "a", "b", and "d" are empirical parameters. The log transformation of both variables was also tried prior to using each equation to see if the algorithm would predict better. In cases where the published algorithms used specific band wavelengths, the closest band wavelength available for the AISA data was substituted.

Algorithm Success

The success of the pigment estimation algorithms are generally measured on two parameters; coefficient of determination (R^2) between reflectance and pigment concentration and the root mean squared error (RMSE) of the prediction. In some cases, only the R^2 is reported for the models ability to predict pigment concentration (Dekker, et al., 1992; Gitelson, 1992; Millie, et al., 1992; Mittenzwey, et al., 1992; Gitelson, 1993; Yacobi,

et al., 1995; Rundquist, et al., 1996; Fraser, 1998; Kuster, et al., 1998; Schalles, et al., 1998; Gons, 1999; Schalles & Yacobi, 2000; Vincent, et al., 2004; Simis, et al., 2005; Wang, et al., 2005), but often both the R^2 and RMSE are reported for the algorithms used (Gitelson, et al., 2000; Kallio, et al., 2001; Kallio, et al., 2003; Dall'Olmo, Gitelson, et al., 2005; Giardino, et al., 2005).

Coefficient of Determination

The coefficient of determination, R^2, is a useful statistic to calculate because it gives the proportion of the variation of one variable that is predictable from the other variable. The total variation of a variable is made up of two parts, the part that can be explained by the regression equation and the part that cannot be explained by the regression equation. The ratio of the explained variation to the total variation is the coefficient of determination. Another way to think of it is that R^2 indicates how well the regression line explains the variation in the dependent variable. If the regression line passes exactly through every point on the scatter plot, it would be able to explain all of the variation in the data set. Thus, R^2 allows us to determine how certain one can be in making predictions from a certain model. An R^2 value of 0 indicates that the variation in the data is poorly explained by the independent variable. A value closer to 1 indicates that one variable can be accurately predicted as a function of the other. The coefficient of determination is calculated from the following equations (Equation 3.2, Equation 3.3, Equation 3.4 and Equation 3.5).

$$R^2 = \frac{SS_{explained}}{SS_{Total}} = 1 - \frac{SS_{Residual}}{SS_{Total}} \quad (3.2)$$

Where SS_{Total}, $SS_{explained}$ and $SS_{residual}$ are,

$$SS_{Total} = \sum_i (y_i - \bar{y})^2 \quad (3.3)$$

$$SS_{explained} = \sum_i (\hat{y}_i - \bar{y})^2 \quad (3.4)$$

$$SS_{residual} = \sum_i (y_i - \hat{y}_i)^2 \quad (3.5)$$

and y_i is the value of observation "i", $\hat{y}_i$ is the predicted observation and $\bar{y}$ is the mean of the observations.

Root Mean Squared Error

The RMSE of a prediction is the average of the error between the actual and predicted values of a model. This error is caused because of the inadequacy of the model to account for all of the variability of the data. The RMSE is calculated by the equation:

$$RMSE = \sqrt{\frac{1}{n}\sum_{i=1}^{n}(y_i - \hat{y}_i)^2} \quad (3.6)$$

where y_i is the value of observation "i", $\hat{y}_i$ is the predicted observation and "n" is the *number of observations in the data set.*

Level of Significance

In hypothesis testing, the p-value is a measure of consistency, indicating the probability of achieving a result as extreme as the given data. Generally, one rejects the null hypothesis if the p-value is smaller than or equal to the significance level. The significance level of this study was set at 0.05.

Geist Reservoir

The AISA spectra extracted for each sample location can be seen in Figure 12. Due to a high error between duplicates, 39%, sample GR - 238 was not used in Chl a algorithm analysis. Additionally, due to a large studentized residual, the deviation from the regression lines, samples GR - 247 and GR - 248 were eliminated from Chl a algorithm development, leaving 24 samples. None of the PC samples from Geist Reservoir were eliminated from the algorithm development, leaving 27 samples for the analysis. The results of the analysis between all of the algorithms and pigment concentrations can be seen in Table 11 and 12, with the best algorithm highlighted. The correlation between pigment concentration and

reflectance with the highest R^2 and a comparison between the concentrations predicted by the best algorithm and measured concentration can be seen in Figure 12, 13 and 14. A summary of all of the Geist Reservoir Parameters can be seen in the Appendix.

Figure 12- AISA Reflectance Spectra for Geist Reservoir

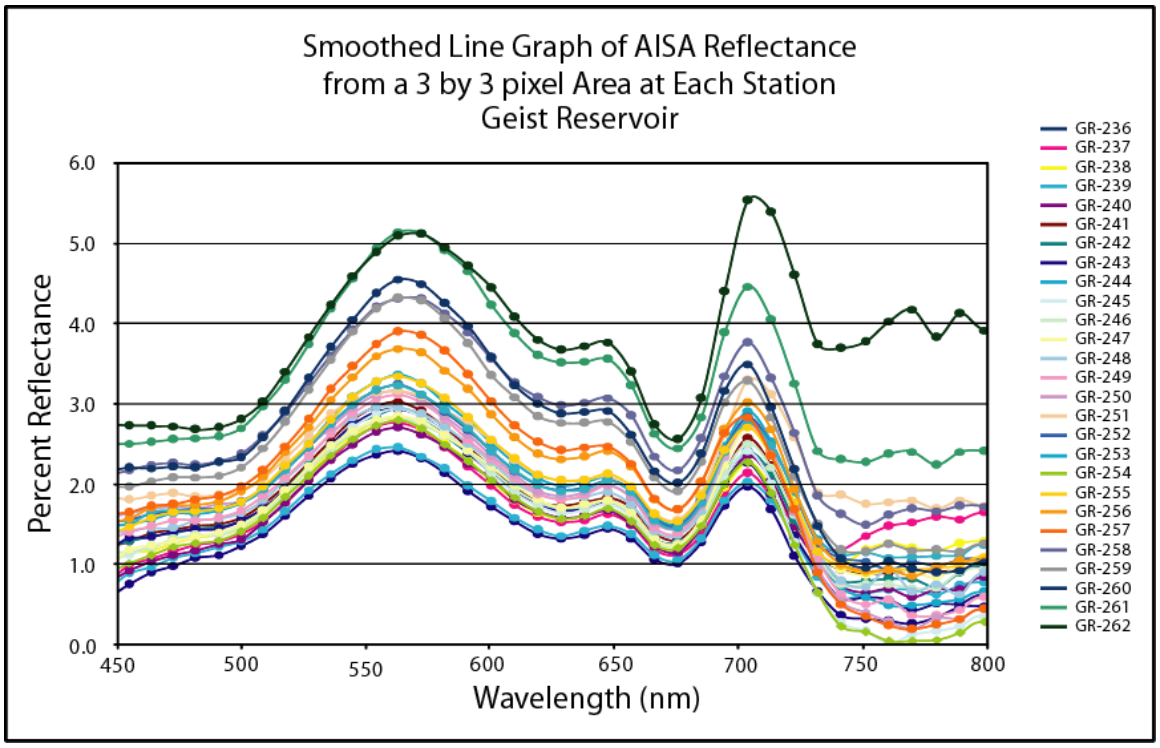

Chlorophyll a

Table 11- Summary of Geist Reservoir Chl a Algorithm Performance

Variable	Band or Band Combination	R^2	RMSE µg/L	Equation Number	Reference
Chl a	R_{704}/R_{675}	0.643	16.16	2.9*	e.g. Dekker, 1993; Gitelson, et al., 2000
Chl a	R_{704}/R_{666}	0.613	20.49	2.9*	e.g. Dekker, 1993; Gitelson, et al., 2000
Chl a	R_{713}/R_{675}	0.661	16.29	3.0	e.g. Dekker, 1993; Gitelson, et al., 2000
Chl a	R_{713}/R_{666}	0.648	16.53	2.9*	e.g. Dekker, 1993; Gitelson, et al., 2000
Chl a	Height of R_{704} above a base line 675 nm to 751 nm.	0.201	21.75	2.9*	e.g. Gitelson, et al., 2000
Chl a	Height of R_{713} above a base line 675 nm to 751 nm.	0.107	23.22	2.9*	e.g. Gitelson, et al., 2000
Chl a	Area above the base line between 675 nm and 751 nm.	0.277	20.77	2.9*	e.g. Gitelson, et al., 2000
Chl a	Area above the base line between 666 nm and 751 nm.	0.262	20.99	2.9	e.g. Gitelson, et al., 2000
Chl a	$R_{699 - 705}/R_{670 - 677}$	0.613	17.26	2.9*	Kallio, et al., 2001
Chl a	$R_{698 - 716}/R_{671 - 684}$	0.624	17.87	2.9*	Dekker, et al., 1993
Chl a	R_{713}/R_{647}	0.712	14.15	3.1	Zimba, et al., 2005
Chl a	$R_{740}/(R_{647} - R_{710})$	0.601	21.84	2.7	Zimba, et al., 2005

*** Indicates the data were log transformed**

Highlighted row indicates the best algorithm based on R^2

Figure 13- Geist Reservoir Chl a Algorithm Statistics

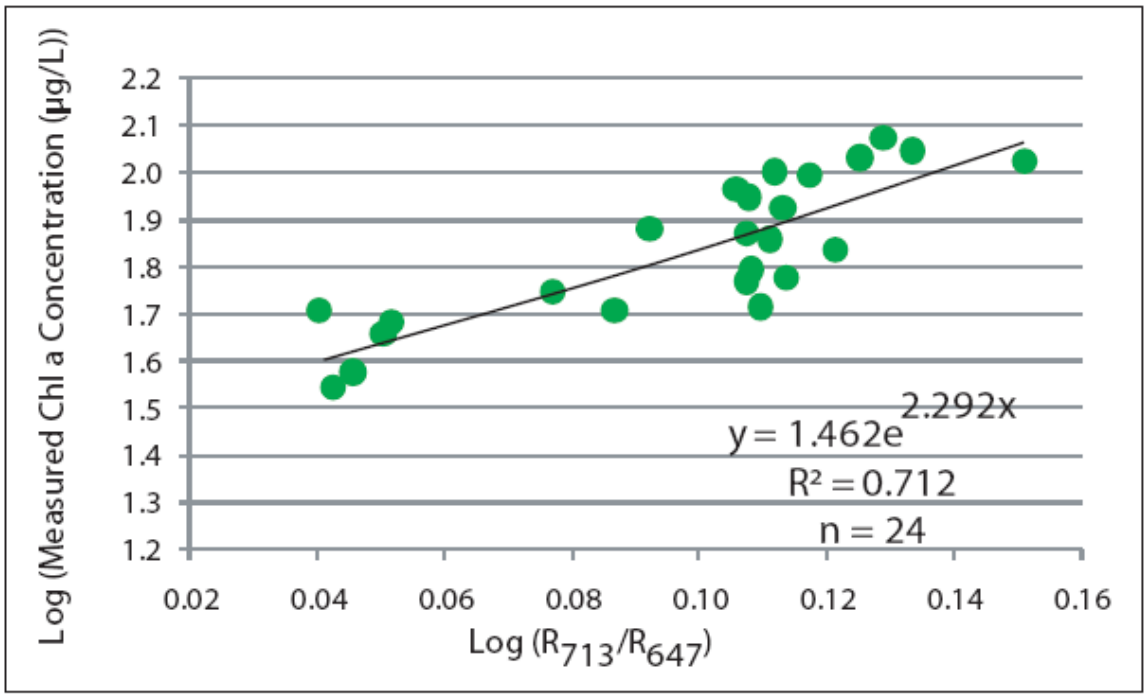

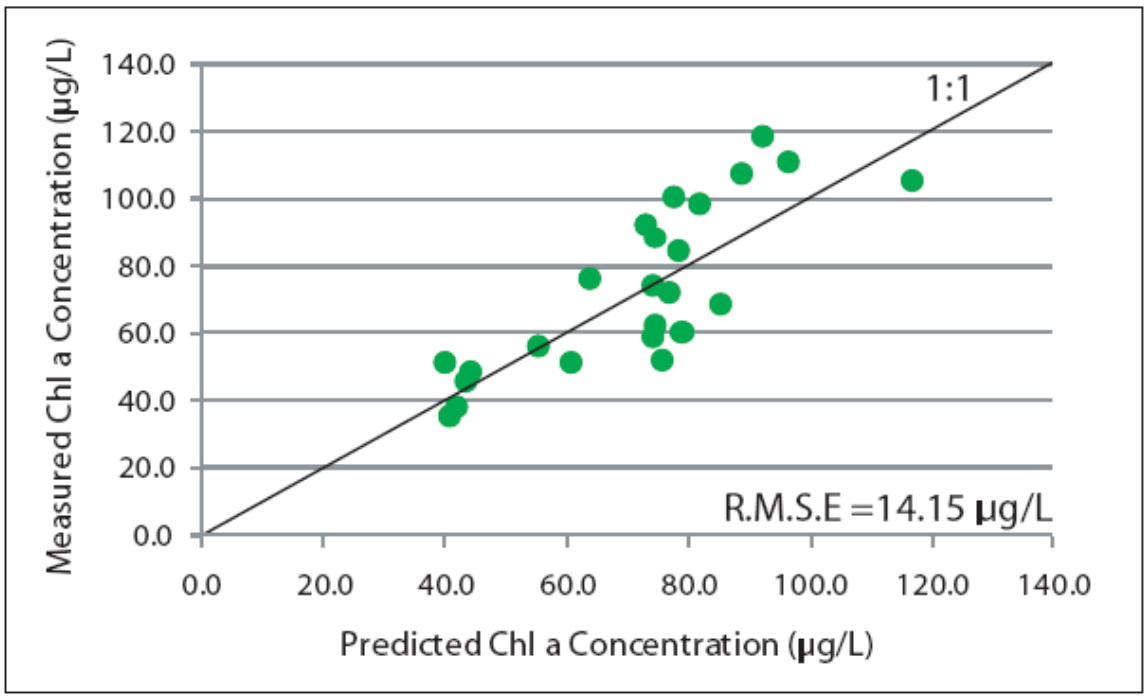

Phycocyanin

Table 12- Summary of Geist Reservoir PC Algorithm Performance

Variable	Band or Band Combination	R^2	RMSE µg/L	Equation Number	Reference
PC	R_{647}/R_{619}	0.199	39.91	2.8*	Schalles & Yacobi, 2000
PC	R_{647}/R_{628}	0.280	38.14	2.8*	Schalles & Yacobi, 2000
PC	R_{704}/R_{628}	0.521	30.98	2.9*	Adapted from Simis, et al., 2005
PC	R_{704}/R_{619}	0.514	31.24	2.9*	Adapted from Simis, et al., 2005
PC	R_{628}	0.796	26.34	3.1*	Adapted from Gitelson, et al., 1995
PC	R_{619}	0.804	26.10	3.1*	Adapted from Gitelson, et al., 1995
PC	$R_{600 - 628}$	0.805	25.25	3.1*	Millie, et al., 1992
PC	$0.5*(R_{591 - 609} + R_{647 - 656})-R_{619 - 638}$	0.735	25.993	3.1*	Dekker, 1993

*** Indicates the data were log transformed**
Highlighted row indicates the best algorithm based on R^2

Figure 14- Geist Reservoir PC Algorithm Statistics

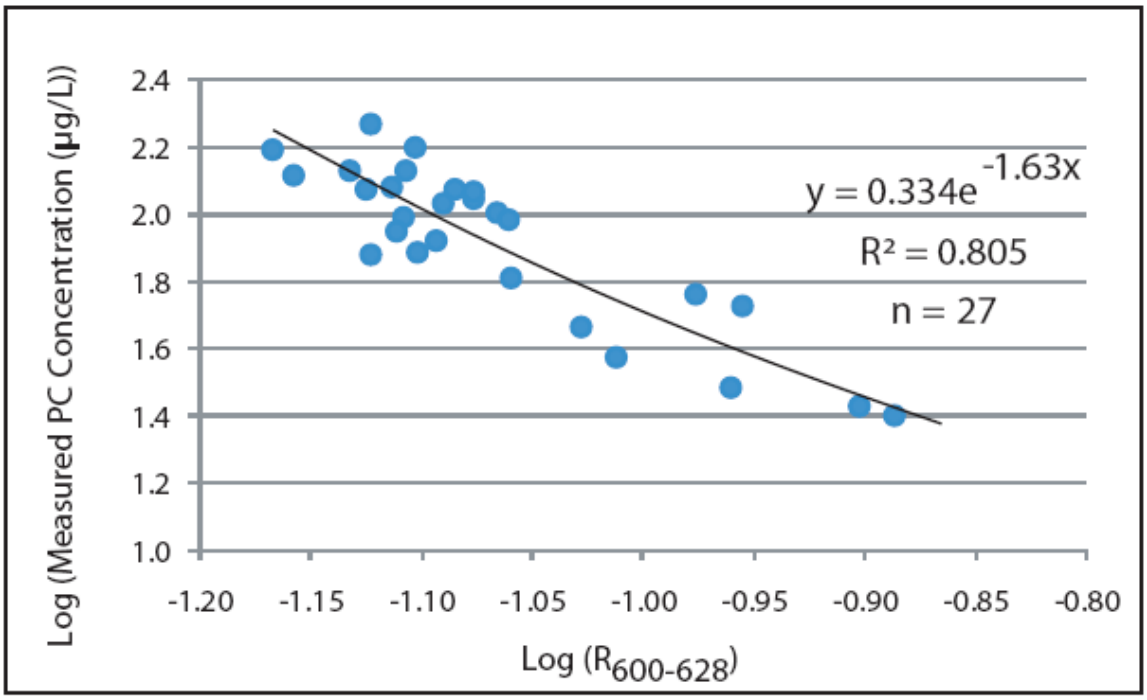

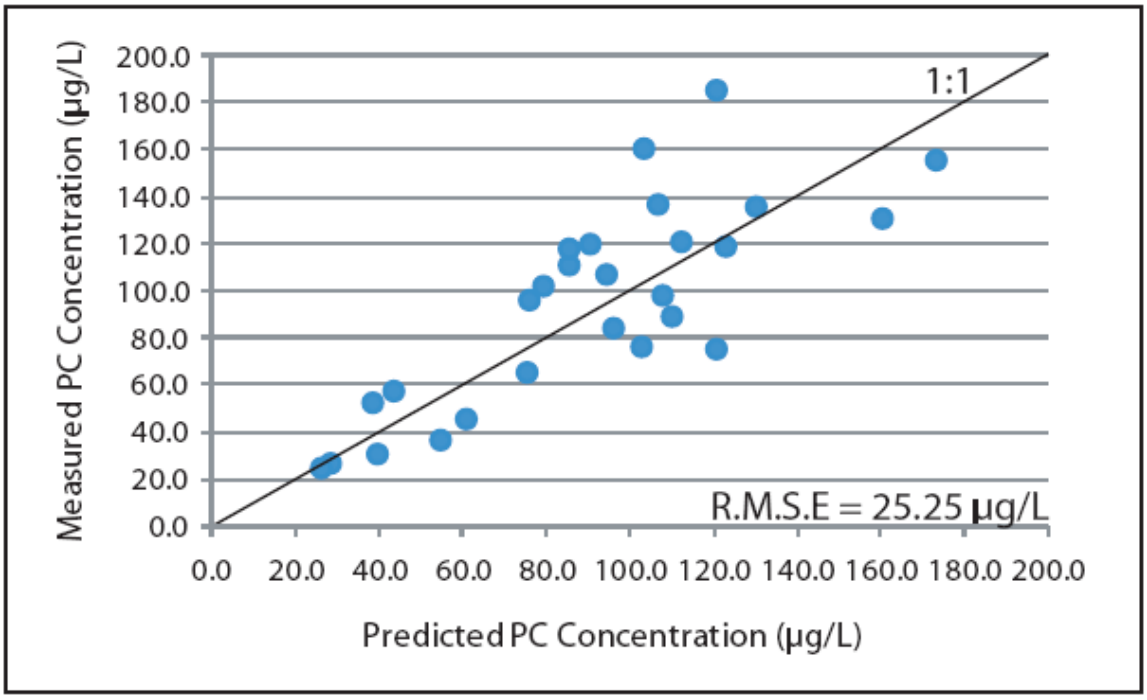

Morse Reservoir

An image of the spectra extracted from each sample site on Morse Reservoir can be seen in Figure 15. Only one sample site was eliminated from the Chl a algorithm development due to the error between the duplicates of greater than 30% (MR - 283), leaving 27 samples. Six sites were excluded from PC algorithm development, three sample locations (MR - 272, MR - 277 and MR - 289) due to missing samples and two other locations (MR - 282, MR - 297 and MR - 298) due to high error (> 30%) between the duplicates; leaving 23 samples. The results of the analysis between all of the algorithms and pigment concentrations can be seen in Table 13 and 14, with the best algorithm highlighted. The correlation between pigment concentration and reflectance with the highest R^2 and a comparison between the concentrations predicted by the best algorithm and measured concentration can be seen in Figure 16 and 17. A summary of all of the Morse Reservoir Parameters can be seen in the Appendix.

Figure 15- AISA Reflectance Spectra from Morse Reservoir

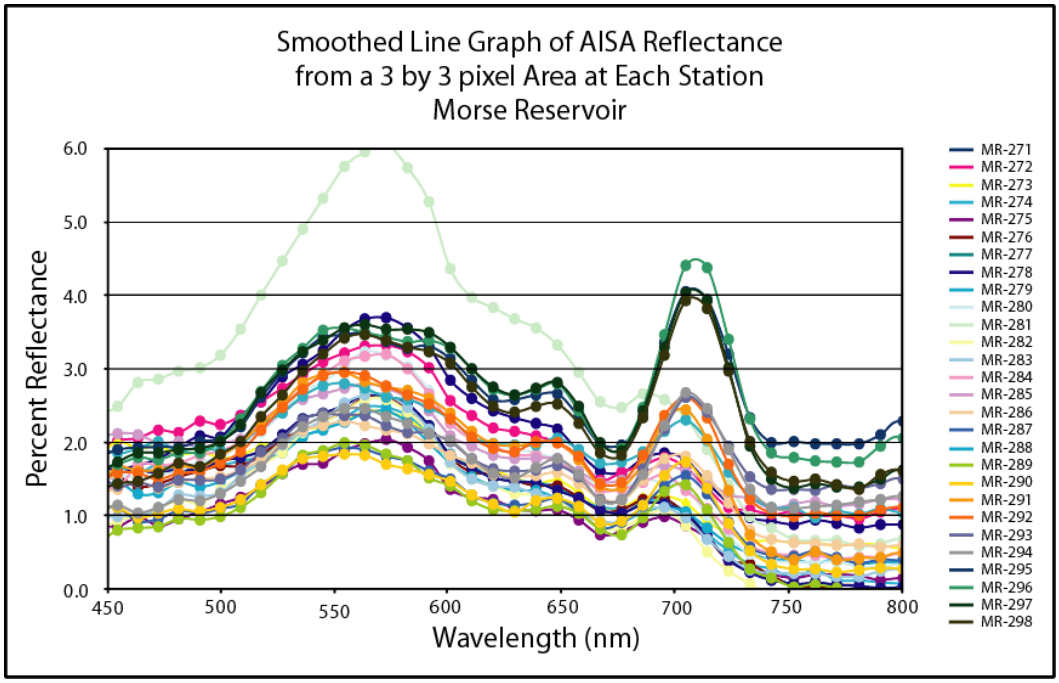

Chlorophyll a

Table 13- Summary of Morse Reservoir Chl a Algorithm Performance

Variable	Band or Band Combination	R^2	RMSE µg/L	Equation Number	Reference
Chl a	R_{704}/R_{675}	0.852	20.68	2.9*	e.g. Dekker, 1993; Gitelson, et al., 2000
Chl a	R_{704}/R_{666}	0.831	23.12	2.9*	e.g. Dekker, 1993; Gitelson, et al., 2000
Chl a	R_{713}/R_{675}	0.882	18.10	2.9*	e.g. Dekker, 1993; Gitelson, et al., 2000
Chl a	R_{713}/R_{666}	0.804	20.03	2.9*	e.g. Dekker, 1993; Gitelson, et al., 2000
Chl a	Height of R_{704} above a base line 675 nm to 751 nm.	0.890	14.56	2.9	e.g. Gitelson, et al., 2000
Chl a	Height of R_{704} above a base line 666 nm to 751 nm.	0.895	14.25	2.9	e.g. Gitelson, et al., 2000
Chl a	Area above the base line between 675 nm and 751 nm.	0.668	25.23	2.9	e.g. Gitelson, et al., 2000
Chl a	Area above the base line between 666 nm and 751 nm.	0.566	27.42	2.9	e.g. Gitelson, et al., 2000
Chl a	$R_{699 - 705}/R_{670 - 677}$	0.824	22.78	2.9*	Kallio, et al., 2001
Chl a	$R_{698 - 716}/R_{671 - 684}$	0.882	18.84	2.9	Dekker, et al., 1993
Chl a	R_{714}/R_{647}	0.884	19.03	2.9*	Zimba, et al., 2005
Chl a	$R_{704}/(R_{647} - R_{710})$	0.110	38.75	2.9	Zimba, et al., 2005

*** Indicates the data were log transformed**

Highlighted row indicates the best algorithm based on R^2

Figure 16- Morse Reservoir Chl a Algorithm Statistics

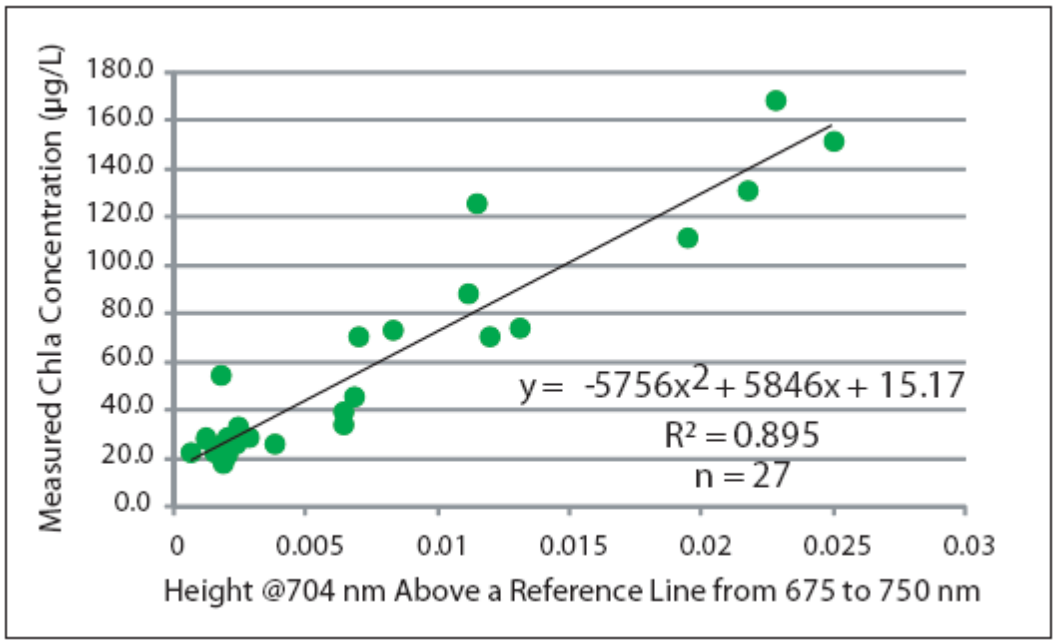

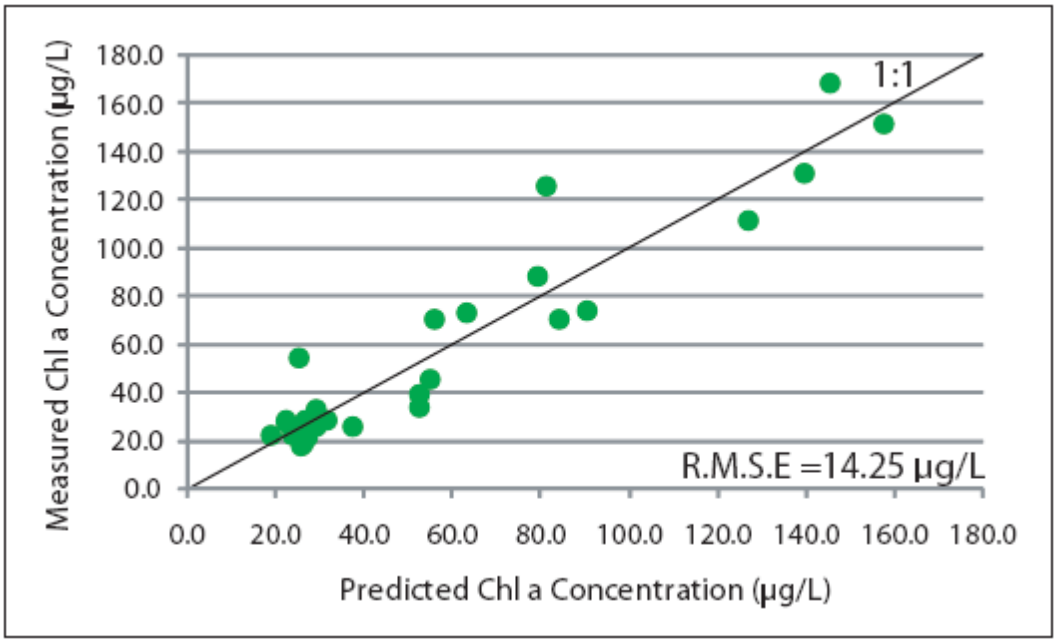

Phycocyanin

Table 14- Summary of Morse Reservoir PC Algorithm Performance

Variable	Band or Band Combination	R^2	RMSE µg/L	Equation Number	Reference
PC	R_{647}/R_{619}	0.713	22.87	2.9*	Schalles & Yacobi, 2000
PC	R_{647}/R_{628}	0.501	59.00	2.9*	Schalles & Yacobi, 2000
PC	R_{704}/R_{628}	0.830	17.41	2.9	Adapted from Simis, et al., 2005
PC	R_{704}/R_{619}	0.878	15.64	2.9	Adapted from Simis, et al., 2005
PC	R_{628}	0.103	38.41	2.9	Adapted from Gitelson, et al., 1995
PC	R_{619}	0.075	165.52	2.9	Adapted from Gitelson, et al., 1995
PC	$R_{600 - 628}$	0.087	405.47	3.1	Millie, et al., 1992
PC	$.5*(R_{591 - 609} + R_{647 - 656})-R_{619 - 638}$	0.132	37.76	2.9	Dekker, 1993

*** Indicates the data were log transformed**
Highlighted row indicates the best algorithm based on R^2

Figure 17- Morse Reservoir PC Algorithm Statistics

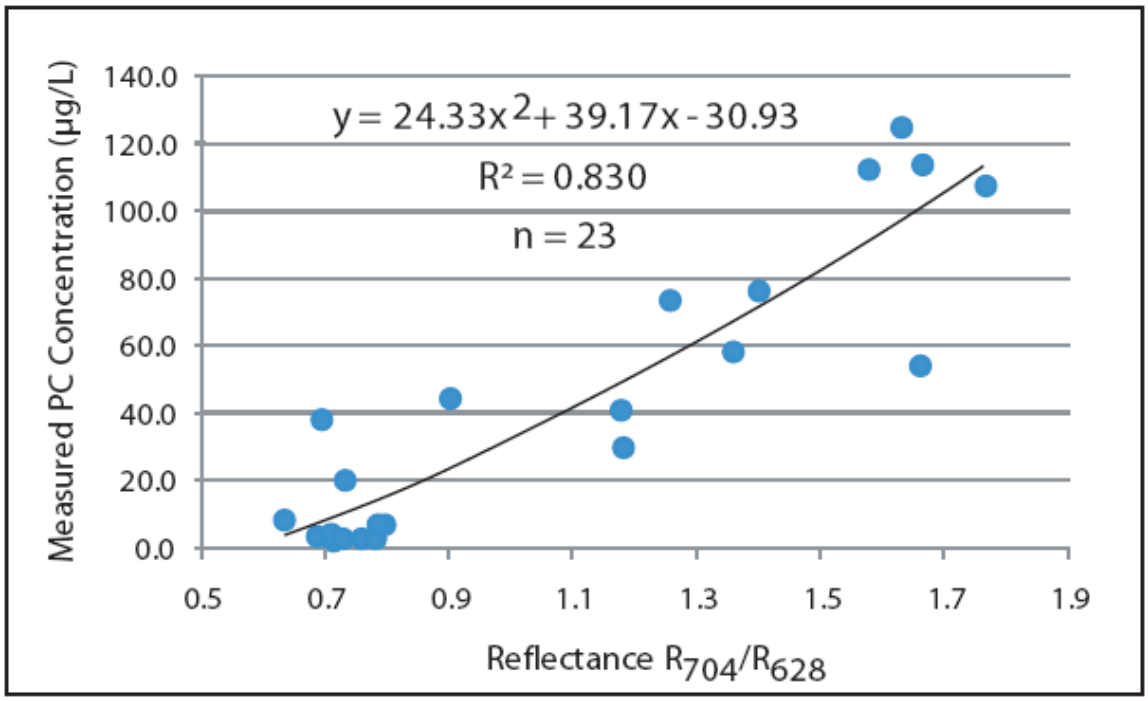

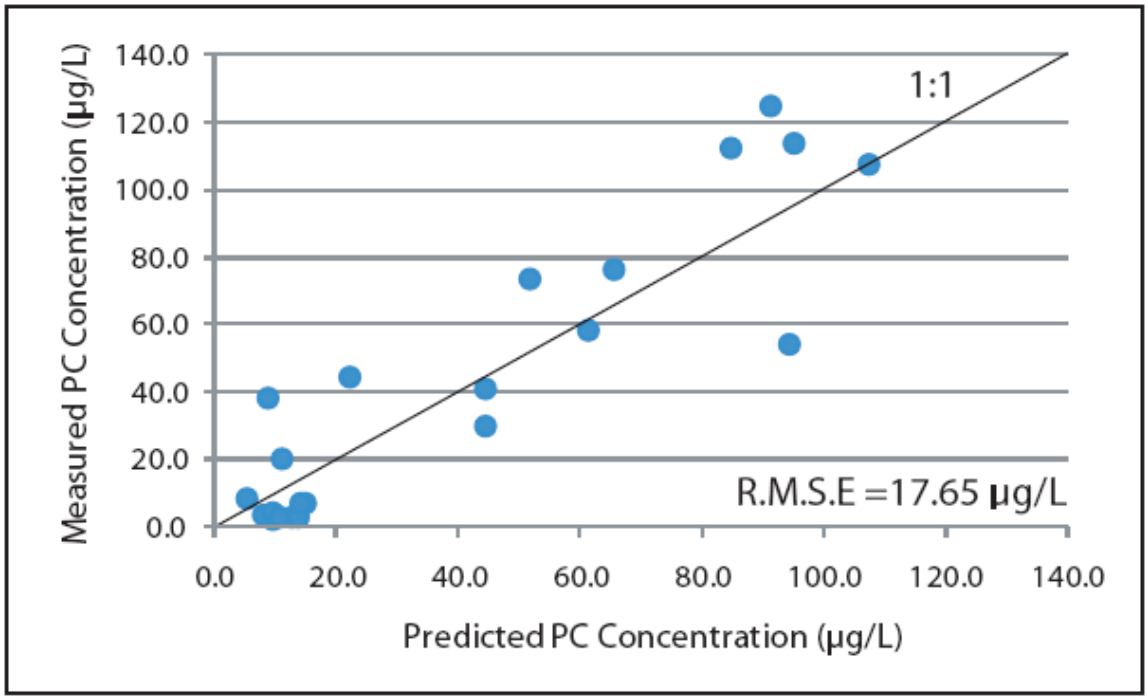

Eagle Creek Reservoir

The AISA spectra extracted for each sample location can be seen in Figure 18. One sample was eliminated from Chl a algorithm development due to an error of 67%, ECR - 208. Three sample locations were eliminated from PC algorithm development due to an error above 30% (ECR - 209, ECR - 216 and ECR - 277). The two best spectral ratios for pigment prediction were used for pigment prediction because spectral ratios, by nature, can account for uniform variation in spectral data (Dekker, et al., 1992). Since there was no ground truth data for this reservoir, it was thought that by using spectral ratio algorithms, a more accurate representation of the water quality parameters could be achieved. It should be noted here that for Chl a estimation, a spectral ratio algorithm did not yield the highest R^2; however, for PC estimation it did. The results of the analysis between all of the algorithms and pigment concentrations can be seen in Table 15 and 16, with the best algorithm highlighted (for Chl a, the best algorithm and the best ratio algorithm are highlighted). The correlation between pigment concentration and reflectance algorithm with the highest R^2 and a comparison between the concentrations predicted by the best algorithm and measured concentration can be seen in Figure 19 and 20. A summary of all of the Eagle Creek Reservoir Parameters can be seen in the Appendix.

Figure 18- AISA Reflectance Spectra from Eagle Creek Reservoir

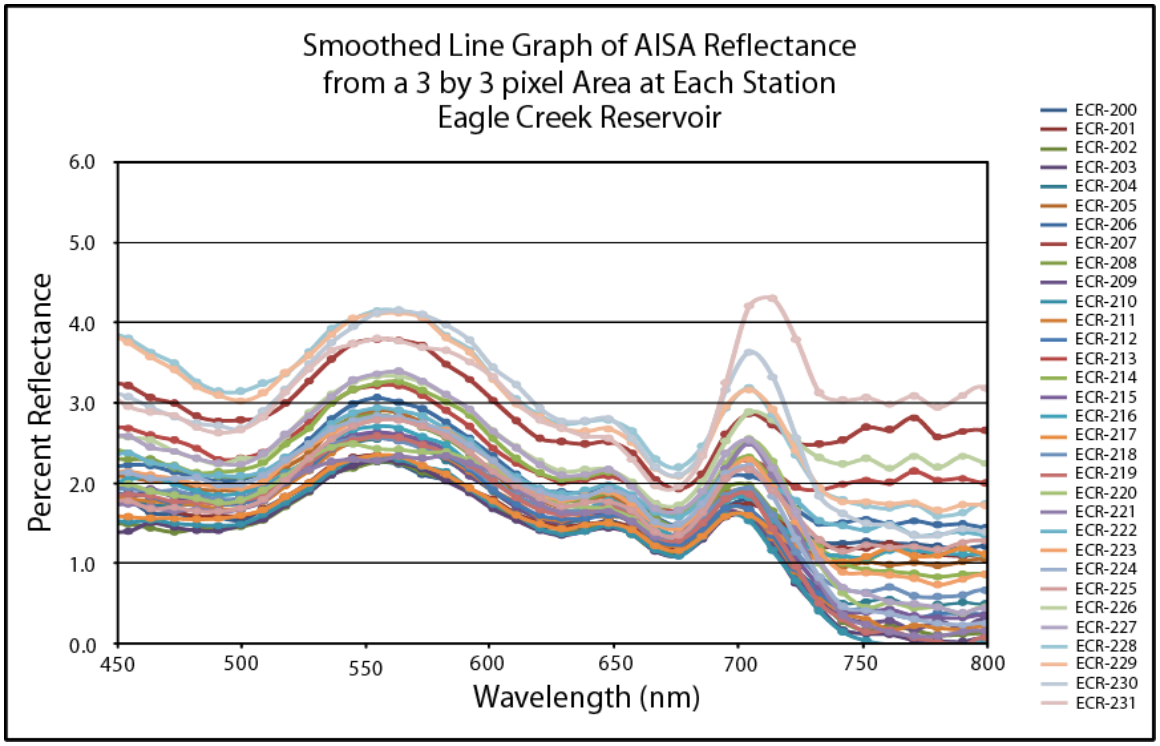

Chlorophyll a

Table 15- Summary of Eagle Creek Reservoir Chl a Algorithm Performance

Variable	Band or Band Combination	R^2	RMSE µg/L	Equation Number	Reference
Chl a	R_{704}/R_{675}	0.201	21.15	2.9	e.g. Dekker, 1993; Gitelson, et al., 2000
Chl a	R_{704}/R_{666}	0.158	21.65	2.9	e.g. Dekker, 1993; Gitelson, et al., 2000
Chl a	R_{713}/R_{675}	0.198	21.19	2.9	e.g. Dekker, 1993; Gitelson, et al., 2000
Chl a	R_{713}/R_{666}	0.162	21.66	2.9	e.g. Dekker, 1993; Gitelson, et al., 2000
Chl a	Height of R_{704} above a base line 675 nm to 751 nm.	0.330	19.64	2.9	e.g. Gitelson, et al., 2000
Chl a	Height of R_{713} above a base line 675 nm to 751 nm.	0.326	19.43	2.9	e.g. Gitelson, et al., 2000
Chl a	Area above the base line between 675 nm and 751 nm.	0.392	18.45	2.9	e.g. Gitelson, et al., 2000
Chl a	Area above the base line between 666 nm and 751 nm.	0.387	18.52	2.9	e.g. Gitelson, et al., 2000
Chl a	$R_{699 - 705}/R_{670 - 677}$	0.172	21.53	2.9	Kallio, et al., 2001
Chl a	$R_{698 - 716}/R_{671 - 684}$	0.229	20.78	2.9	Dekker, et al., 1993
Chl a	R_{714}/R_{647}	0117	22.23	2.9*	Zimba, et al., 2005
Chl a	$R_{704}/(R_{647} - R_{710})$	0.072	22.80	2.9	Zimba, et al., 2005

*** Indicates the data were log transformed**
Highlighted row indicates the best algorithm based on R^2

Figure 19- Eagle Creek Reservoir Chl a Algorithm Statistics

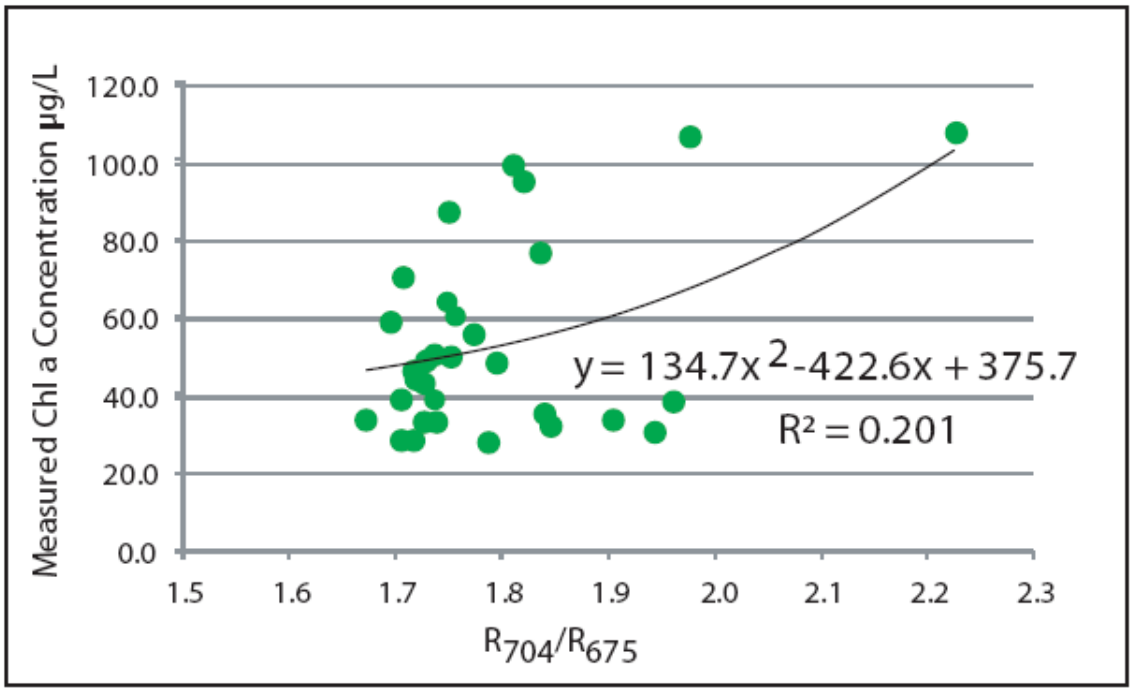

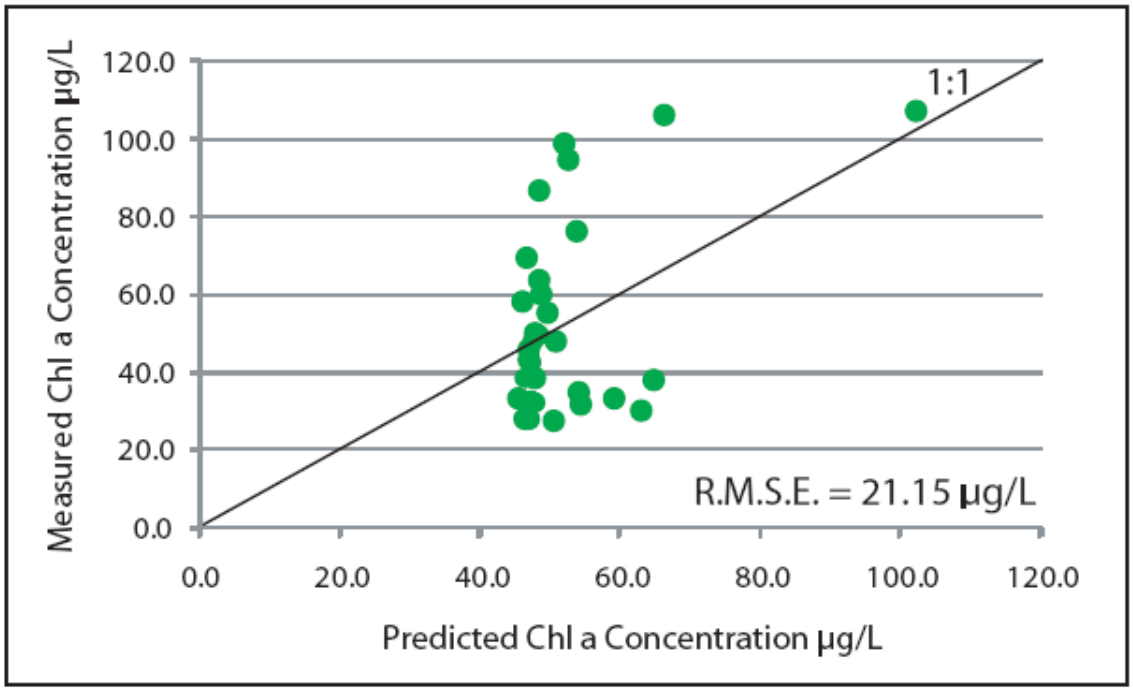

Phycocyanin

Table 16- Summary of Eagle Creek Reservoir PC Algorithm Performance

Variable	Band or Band Combination	R^2	RMSE µg/L	Equation Number	Reference
PC	R_{647}/R_{619}	0.069	24.44	2.9	Schalles & Yacobi, 2000
PC	R_{647}/R_{628}	0.012	25.18	2.7	Schalles & Yacobi, 2000
PC	R_{704}/R_{628}	0.290	34.36	2.9*	Adapted from Simis, et al., 2005
PC	R_{704}/R_{619}	0.316	22.13	2.9	Adapted from Simis, et al., 2005
PC	R_{628}	.122	1100.31	2.9	Adapted from Gitelson, et al., 1995
PC	R_{619}	0.139	1798.36	2.9*	Adapted from Gitelson, et al., 1995
PC	$R_{600 - 628}$	0.145	912.35	2.9*	Millie, et al., 1992
PC	$.5*(R_{591 - 609} + R_{647 - 656})-R_{619 - 638}$	0.017	44.61	2.9*	Dekker, 1993

*** Indicates the data were log transformed**
Highlighted row indicates the best algorithm based on R^2

Figure 20- Eagle Creek Reservoir PC Algorithm Statistics

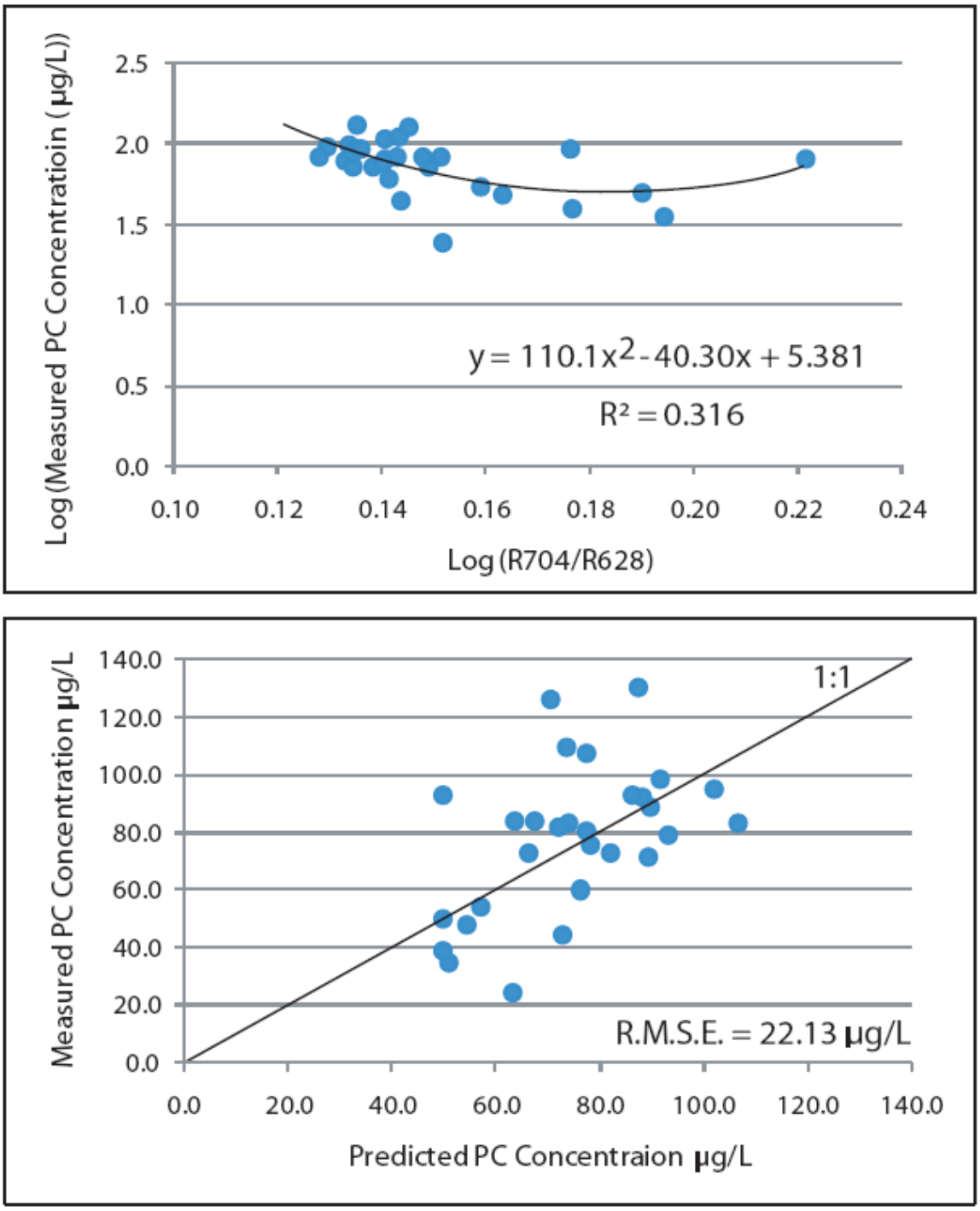

8.0 Maps of Pigment Concentration

Chlorophyll a

Geist Reservoir

Figure 21- Geist Reservoir Predicted Chl a Concentration Map

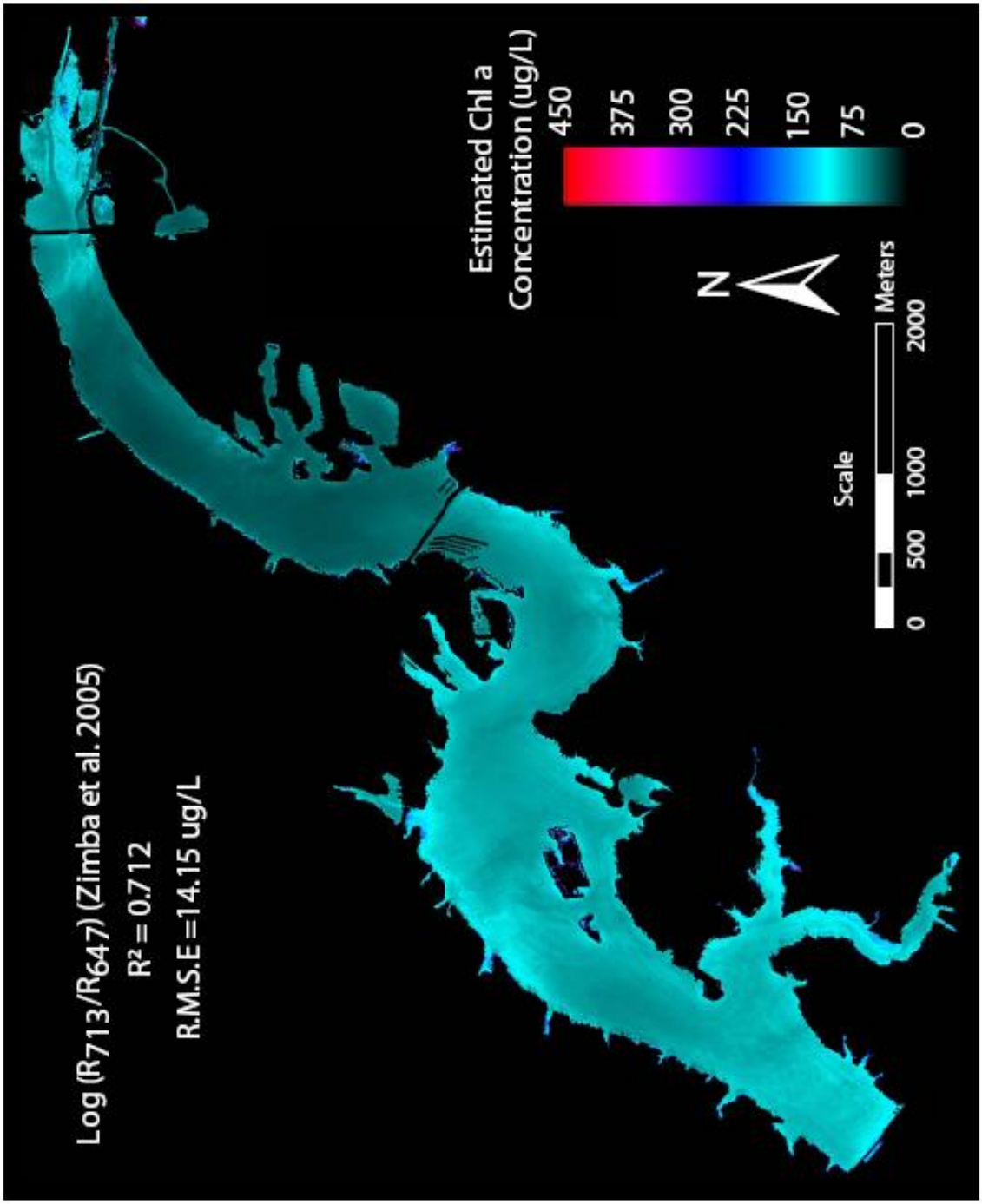

Figure 22- Geist Reservoir Interpolated Measured Chl a Concentration

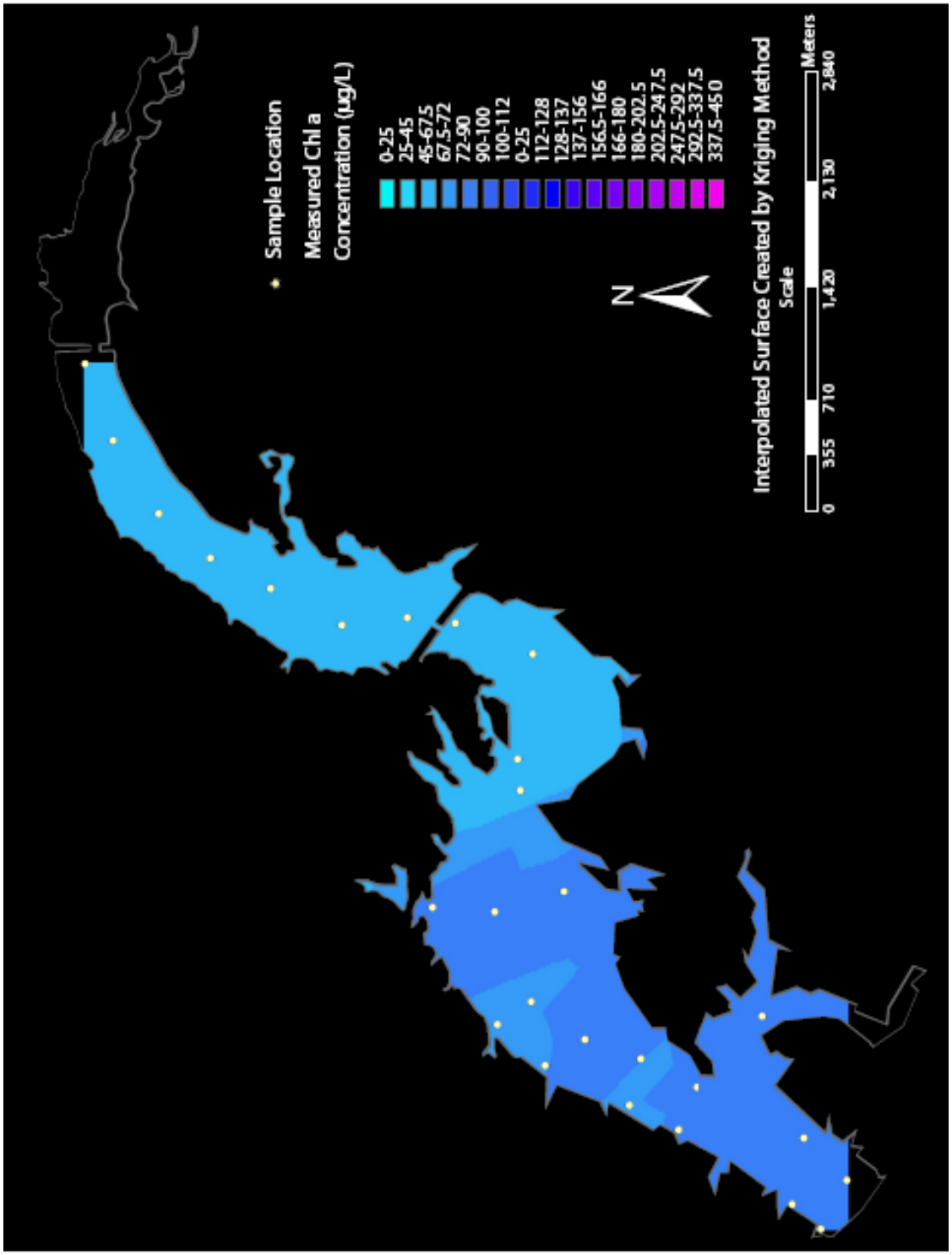

Morse Reservoir

Figure 23- Morse Reservoir Predicted Chl a Concentration Map

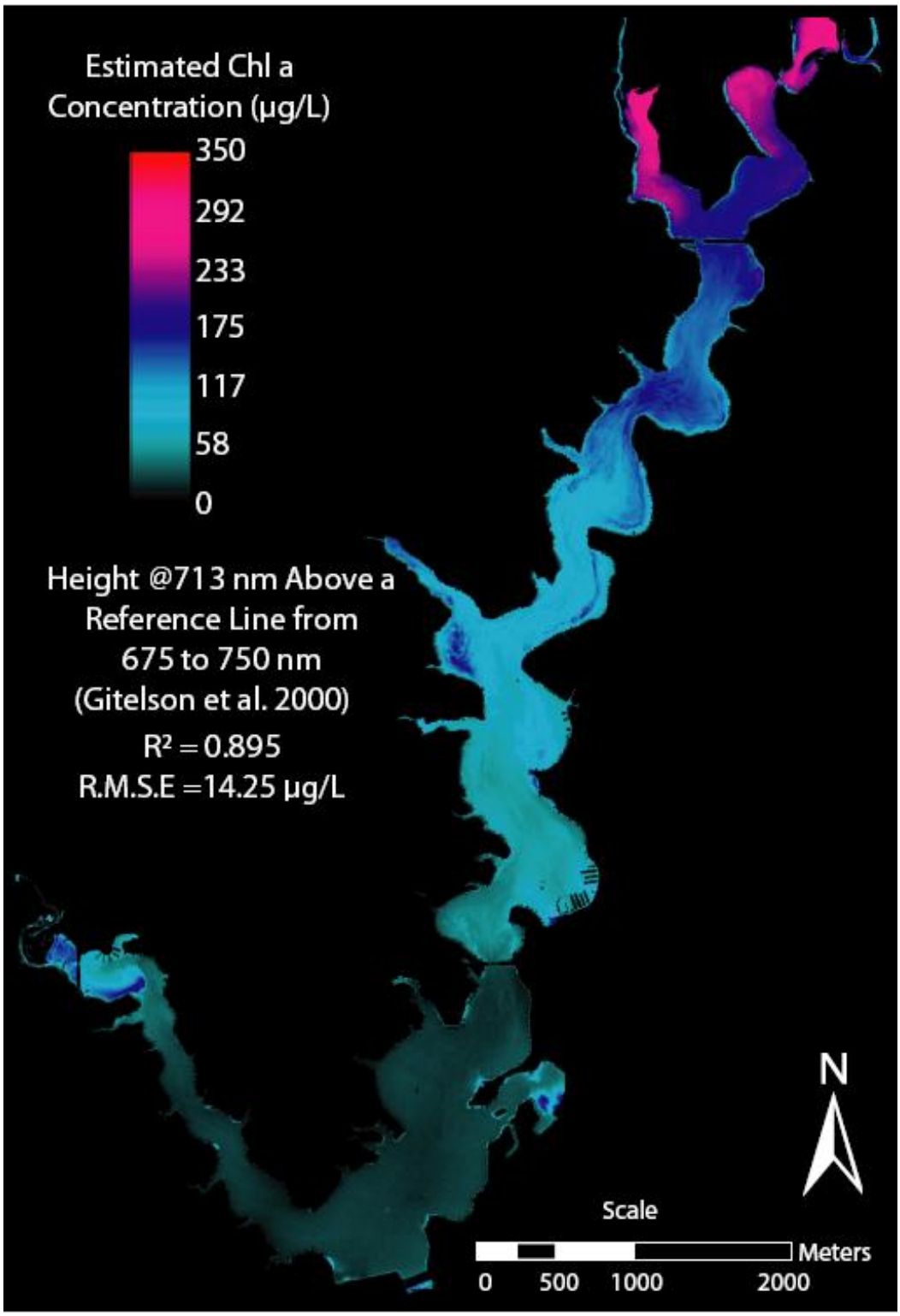

Figure 24- Morse Reservoir Interpolated Measured Chl a Concentration

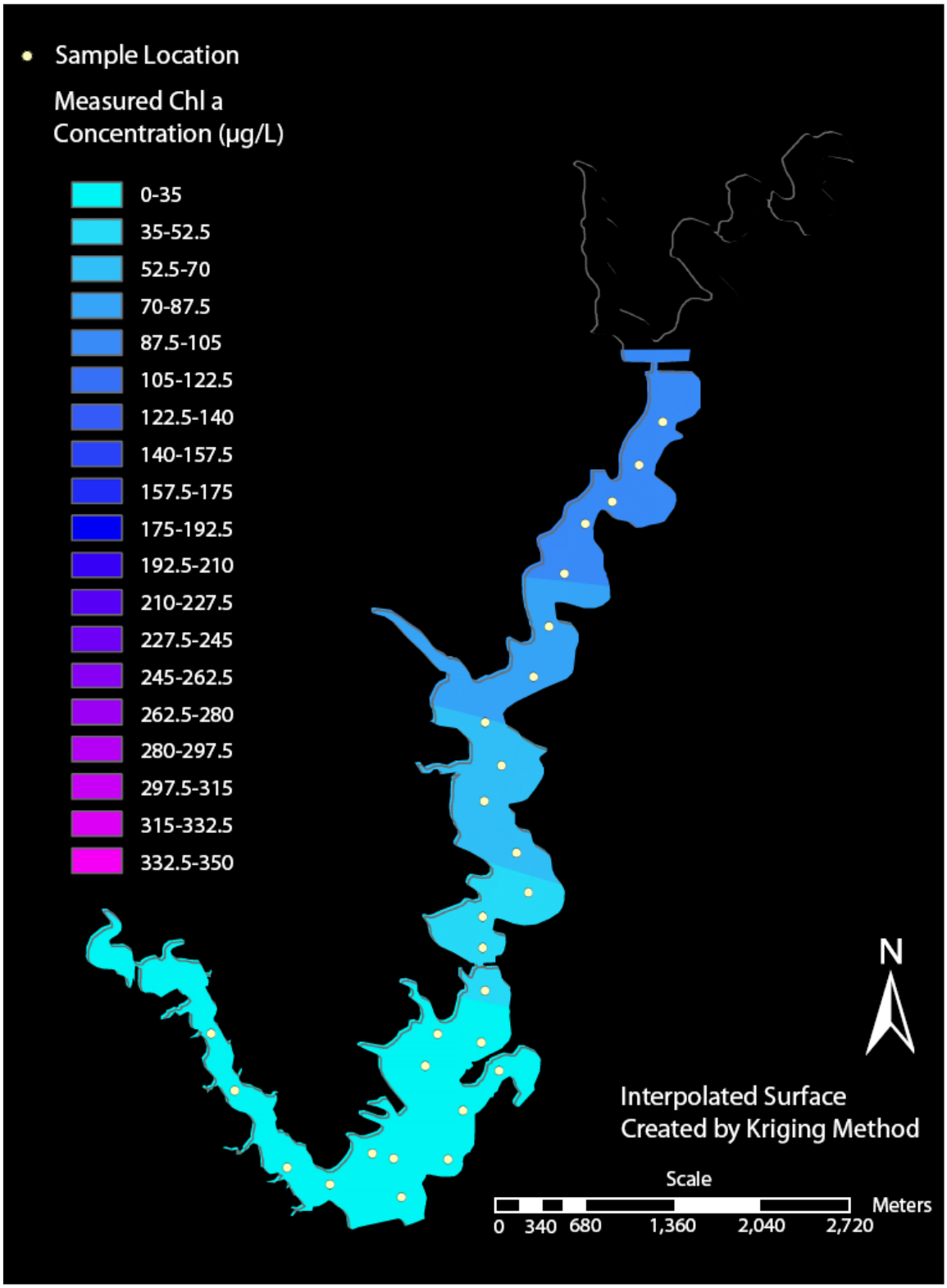

Eagle Creek Reservoir

Figure 25- Eagle Creek Reservoir Predicted Chl a Concentration Map

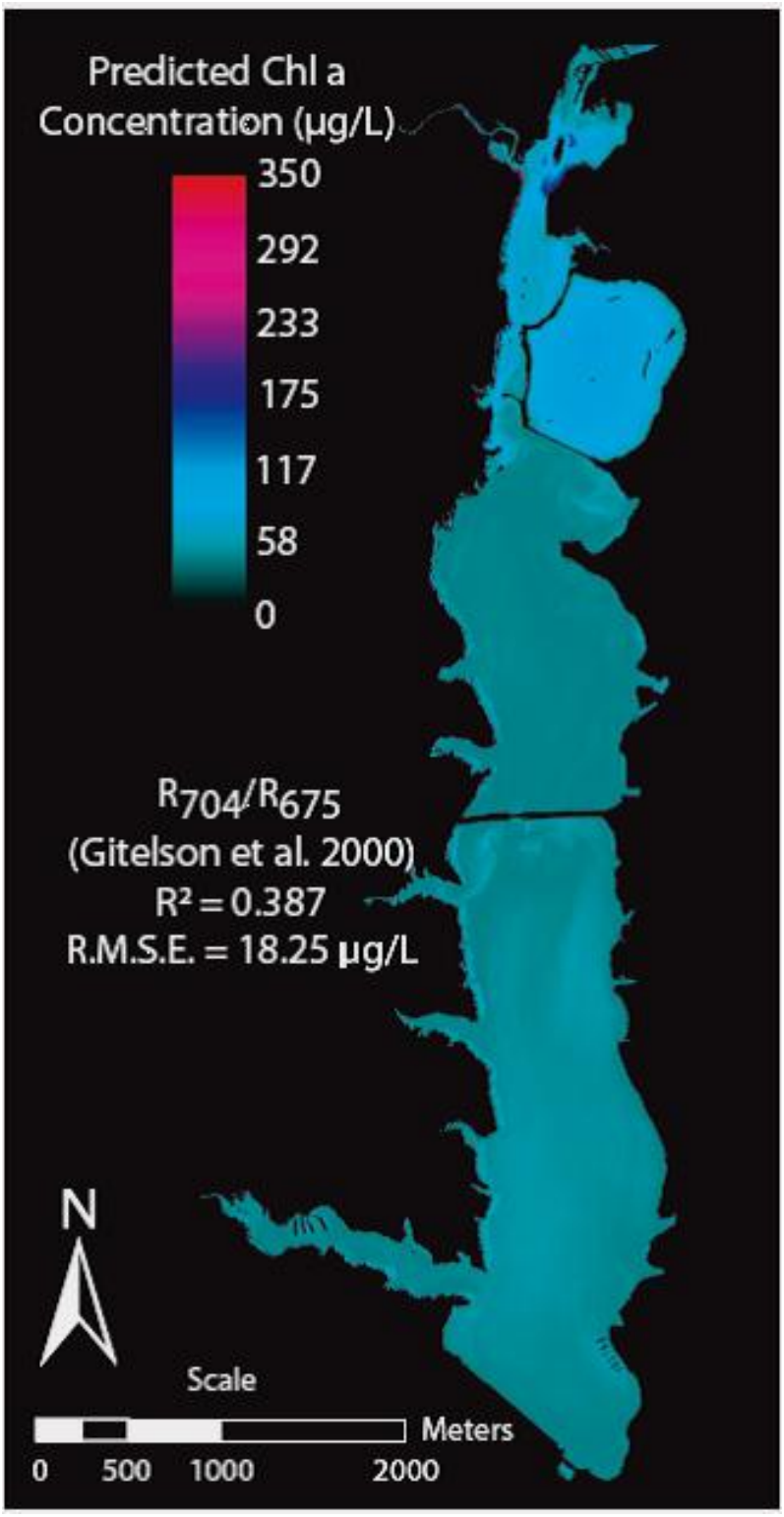

Figure 26- Eagle Creek Reservoir Interpolated Measured Chl a Concentration

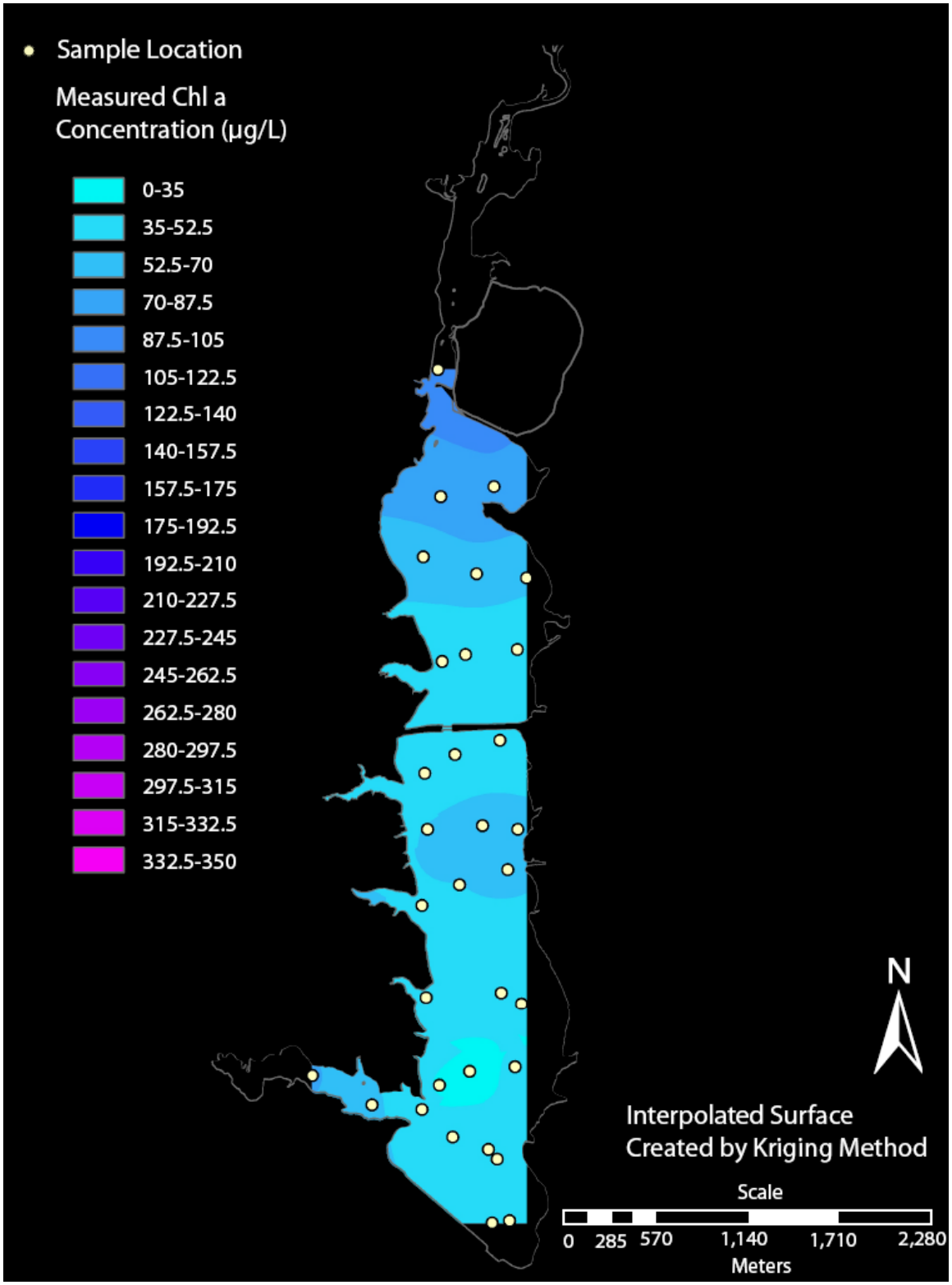

Phycocyanin

Geist Reservoir

Figure 27- Geist Reservoir Predicted PC Concentration Map

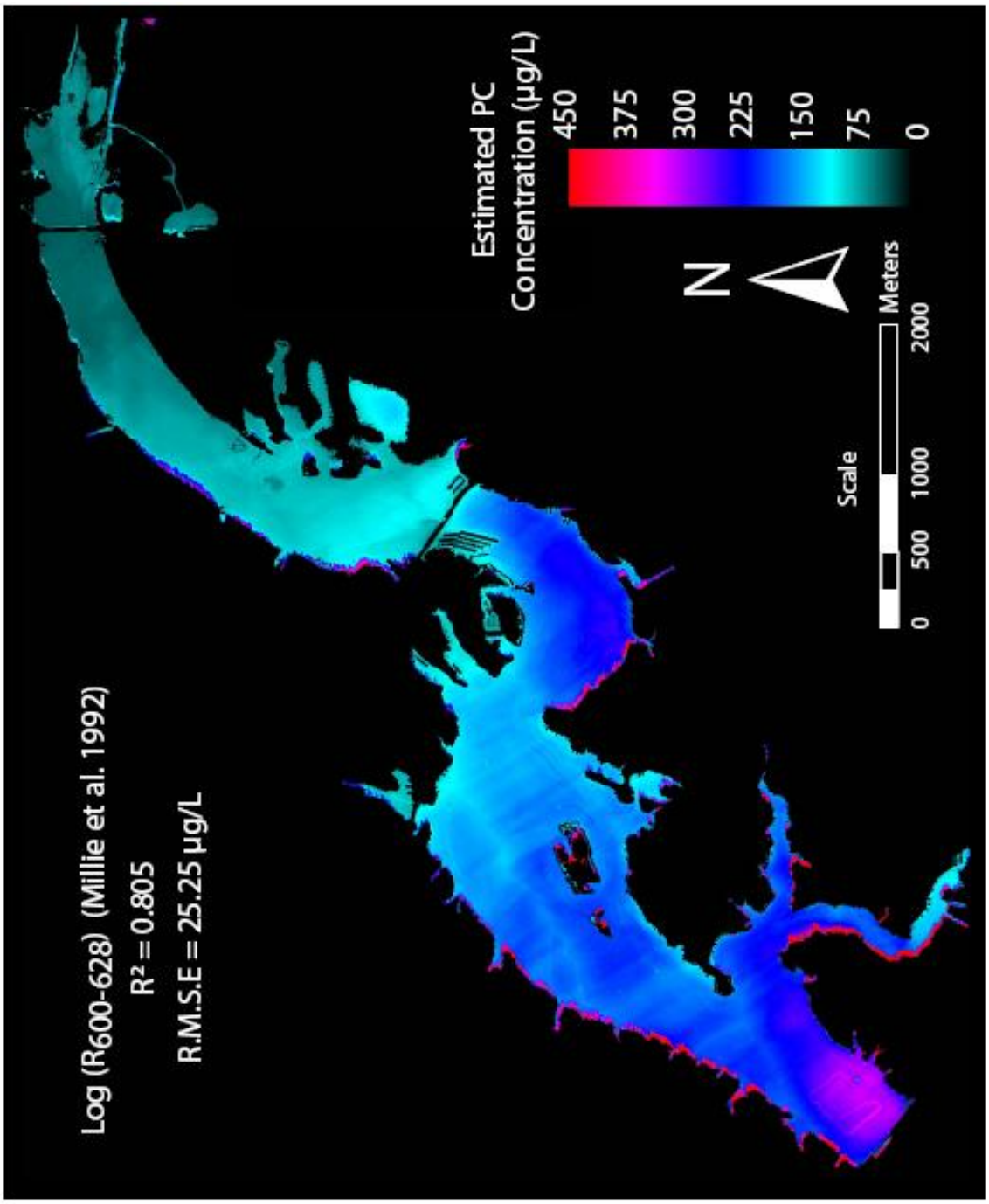

Figure 28- Geist Reservoir Interpolated Measured PC Concentration

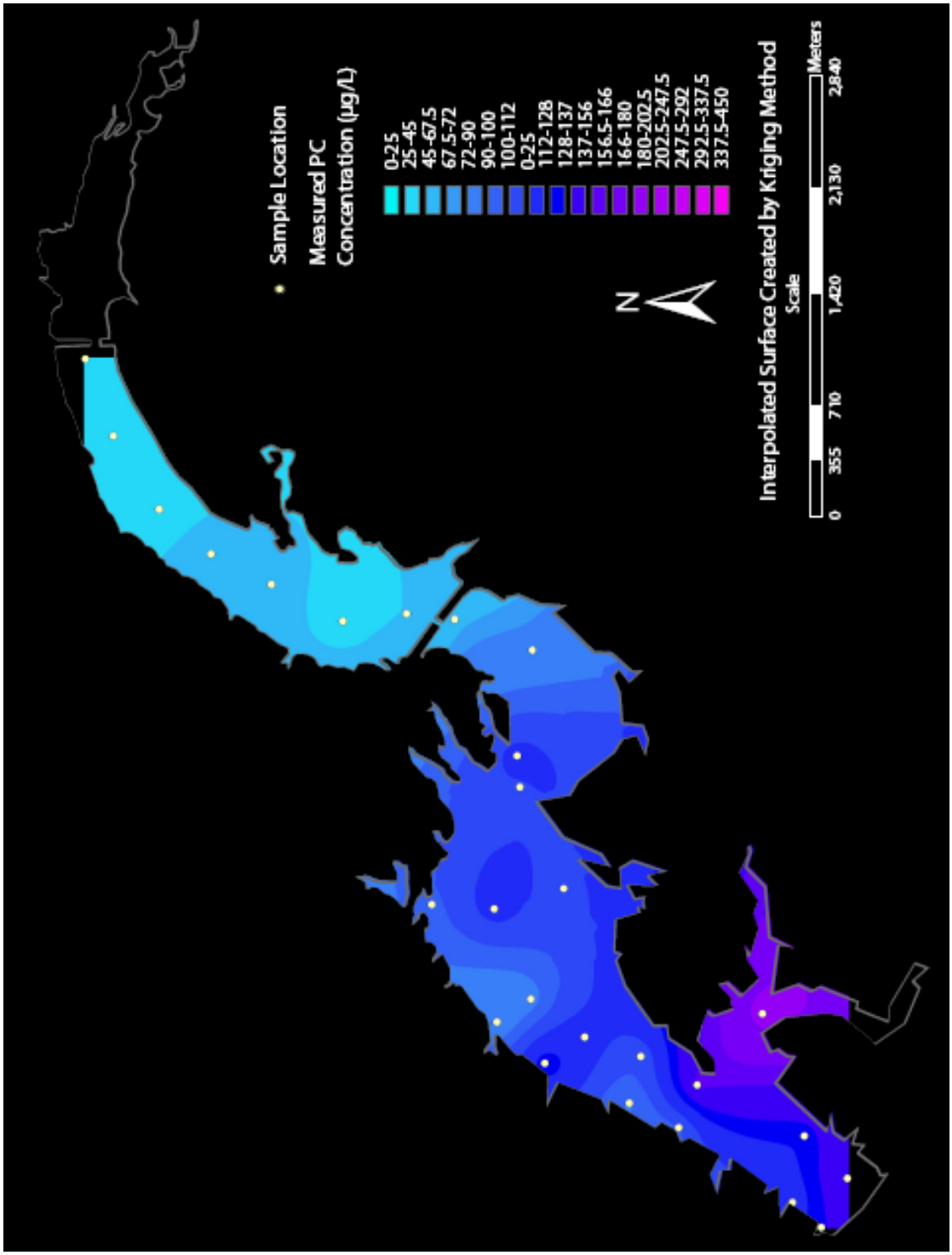

Morse Reservoir

Figure 29- Morse Reservoir Predicted PC Concentration Maps

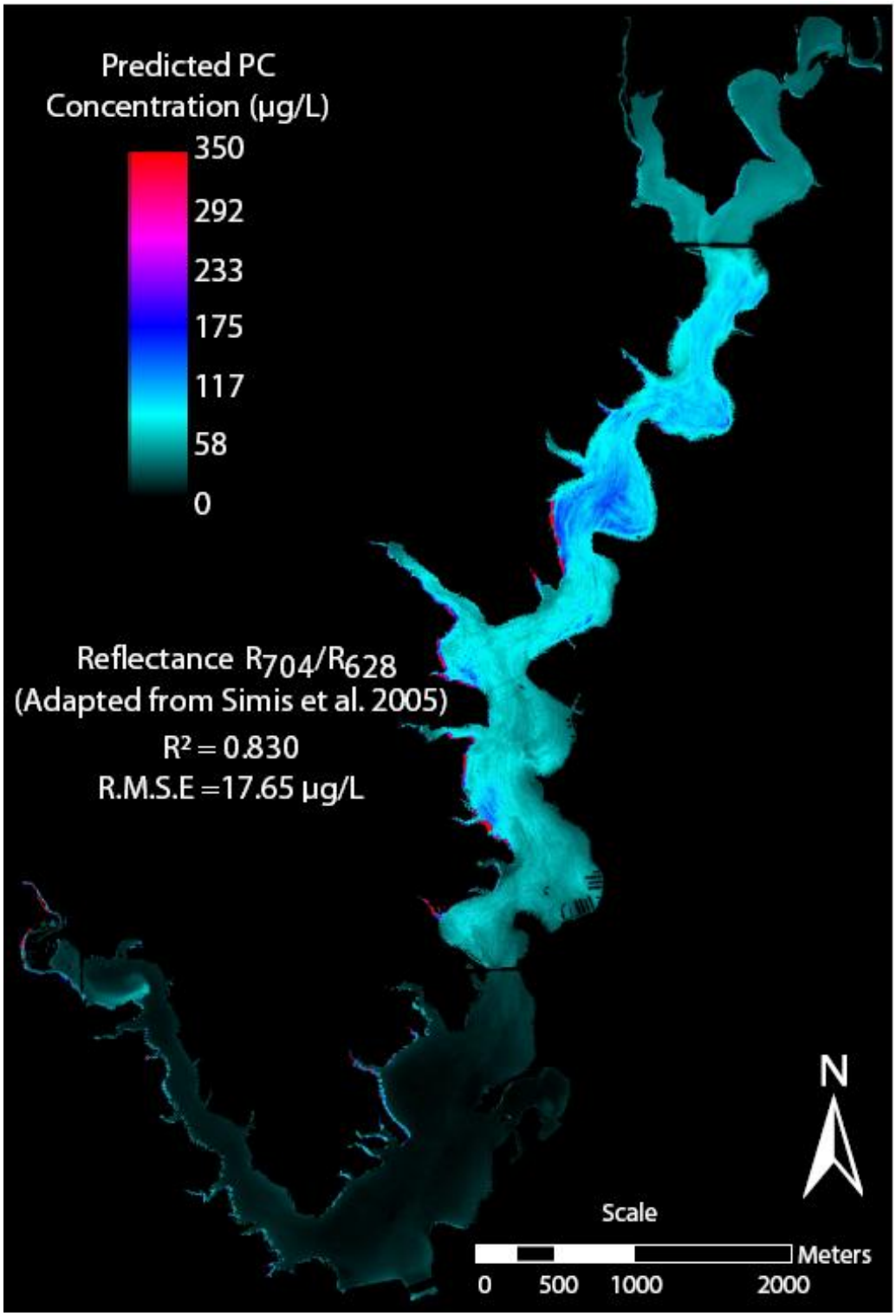

Figure 30- Morse Reservoir Interpolated Measured PC Concentration

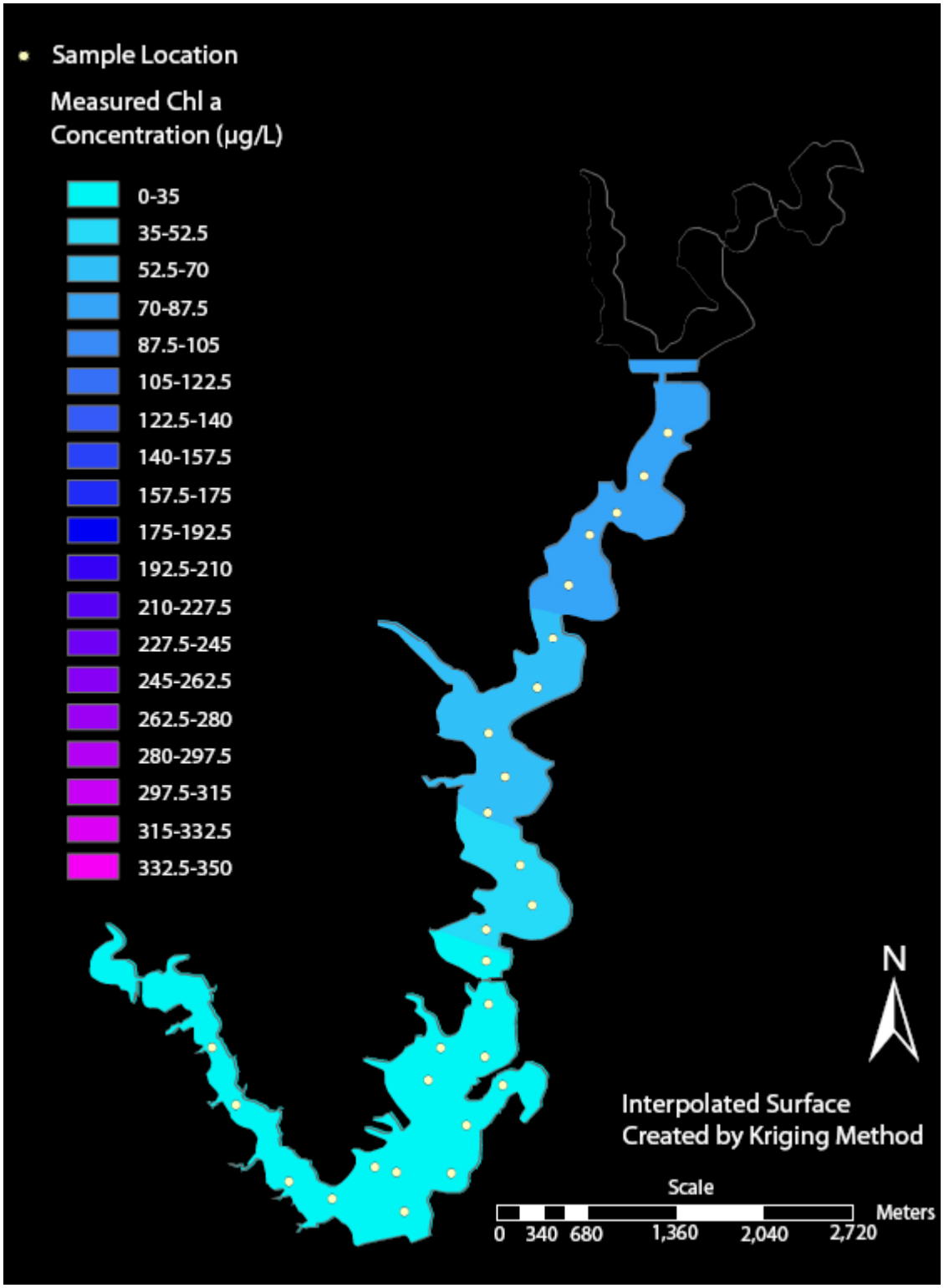

Eagle Creek Reservoir

Figure 31- Eagle Creek Reservoir Predicted PC Concentration Map

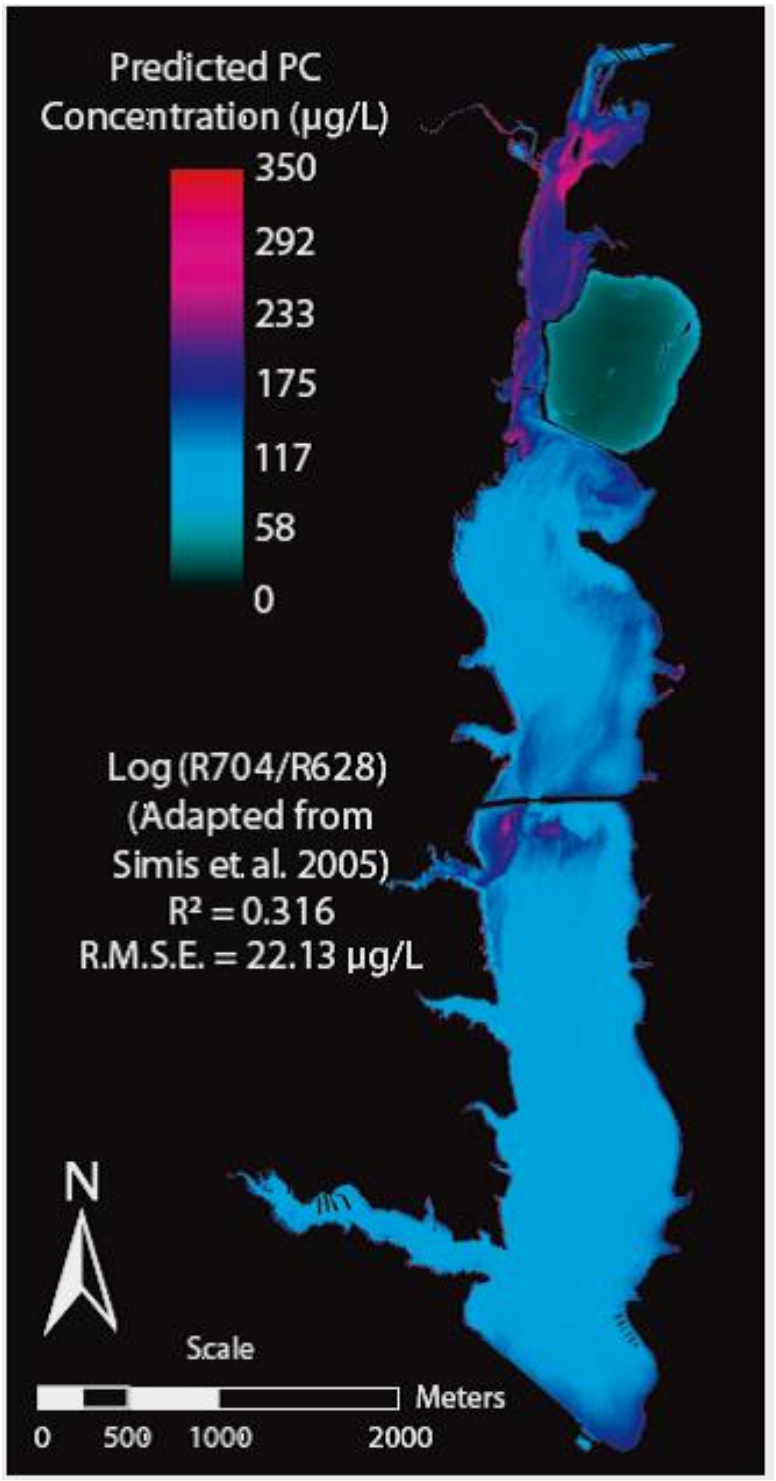

Figure 32- Eagle Creek Reservoir Interpolated Measured PC Concentration

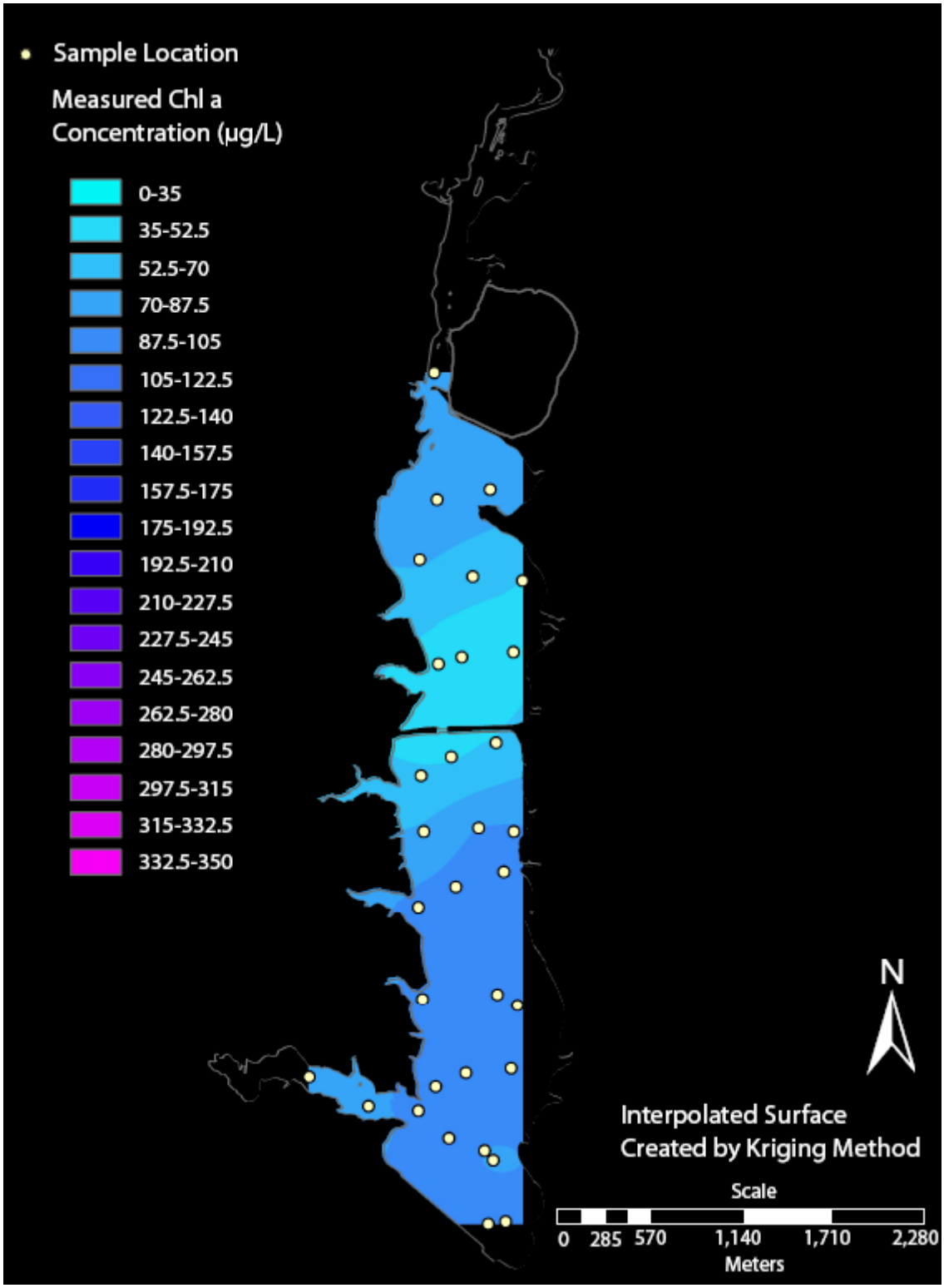

9.0 Discussion

Relationship between Phycocyanin and Cyanobacterial Abundance

In order to predict algal abundance from pigment concentration, it is assumed that the differences in pigment concentration reflect differences in cyanobacterial concentration. It is possible for cyanobacteria to exist in a reservoir without the presence of PC. This situation can occur because of the physiological state of the cyanobacteria, i.e. little or no PC produced or the breakdown of the pigment in times of nitrogen limitation (Simis, et al., 2007). To determine whether this assumption is correct, the relationship between phycocyanin pigment concentrations and cyanobacterial abundance was determined using a subset of 25 samples from all three reservoirs in a companion study done by Li et al. (2006). This study correlated pigment concentration to biovolume, which was calculated from phytoplankton identification and enumeration. These data show a strong correlation between ground truth phycocyanin concentrations and biovolume measurements (R^2 = 0.946, $p < 0.01$, Figure 33) and a moderately strong relationship between phycocyanin concentrations and phytoplankton counts as natural units-m/L (R^2 = 0.755, $p = 0.06$; Figure 34).

Figure 33- Regression between Biovolume and PC Concentration (Li, et al., 2006)

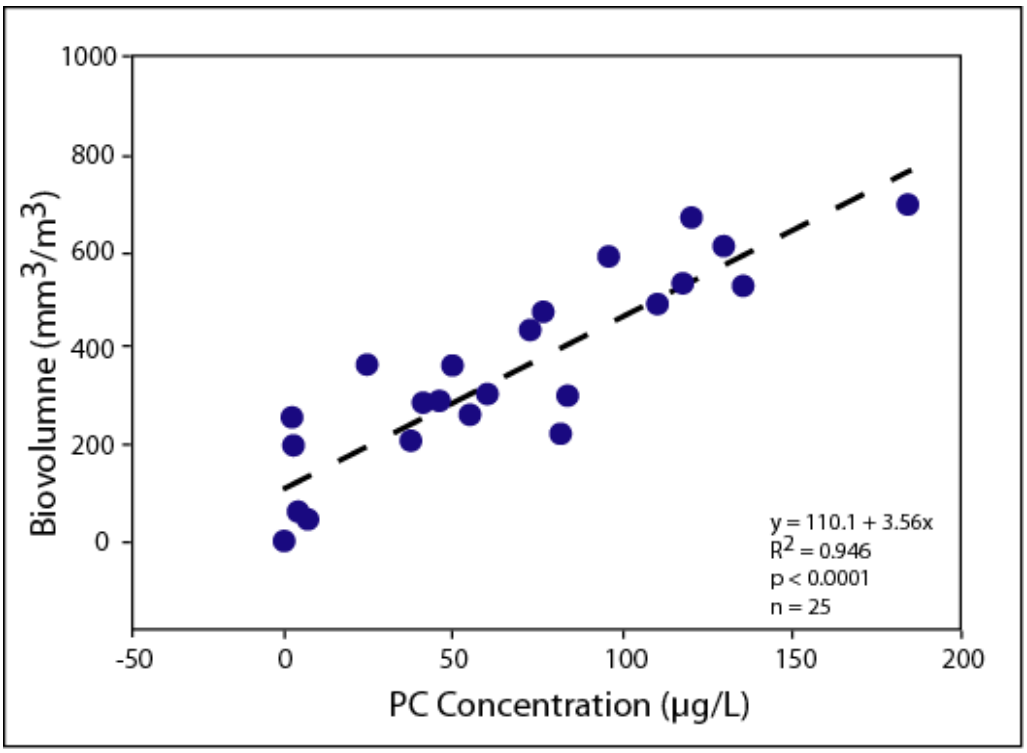

Figure 34- Regression between Cyanobacterial Natural Units and PC Concentration (Li, et al., 2006)

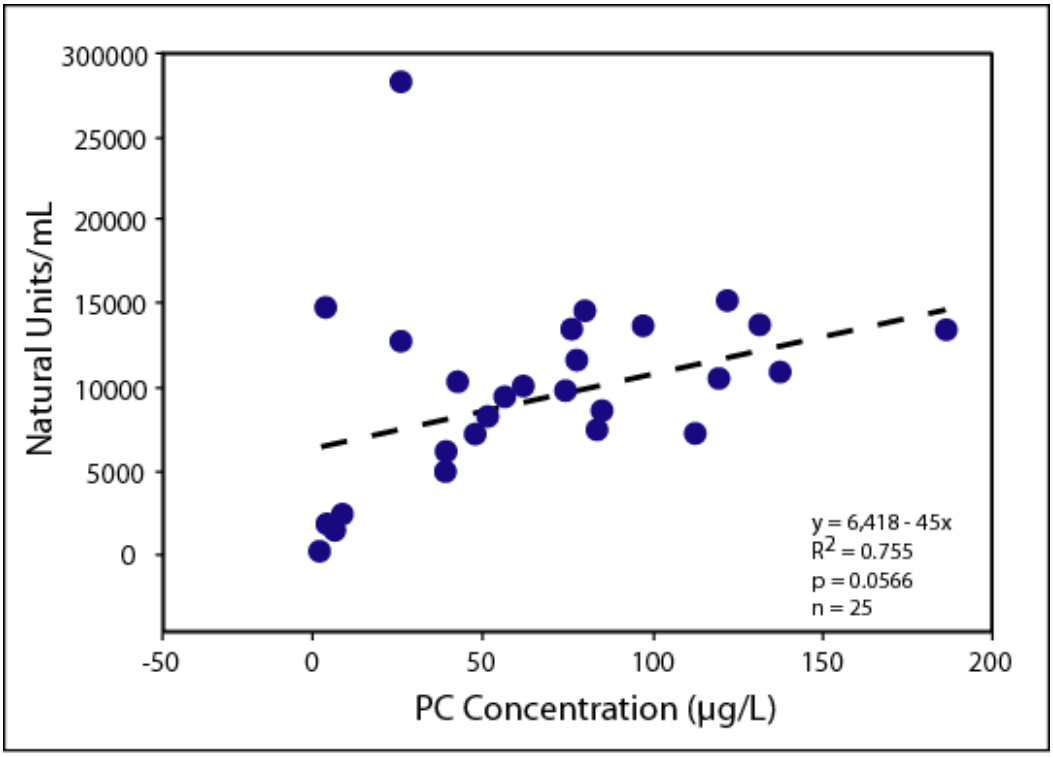

While most management decisions are based on the number of cells or natural units, biovolume is a better measure of the actual biomass for cyanobacterial populations because they are not uniform in size and shape (Li, et al., 2006). With the information from these regressions, both biovolume and natural unit measures for cyanobacterial concentration can be reasonably estimated from phycocyanin concentrations (Equation 3.7 and Equation 3.8, (Li, et al., 2006)), allowing managers a method in which to compare phycocyanin concentrations to cyanobacterial algal abundance.

3.7 $$Cyanobacterial\ Biovolume\ \left(\frac{mm^3}{m^3}\right) = 110.1 + 3.56 * [PC](\mu g/L)$$

3.8 $$Cyanobacterial\ Natural\ Units\ (NU)\left(\frac{NU}{mL}\right) = 3{,}629 + 67 * [PC]\ (\mu g/L)$$

Factors Affecting Algorithm Performance

Because none of the algorithms were able to perfectly predict either pigment concentration, implies that there are other factors affecting the either the pigment concentrations or the spectral reflectance. These factors can be broken up into several sections: errors due to sampling times, errors due to image processing, errors due to sample collection and processing and errors caused by other optically active constituents in the water. The following sections will discuss some possible causes of error.

Image Acquisition versus Sampling Time

Because these reservoir systems are not static, it is expected that changes in water quality parameters to occur over time. One major problem is the comparison of ground data and airborne data as if they were collected at the same instant; when they were not. Table 17 summarizes the time of imagery acquisition, time of sample collection and lag time between the data sets for each reservoir.

Table 17- Comparison of Image Acquisition and Field Sampling Times

Reservoir	Median Sample Acquisition Time	Median Airborne Acquisition Time	Lag Time
Geist	11:15 am	5:45 pm	6 h 30 min
Morse	10:45 am	4:20 pm	5 h 35 min
Eagle Creek	11:02 am	5:20 pm	6 h 18 min

During time between data sets, the characteristics of the water in the sample site may have changed due to the flow of water in the reservoir, movement due to wind currents or mixing due to boat and wind activity and the movement of cyanobacteria within the water column. The difference in acquisition times is a source of error that cannot be eliminated from this data.

Normalization and Atmospheric Calibration

Ideally, normalization and atmospheric calibration would remove all radiometric differences between measurements taken at the surface and the airborne imagery in this study. However, as good as the normalization and atmospheric calibration is, it is likely that there are some atmospheric effects and possibly some spectral artifacts from the calibration processes still present in the data. The calibration of the imagery is a source of error that cannot be accounted for in the data, this would cause the spectra to predict pigment concentration erroneously.

Sample Collection, Processing and Size

Error may have also been introduced during the sample collection and sample processing. If mistakes were made during field spectral collection they would affect the calibration of the airborne imagery. One cause of error with the sample collection is that these samples were surface samples, yet the reflectance is measured over the depth of photic zone. Therefore, differences between pigment concentration throughout the water

column and the surface, while likely minimal, could be causing error based on how the data was collected.

Water samples must be collected, filtered, extracted, diluted and then read fluorometrically, an error in anyone of these steps can affect the measured concentration of pigment in the sample. If problems occurred during water sample collection and pigment extraction it would affect the ability of the spectra to predict the measured pigment concentration.

Another issue is the sample size for this study. Because of difficulty associated with field data collection, approximately 30 samples were taken per reservoir. Unfortunately, due to missing samples and analysis errors, samples had to be eliminated from algorithm development in all of the reservoirs. A greater number of samples would reduce the error of the measurements and improve the predictive power of the algorithms. This occurs because with a greater the sample size, the data is more similar to the actual population itself (Lenth, 2001).

Other Optically Active Constituents

If other optically active constituents, besides Chl a and PC, are present in water it will affect the spectral response of the water column. While algorithms were chosen in this study specifically were developed to eliminate the effect of other constituents it is possible that all of the variability was not accounted for. The presence of other optically active constituents would change the spectral signature recorded by the sensor, affecting its ability to predict pigment concentration. To investigate if any of the other optically active constituents are causing the algorithms to erroneously predict pigment values regressions were performed in excel. The data from these regressions is shown in the following section.

Regression Statistics

Geist Reservoir

Regressions on Chl a Concentration

Regression analysis of Geist reservoir has yielded interesting results concerning the source obfuscation in the prediction of Chl a and PC from reflectance data. Table 18 shows the results of a linear regression performed between the reflectance ratio which had the highest R^2 (R_{713}/R_{647} (Zimba & Gitelson, 2006)) and Chl a concentration, yielding a p-value of $2.6*10^{-6}$ and an R^2 of 0.641.

Table 18- Geist Reservoir: Regression between Chl a Concentration and AISA Reflectance

Geist Regression Statistics Chl a Concentration					
R^2	0.641	Observations	24		
Standard Error	15.29				
	Regression Coefficients	Standard Error	p-value	Lower 95%	Upper 95%
Intercept	10.01	10.56	0.35	-11.87	31.89
R_{704}/R_{666}	641.72	102.40	$2.6*10^{-6}$	429.35	854.08

The p-value shows the likelihood that the coefficient of the reflectance is zero. If a coefficient of the variable is zero, it will make the effect of that coefficient zero in the regression equation, indicating that variable may as well not be included. Since this value is very low, it indicates that chance that coefficient of reflectance is zero is very unlikely, .000003% chance. Therefore, reflectance is a significant factor in predicting Chl a concentration. However, the R^2 of 0.641 indicates that a linear relationship between reflectance only explains 64.1% of the variation in Chl a concentration, so other variables should be included in the regression equation in order to explain the variation in Chl a more completely. Table 19 shows the regression of Chl a against reflectance, TSS and turbidity. While adding all of the water quality constituents measured was possible, this study was

only interested in variables that would be affecting reflectance. Thus allowing the detection of constituents that affect pigment concentration, but were effectively 'eliminated from the picture' with the use of an algorithm. In this regression, R^2 has slightly increased to 0.643, because there are more variables involved in the regression to explain variation.

Table 19- Geist Reservoir: Regression between Chl a Concentration and AISA Reflectance, TSS and Turbidity

Geist Regression Statistics Chl a Concentration					
R^2	0.643	Observations	24		
Standard Error	15.98				
	Regression Coefficients	Standard Error	p-value	Lower 95%	Upper 95%
Intercept	9.37	17.37	0.60	-26.87	45.60
R_{704}/R_{666}	615.01	135.36	$2.0*10^{-3}$	332.65	897.37
TSS	0.46	1.22	0.71	-2.08	3.00
Turbidity	-0.59	2.16	0.79	-5.084	3.91

It is also important to note the p-values of reflectance is still low, $p < 0.01$, indicating that it is still significant in explaining Chl a concentration. Also, it is important to notice the p-values of turbidity and TSS. The values are very high, indicating that they are not statistically different from zero and may as well not be included in the regression. One more regression was done to identify more confounding factors in the relationship between Chl a and the reflectance ratio. The dissolved component is another optically active constituent in the water that may affect spectral response. A regression was performed between Chl a, the reflectance ratio and TDS (Table 20).

Table 20- Geist Reservoir: Regression between Chl a Concentration and AISA Reflectance and TDS

Geist Regression Statistics Chl a Concentration					
R^2	0.652	Observations	24		
Standard Error	15.41				
	Regression Coefficients	Standard Error	P-value	Lower 95%	Upper 95%
Intercept	72.60	77.13	0.36	-87.80	233.00
R_{704}/R_{666}	525.40	175.49	$7.0*10^{-3}$	160.44	890.36
TDS	-157.81	192.60	0.42	-558.343	242.73

This regression yields interesting results. The R^2 increased to 0.652, indicating that more of the variation in Chl a concentration is explained by adding TDS, and removing TSS and turbidity, to the regression. Additionally, the p-value of reflectance is quite small, indicating that reflectance is still a statistically significant factor in predicting Chl a concentration. However, with the high p-value of TDS it shows that the variable need not be included in the regression equation.

Regression on Chl a Estimation Error

The residuals from the regression between Chl a and the reflectance ratio were squared and regressed against several variables to find any statistically significant relationships. The variables chosen were the ratio between Chl a concentration and PC concentration, TSS, turbidity and TDS. The results of this regression are displayed in Table 21.

Table 21- Geist Reservoir: Regression between Chl a Squared Prediction Residuals and Chl a: PC, TDS, TSS and Turbidity

Geist Regression Statistics Chl a Squared Residuals					
R^2	0.233	Observations	24		
	Regression Coefficients	Standard Error	p-value	Lower 95%	Upper 95%
Intercept	679.34	1595.35	0.67	-2659.71	4018.51
PC : Chl a Ratio	239.57	232.89	0.32	-24.884	727.01
TDS	-37.91.30	3853.01	0.34	-1185.70	4273.14
TSS	-24.41	30.70	0.44	-88.66	37.85
Turbidity	102.47	62.96	0.12	-29.30	234.24

The results of the regression indicate that very little of the variation in the error is explained by the combination of these variables ($R^2 = 0.233$). Additionally, because of the high p-values, none of these parameters are statistically significant for predicting the error in the Chl a estimation. These regressions indicate that the concentrations of these water quality parameters in Geist Reservoir are not causing error in the prediction of pigment concentration.

Another consideration is whether or not the errors change with the value of the prediction. This is done by graphing the residuals of the regression versus the independent variable, Figure 35. The data in this case show heteroskedasticity, $p = 0.06$, indicating that a relationship exists between the error and the reflectance ratio. Since the relationship between the reflectance ratio and Chl a concentration is positive, as the predicted value of Chl a increases in Geist reservoir, there is a statistically significant chance that the error of that estimated value would increases as well.

Figure 35- Geist Reservoir Chl a Prediction Residuals vs. Reflectance Algorithm

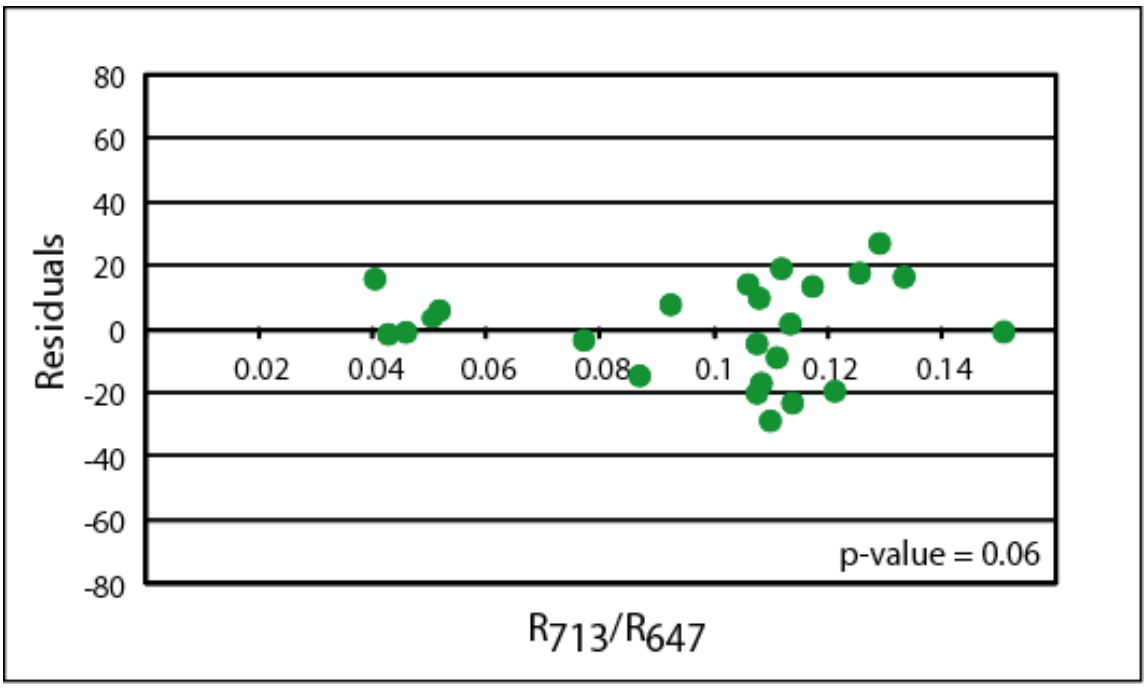

Regressions on PC Concentration

The regression of Geist Reservoir's PC concentration yielded similar results to that of the Chl a regressions. The results of the initial regression between PC and the reflectance algorithm ($R_{600-628}$ (Millie, et al., 1992)) can be seen in Table 22.

Table 22- Geist Reservoir: Regression between PC Concentration and AISA Reflectance

Geist Regression Statistics PC Concentration					
R^2	0.639	Observations	27		
Standard Error	26.21				
	Regression Coefficients	Standard Error	p-value	Lower 95%	Upper 95%
Intercept	280.11	28.27	$3.9*10^{-10}$	221.88	338.33
$R_{600-628}$	-2127.51	319.64	$5.7*10^{-07}$	-2785.82	-1469.20

With an R^2 of 0.639, this algorithm explains 64% of the variation in PC concentration, and because of the very low p-value, it is shown that the reflectance is significant for predicting

PC concentration. A second regression between PC, reflectance, TSS and turbidity can be seen in Table 23.

Table 23- Geist Reservoir: Regression between PC Concentration and AISA Reflectance, TSS and Turbidity

Geist Regression Statistics PC Concentration					
R^2	0.735	Observations	27		
Standard Error	23.44				
	Regression Coefficients	Standard Error	p-value	Lower 95%	Upper 95%
Intercept	207.41	36.91	$1.0*10^{-05}$	131.06	283.76
$R_{600 - 628}$	-1741.77	340.63	$3.5*10^{-05}$	-2446.41	-1037.13
TSS	4.54	1.68	0.01	1.06	8.02
Turbidity	-5.25	3.64	0.16	-12.78	2.27

With this regression the R^2 increased, and more variation in PC concentration is explained. The coefficient of reflectance changed significantly indicating that TSS and turbidity have a statistically significant affect on this reflectance algorithm. The low p-values of TSS and reflectance indicated that they are both important for predicting PC concentration, but because of the high p-value of turbidity in this regression, it indicates that it is not significant factor for explaining variation in PC concentration. A third regression included the variables PC, TSS and TDS (Table 24).

Table 24- Geist Reservoir: Regression between PC Concentration and AISA Reflectance, TDS and TSS

Geist Regression Statistics PC Concentration					
R^2	0.764	Observations	27		
Standard Error	22.12				
	Regression Coefficients	Standard Error	p-value	Lower 95%	Upper 95%
Intercept	402.60	89.69	$1.7*10^{-4}$	217.06	588.14
$R_{600-628}$	-942.80	539.09	0.09	-2057.98	172.39
TDS	-781.11	343.36	0.03	-1491.41	-70.82
TSS	1.26	1.18	0.30	-1.19	3.71

The R^2 increased to 0.76, meaning that this combination of variables is better at explaining pigment concentration than the previous regression. What is important to note in this regression is the significance that TDS has on PC concentration, and the statistically insignificant role TSS now plays on PC concentration prediction compared to the other variables. Therefore, TDS has a statistically significant effect on PC concentration in Geist Reservoir.

Regression on PC Estimation Errors

To find any statistically significant relationships with the error of prediction, the squared residuals from the first regression between PC and the reflectance were squared and regressed against several variables. The results of the regression between the residuals and the Chl a: PC ratio, turbidity, TSS and TDS is shown in Table 25.

Table 25- Geist Reservoir: Regression between PC Squared Prediction Residuals and Chl a: PC, TDS, TSS and Turbidity

Geist Regression Statistics PC Squared Residuals					
R^2	0.045	Observations	24		
	Regression Coefficients	Standard Error	p-value	Lower 95%	Upper 95%
Intercept	-2769.78	4857.26	0.58	-12936.1	7396.57
PC: Chl a Value	588.6744	709.07	0.42	-895.43	2075.78
TDS	5768.65	11730.98	0.63	-18784.6	30321.86
TSS	15.03	93.47	0.87	-180.603	210.66
Turbidity	45.02	191.68	0.81	-855.18	447.21

The results of the regression indicate that very little of the variation in the error is explained by the combination of these variables ($R^2 = 0.045$). Additionally, because of the high p-values, none of these parameters are statistically significant for predicting the error in PC estimation.

To investigate any relationships between error and the value of the prediction, a graph of the two was created (Figure 36). The data in this case do not show heteroskedasticity, $p = 0.35$, indicating that there are no statistically significant relationships between the error and the reflectance.

Figure 36- Geist Reservoir PC Prediction Residuals vs. Reflectance Algorithm

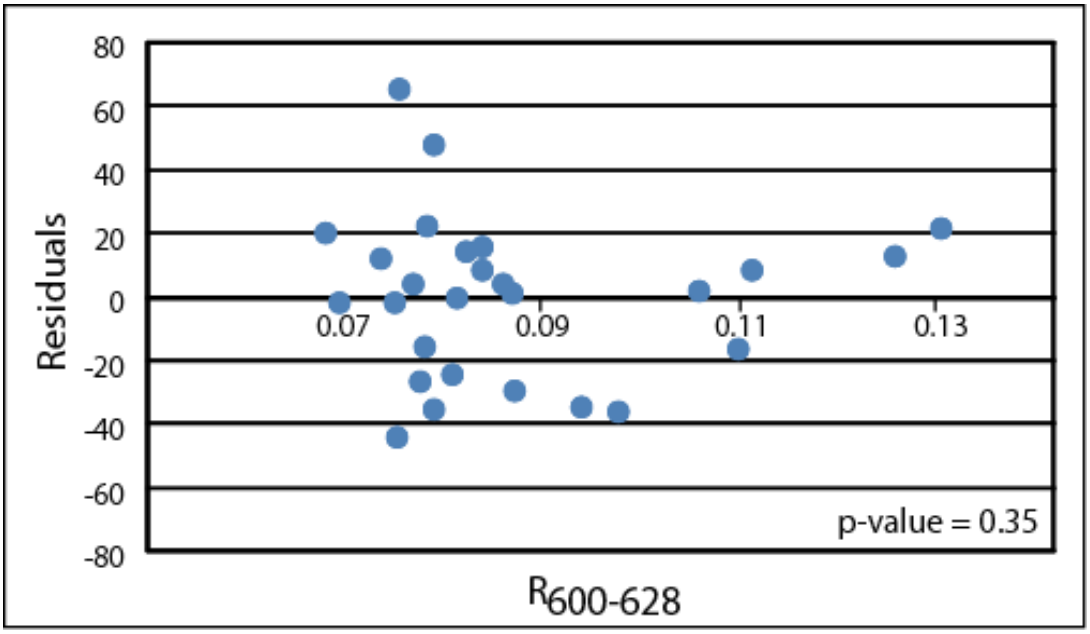

Summary of Geist Reservoir Statistics

The first regressions of either pigment on Geist Reservoir show that reflectance gathered by the AISA sensor is statistically significant in predicting concentration. With the first several regressions on the pigments, of the constituents that may affect reflectance, TDS was the only one which was statistically significant for predicting the concentration of Chl a or PC. With the last regressions on the error of the pigment estimations, none of the water constituents affect the error of the prediction. This shows that while TDS is significant for predicting the concentration of Chl a and PC in the reservoir, the algorithms can remove or are not affected by any of the spectral attenuation it may cause. Furthermore, the graphs of error versus reflectance indicate that only the Chl a algorithm has heteroskedasticity, causing the error of the estimation to increase with increasing predicted concentration. A correlation between the pigments and the other parameters considered in the regressions of Geist Reservoir is shown in Table 48.

Morse Reservoir

Regressions on Chl a Concentration

Several regressions of Chl a concentration for Morse reservoir can be seen in Table 26, 27, 28 and 29. The linear regression between Chl a and the best algorithm (Height of R_{704} above a base line 66 nm to 751 nm, e.g. (Gitelson, et al., 2000)) is shown in Table 26.

Table 26- Morse Reservoir: Regression between Chl a Concentration and AISA Reflectance

Morse Regression Statistics Chl a Concentration					
R^2	0.887	Observations	27		
Standard Error	15.17				
	Regression Coefficients	Standard Error	p-value	Lower 95%	Upper 95%
Intercept	6.29	4.71	0.19	-3.41	15.98
Reference Line Height	5798.60	413.71	$2.4*10^{-13}$	4946.54	6650.66

The R^2 is quite high, indicating that the algorithm explains the variation seen in Chl a concentration. Furthermore, the p-value is quite low, indicating that it is statistically unlikely that the coefficient is equal to zero, and the algorithm is an important variable for predicting Chl a concentration. A second regression was done using the reflectance algorithm, TSS and Turbidity (Table 27).

Table 27- Morse Reservoir: Regression between Chl a Concentration and AISA Reflectance, TSS and Turbidity

Morse Regression Statistics Chl a Concentration					
R^2	0.900	Observations	27		
Standard Error	14.86				
	Regression Coefficients	Standard Error	p-value	Lower 95%	Upper 95%
Intercept	8.50	4.78	0.09	-1.39	18.38
Reference Line Height	4315.31	1106.77	$7.2*10^{-4}$	2025.78	6604.84
TSS	1.40	0.84	0.11	-0.33	3.13
Turbidity	-1.64	1.60	0.32	-4.95	1.67

Because more variables were added to the regression, more variability in Chl a concentration was explained, yielding a slightly higher R^2 of 0.900. The high p-values of turbidity and TSS indicate that they are relatively statistically insignificant for predicting Chl a concentration. As with Geist reservoir, the Chl a concentration was regressed against the reflectance algorithm and TDS, Table 28.

Table 28- Morse Reservoir: Regression between Chl a Concentration and AISA Reflectance and TDS

Morse Regression Statistics Chl a Concentration					
R^2	0.888	Observations	27		
Standard Error	15.41				
	Regression Coefficients	Standard Error	p-value	Lower 95%	Upper 95%
Intercept	-75.40	173.23	0.67	-432.93	282.14
Reference Line Height	5722.17	450.45	$3.8*10^{-12}$	4792.49	6651.85
TDS	308.18	653.35	0.64	-1040.26	1656.63

Conversely, the regression of Morse reservoir indicates that TDS has very little significance for predicting Chl a. This is seen with a small increase in R^2 from the original regression of Chl a and reflectance and the high p-value of TDS.

Regression on Chl a Estimation Error

To explore the relationships between the errors of prediction, the residuals from the first regression between Chl a concentration and reflectance were squared and regressed against several variables. The results of the regression between the residuals and the Chl a: PC ratio, turbidity, TSS and TDS is shown in Table 29.

Table 29- Morse Reservoir: Regression between Chl a Squared Prediction Residuals and Chl a: PC, TDS, TSS and Turbidity

Morse Regression Statistics Chl a Squared Residuals					
R^2	0.347	Observations	21		
	Regression Coefficients	Standard Error	p-value	Lower 95%	Upper 95%
Intercept	24885.33	7412.74	$4.0*10^{-3}$	9171.03	40599.62
PC: Chl a Value	-517.49	26.94	0.074	-1089.77	54.78
TDS	-92081.90	27701.05	$4.0*10^{-3}$	-150806	-33358.3
TSS	55.88	36.44	0.14	-21.37	133.12
Turbidity	-100.83	95.50	0.31	-303.28	101.62

The results of the regression indicate that very little of the variation in the error is explained by the combination of these variables ($R^2 = 0.347$). The high p-values of the Chl a: PC ratio, turbidity and TSS indicate that these parameters are statistically insignificant for predicting the error in Chl a estimation. The low p-value of TDS indicates that it is statistically significant for predicting error in Morse Reservoir. However, because the value of the coefficient is negative it indicates that as TDS increases, error decreases. This relationship is counter intuitive, because it would seem that as there are more dissolved substances in the water column it should interfere with the spectral signatures, decreasing the algorithms ability to predict pigment concentration.

To investigate any relationships between error and the value of the prediction, a graph of the two variables was created (Figure 37). The data in this case shows little relationship between the error of prediction and the reflectance (p = 0.32). This reveals that the error is independent of the reflectance value.

Figure 37- Morse Reservoir Chl a Prediction Residual vs. Reflectance Algorithm

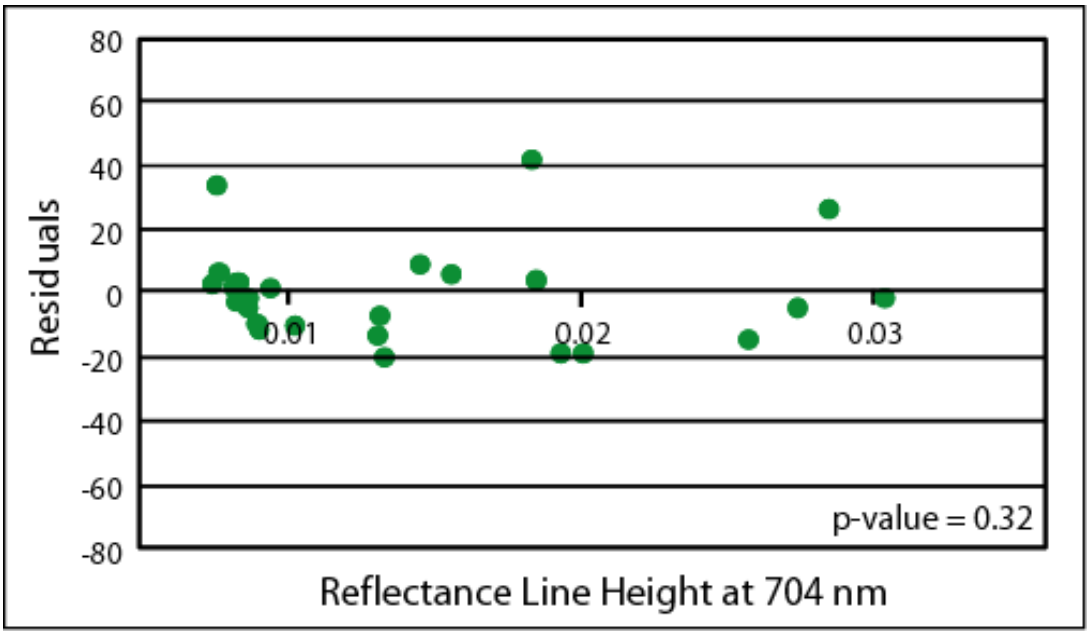

Regressions on PC Concentration

A regression was performed between PC concentration and the reflectance ratio which best predicted PC concentration (R_{704}/R_{619} (Simis, Peters, & Gons, 2005)) (Table 30).

Table 30- Morse Reservoir: Regression between PC Concentration and AISA Reflectance

Morse Regression Statistics PC Concentration					
R^2	0.827	Observations	22		
Standard Error	17.90				
	Regression Coefficients	Standard Error	p-value	Lower 95%	Upper 95%
Intercept	-60.05	11.15	$2.9*10^{-05}$	-83.31	-36.79
R_{704}/R_{628}	95.87	9.80	$4.6*10^{-09}$	75.43	116.30

The high R^2 indicates that this algorithm accounts for approximately 83% of the variation in PC concentration. Additionally, the very low p-value indicates that this reflectance algorithm should be included in the regression equation to predict PC concentration. A regression was carried out between PC concentration and reflectance, turbidity and TSS (Table 31).

Table 31- Morse Reservoir: Regression between PC Concentration and AISA Reflectance, TSS and Turbidity

Morse Regression Statistics PC Concentration					
R^2	0.896	Observations	22		
Standard Error	14.66				
	Regression Coefficients	Standard Error	p-value	Lower 95%	Upper 95%
Intercept	-39.51	11.01	$2.1*10^{-3}$	-62.65	-16.37
R_{704}/R_{628}	63.18	12.83	$1.1*10^{-4}$	36.22	90.13
TSS	2.92	1.44	0.06	-0.11	5.96
Turbidity	-4.37	3.77	0.26	-12.29	3.55

With this regression, R^2 increased slightly, indicating that more of the variation in PC concentration is explained by adding the variables turbidity and TSS. The p-values show that only the reflectance ratio is important for predicting PC concentration, while turbidity and TSS need not be included in the regression equation. To assess the role of TDS, it was added to the regression (Table 32).

Table 32- Morse Reservoir: Regression between PC Concentration and AISA Reflectance, TDS and TSS

Morse Regression Statistics PC Concentration					
R^2	0.831	Observations	22		
Standard Error	18.16				
	Regression Coefficients	Standard Error	p-value	Lower 95%	Upper 95%
Intercept	-258.54	304.34	0.41	-815.54	378.45
R_{704}/R_{628}	98.03	10.48	$1.5*10^{-08}$	76.10	119.96
TDS	737.02	1129.27	0.52	-1626.56	3100.60

The result of this regression reveals that TDS has very little effect on the prediction of PC concentration, similar to the Chl a regression.

Regression on PC Estimation Error

A regression between the squared errors of prediction from the first regression between PC concentration and the reflectance and several other variables is shown in Table 33.

Table 33- Morse Reservoir: Regression between PC Squared Prediction Residual and Chl a: PC, TDS, TSS and Turbidity

Morse Regression Statistics PC Squared Residuals					
R^2	0.191	Observations	21		
	Regression Coefficients	Standard Error	p-value	Lower 95%	Upper 95%
Intercept	7635.94	9404.50	0.43	-12300.70	27572.60
PC: Chl a Value	246.06	342.48	0.48	-479.97	972.09
TDS	-28.762.90	35144.19	0.43	-103.265	45739.45
TSS	-54.53	46.23	0.26	-152.53	43.47
Turbidity	147.68	121.16	0.24	-109.16	404.53

The results of the regression indicate that very little of the variation in the error is explained by the combination of these variables ($R^2 = 0.191$). The high p-values of the Chl a:

PC ratio, turbidity, TSS and TDS indicate that these parameters are statistically insignificant for predicting the error in PC estimation.

To determine the presence of any relationships between error and the value of the prediction, a graph of the two was created (Figure 38). The data in this case may show some heteroskedasticity, p = 0.08, but it is not statistically significant at the 95% level. Therefore, as the predicted value of PC increases, there is no statistically significant effect on the error of that estimated value.

Figure 38- Morse Reservoir PC Prediction Residuals vs. Reflectance Algorithm

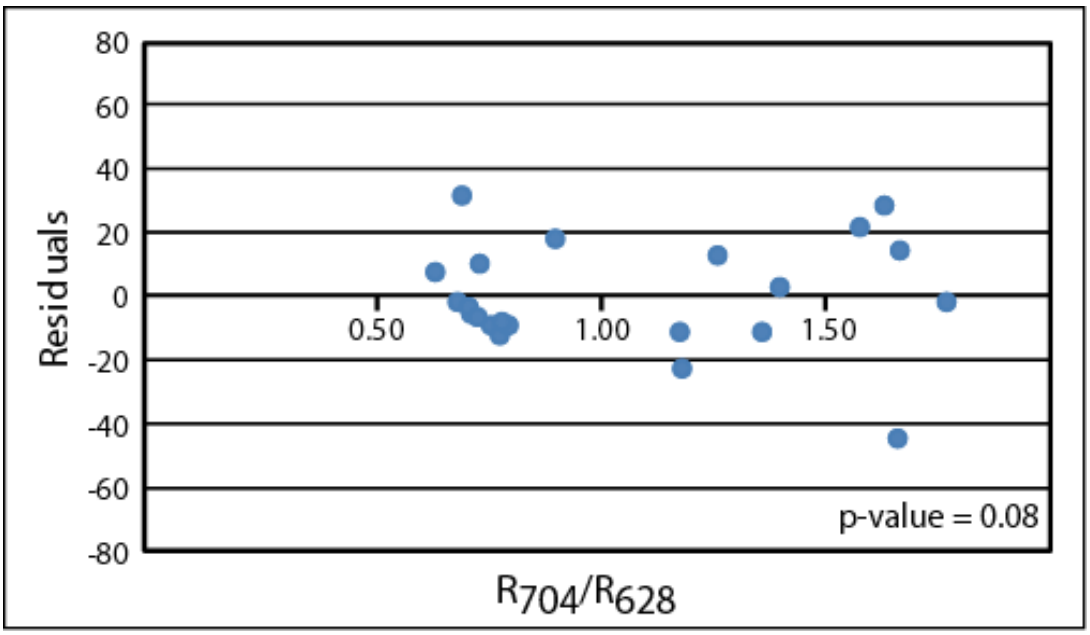

Summary of Morse Reservoir Statistics

The first regressions of either pigment, on Morse Reservoir show that reflectance gathered by the AISA sensor is statistically significant in predicting concentrations of Chl a and PC. With the first several regressions on Chl a, none of the selected constituents were statistically significant for predicting the concentration of the pigment. However, when the regression between the error of prediction and the constituents was performed, TDS is statistically significant for predicting the error. However, the negative relationship that TDS

had with error of prediction is opposite than expected. It would seem that with higher concentrations of TDS the error should increase, not the opposite. The regressions on PC concentration showed that only reflectance is statistically significant for predicting the pigment concentration. Furthermore, when the error was regressed against the water constituents, none of the constituents had a statistically significant relationship. The graphs of error versus reflectance indicate that the Chl a algorithm does not exhibit heteroskedasticity, while the PC algorithm weakly exhibits that property but is not statistically significant. A correlation between the pigments and the other parameters considered in the regressions of Morse Reservoir is shown in Table 49.

Eagle Creek Reservoir

The two best spectral ratios for pigment prediction were used for the regressions because spectral ratios, by nature, can account for uniform variation in the spectral data (Dekker, et al. 1992). Since there was no ground truth data for this reservoir, it was thought that by regressing spectral ratio algorithms, along with other constituents, a more accurate representation of how other water quality parameters affected pigment estimates could be achieved. It should be noted here that for Chl a estimation a spectral ratio algorithm did not yield the highest R^2; however, for PC estimation it did.

Regressions on Chl a Concentration

A regression of Chl a concentration and the best ratio algorithm (R_{704}/R_{675} (e.g. Dekker, 1993; Gitelson, et al., 2000)) can be seen in Table 34.

Table 34- Eagle Creek Reservoir: Regression between Chl a Concentration and AISA Reflectance

Eagle Creek Regression Statistics Chl a Concentration					
R^2	0.188	Observations	31		
Standard Error	22.05				
	Regression Coefficients	Standard Error	p-value	Lower 95%	Upper 95%
Intercept	-112.258	63.79	0.09	-242.72	-18.20
R_{704}/R_{675}	92.095	35.52	0.02	19.45	164.74

The R^2 in this regression is quite low, indicating that this algorithm explains very little of the variation in Chl a concentration in Eagle Creek Reservoir. However, because the p-value is 0.02, this regression shows that with only the reflectance variable in the regression equation, this ratio is statistically significant in predicting Chl a concentration. Table 35 shows the results of adding TSS and turbidity into the regression.

Table 35- Eagle Creek Reservoir: Regression between Chl a Concentration and AISA Reflectance, TSS and Turbidity

Eagle Creek Regression Statistics Chl a Concentration					
R^2	0.633	Observations	31		
Standard Error	15.364				
	Regression Coefficients	Standard Error	p-value	Lower 95%	Upper 95%
Intercept	134.66	65.656	0.05	-0.057	269.37
R_{704}/R_{675}	-79.728	39.77	0.06	-161.32	1.88
TSS	0.385	2.49	0.88	-4.73	5.50
Turbidity	9.87	4.15	0.03	1.36	18.38

The R^2 increases dramatically, so much more of the pigment variation is explained by this regression equation. Turbidity is much more important for predicting Chl a than TSS, and is the only variable, of the parameters tested, that is statistically significant. The third regression between Chl a and reflectance, TDS and turbidity is shown in Table 36.

Table 36- Eagle Creek Reservoir: Regression between Chl a Concentration and AISA Reflectance and TDS

Eagle Creek Regression Statistics Chl a Concentration					
R^2	0.704	Observations	31		
Standard Error	13.79				
	Regression Coefficients	Standard Error	p-value	Lower 95%	Upper 95%
Intercept	428.50	126.75	2.0*10-3	168.42	688.58
R_{704}/R_{675}	-44.14	37.905	0.25	-121.91	33.63
TDS	-1496.15	585.41	0.02	-2697.3	-294.98
Turbidity	13.18	1.96	$3.1*10^{-7}$	9.163	17.19

This regression indicates that TDS and turbidity account 70% of the variation on pigment concentration is described by this regression equation. What it also revealed in this regression is that both TDS and turbidity are statistically significant in predicting Chl a concentration, while the reflectance ratio does not.

Regression on Chl a Estimation Error

The squared residuals from the first regression were regressed against several other water quality parameters to investigate any relationships (Table 37).

Table 37- Eagle Creek Reservoir: Regression between Chl a Prediction Squared Residuals and Chl a: PC, TDS, TSS and Turbidity

Eagle Creek Regression Statistics Chl a Squared Residuals					
R^2	0.316	Observations	28		
	Regression Coefficients	Standard Error	p-value	Lower 95%	Upper 95%
Intercept	8839.61	4959.53	0.09	-1419.95	19099.18
PC: Chl a Value	-374.658	159.94	0.03	-705.527	-43.79
TDS	-33410.60	20696.02	0.12	-76223.60	9402.34
TSS	-14.13	88.14	0.87	-196.46	168.204
Turbidity	118.06	165306	0.48	-223.39	459.51

This regression shows that while these variables predict the variation in the error poorly, the PC: Chl a value has a significant positive effect on the prediction error.

Additionally, a graph of the relationship between the residuals and predicted Chl a concentration (Figure 39) shows that there is a high variability in the error, and it is statistically significantly related to the value of the independent variable ($p = 0.04$).

Figure 39- Eagle Creek Reservoir Chl a Prediction Residual vs. Reflectance Algorithm

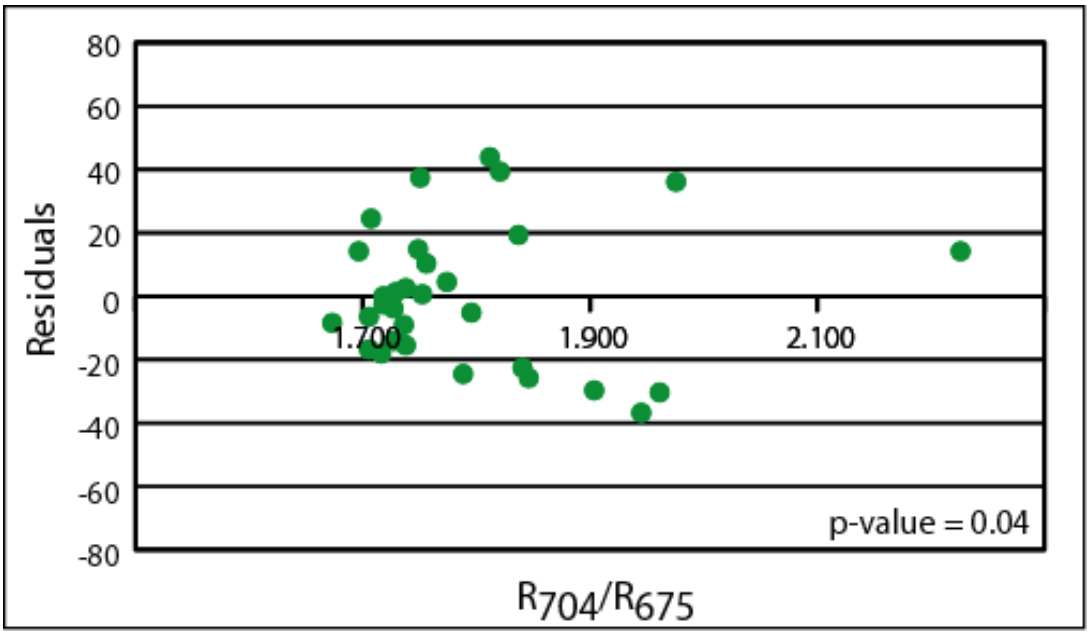

Regressions on PC Concentration

A regression between the measured PC concentration and the reflectance ratio R_{704}/R_{675} can be seen in Table 38.

Table 38- Eagle Creek Reservoir: Regression between PC Concentration and AISA Reflectance

Eagle Creek Regression Statistics PC Concentration					
R^2	0.159	Observations	29		
Standard Error	24.07				
	Regression Coefficients	Standard Error	p-value	Lower 95%	Upper 95%
Intercept	272.23	82.03	4.0*10-3	95.71	448.74
R_{704}/R_{619}	-137.244	60.70	0.03	-261.80	-12.69

The R^2 in this regression is low, revealing that the reflectance algorithm explains very little (16%), of the variation in PC concentration. However, because the p-value is 0.03, the reflectance is significant in predicting pigment concentration in the reservoir. A regression of reflectance, TSS and turbidity on PC is shown in Table 39.

Table 39- Eagle Creek Reservoir: Regression between PC Concentration and AISA Reflectance, TSS and Turbidity

Eagle Creek Regression Statistics PC Concentration					
R^2	0.405	Observations	29		
Standard Error	21.04				
	Regression Coefficients	Standard Error	p-value	Lower 95%	Upper 95%
Intercept	374.67	92.90	$4.6*10^{-4}$	183.04	565.69
R_{704}/R_{628}	-244.80	69.171	$1.6*10^{-3}$	-387.26	-102.342
TSS	5.54	3.44	0.12	-1.55	12.64
Turbidity	-2.23	5.45	0.69	-13.44	8.99

R^2 increases quite a bit, so much more of the pigment variation is explained by this regression equation. The p-values indicate that reflectance is still the most important variable for predicting PC, while TSS and turbidity are not statistically significant. To assess the effect of the dissolved component, a regression between pigment concentration, reflectance and TDS is shown in Table 40.

Table 40- Eagle Creek Reservoir: Regression between PC Concentration and AISA Reflectance and TDS

Eagle Creek Regression Statistics PC Concentration					
R^2	0.176	Observations	29		
Standard Error	24.28				
	Regression Coefficients	Standard Error	p-value	Lower 95%	Upper 95%
Intercept	192.73	139.90	0.18	-94.82	480.29
R_{704}/R_{628}	-177.22	82.43	0.04	-346.66	-7.78
TDS	547.21	755.23	0.48	-105.19	2099.60

This third regression indicates that 17.6% of the variation on pigment concentration is described by this regression equation. This R^2 is slightly increased from the first regression, but a drop from the second regression. TDS is statistically insignificant for predicting PC concentration.

Regression on PC Estimation Error

The squared residuals from the first regression between PC concentration and reflectance were regressed against other water quality parameters to discover any relationships (Table 41).

Table 41- Eagle Creek Reservoir: Regression between PC Squared Prediction Residuals and Chl a: PC, TDS, TSS and Turbidity

Eagle Creek Regression Statistics PC Squared Residuals					
R^2	0.277	Observations	28		
	Regression Coefficients	Standard Error	p-value	Lower 95%	Upper 95%
Intercept	-14054.5	6668.82	0.05	-27849.6	-259.42
PC: Chl a Value	-372.22	215.06	0.10	-817.1	-817.11
TDS	64263.61	27828.04	0.03	6696.92	121830.3
Turbidity	75.82	118.51	0.53	-169.34	320.98
TSS	-298.82	221.94	0.19	-757.99	160.25

This regression shows that the combination of these variables (PC: Chl a value, TDS, Turbidity and TSS) explains 27% of the variation in the prediction error. Only TDS has a significant effect on the prediction error. The regression coefficient is positive, so as the TDS concentration increases, so will the error of the prediction.

A graph of the relationship between the residuals and predicted PC concentration can be found in Figure 40. While this graph shows that there is a high variability in the error, it is not related to the value of the independent variable ($p = 0.23$).

Figure 40- Eagle Creek Reservoir PC Prediction Residuals vs. Reflectance Algorithm

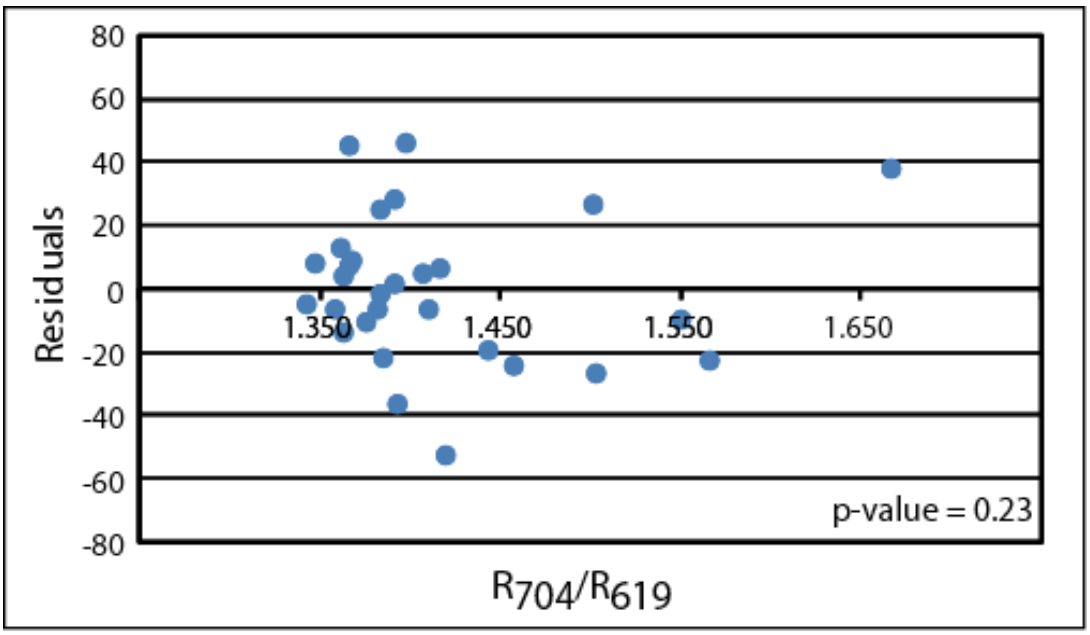

Summary of Eagle Creek Reservoir Statistics

If no other variables are considered, reflectance is statistically significant in predicting the concentrations of pigments in Eagle Creek Reservoir. The regressions of Chl a concentration indicate that turbidity and TDS are significant for predicting the concentration of the pigment. However, when the error is considered, it shows that the ratio of PC to Chl a is related to the error of the prediction, and not turbidity and TDS. The regressions on PC concentration indicate that none of the other water quality constituents

were significant for predicting pigment concentration. Yet, when the squared error was regressed against, the concentration of TDS in the reservoir was significantly related to the error. All of the regressions in Eagle Creek Reservoir were done with the assumption that the atmospheric calibration has accounted for all of the spectral effects caused by the atmospheric path radiance. A correlation between the pigments and the other parameters considered in the regressions of Eagle Creek Reservoir is shown in Table 42.

Table 42- Eagle Creek Reservoir Correlation Matrix

		Chl a	*PC*	*TDS*	*TSS*	*Turbidity*
Eagle Creek Reservoir	*Chl a*	1.00				
	PC	0.40	1.00			
	TDS	0.41	-0.14	1.00		
	TSS	0.75	0.25	0.69	1.00	
	Turbidity	0.76	0.12	0.81	0.95	1.00

Only sites where all of the data was available were used for the correlations.

While this assumption was also made with the other reservoirs, because of the lack of ground truth data this assumption is more likely to be incorrect, causing all of these regression values and the relationships to be meaningless.

PC: Chl a Value

The PC: Chl a value may indicate the proportion of cyanobacteria in the overall population of phytoplankton. For example the PC: Chl a value of Geist Reservoir, 0.637, indicates that there is either a low intercellular PC: Chl a value or the phytoplankton community is dominated y other species (Simis, et al., 2007). Variable PC: Chl a values are not accounted for by semi-empirical algorithms (Simis, et al., 2007), however work done by Schalles, et al. (1998) indicates that this is not an issue for Chl a estimation. In their work, they found that throughout an entire season of their study site, a single NIR/RED prediction algorithm could be used which was not hampered by differing dominant phytoplankton species. This is mirrored by the findings of this study in Geist and Morse Reservoirs, where the ratio of PC: Chl a, whether it is related to differing phytoplankton species or intercellular

concentration, is not significantly related to the prediction error. This also seems to be the situation with PC, where the pigment concentration ratio is not significantly related to the PC prediction error in either reservoir. However, Eagle Creek Reservoir seems to be a different situation altogether. The PC: Chl a value did have an effect on the Chl a prediction error, while this was shown to not be a significant issue with the type of algorithm used by Schalles et al. (1998). What is also interesting is the ratio of the pigment concentration does not have a significant effect on the PC prediction error. While the Ratio of PC: Chl a seems on par with the other reservoirs, the standard deviation of the ratio is higher, and the correlation between Chl a and PC is low compared to the other reservoirs (Table 43). For Eagle Creek Reservoir, this indicates that as Chl a concentration increases, PC concentration may or may not increase and vice versa.

Table 43- Correlation between Chl a Concentration and PC Concentration for each Reservoir

Reservoir	Average PC: Chl a Value	Standard Deviation of the PC: Chl a Value	Correlation between Measured Chl a and PC Concentrations
Geist	0.637	0.46	0.723
Morse	1.92	0.46	0.878
Eagle Creek	1.62	0.66	0.398

It is not known whether the correlation between the pigment concentrations is something that needs to be considered when predicting pigment concentrations from reflectance data of Eagle Creek Reservoir, but because of the image processing issue the answer cannot be determined from this data.

Algorithm Comparison, Geist and Morse Reservoirs

Another aspect of this research was to elucidate the causes of algorithm success between these reservoirs. To do this regression, analyses were performed similar to before, yet looking at the causes of poor prediction of an algorithm in one reservoir which

preformed best in another reservoir (Eagle Creek Reservoir data was left out of this analysis). The algorithms which performed best in Morse Reservoir (Chl a: Height of a reference line at 704 nm and PC: R_{704}/R_{619}) were chosen from the Geist Reservoir data set. The error of prediction of these algorithms was then regressed against the parameters Chl a: PC ratio, TDS, TSS and Turbidity to reveal what impedes the success of these algorithms in Geist Reservoir (Table 44). This was also preformed for Morse Reservoir (Table 45). For ease of clarification, these will be referred to as "reverse-best algorithms".

Table 44- Geist Reservoir Regression between Chl a Residuals and PC: Chl a Value, TDS, TSS and Turbidity

Geist Regression Statistics Chl a Squared Residuals					
R^2	0.147	Observations	24		
	Regression Coefficients	Standard Error	p-value	Lower 95%	Upper 95%
Intercept	1029.25	2262.58	0.65	-3706.41	5764.86
PC: Chl a Value	-126.81	330.30	0.71	-818.13	564.50
TDS	-229.52	5464.46	0.97	-11666.80	11207.72
Turbidity	-13.46	89.29	0.88	-200.344	173.42
TSS	-5.79	43.54	0.90	-96.92	85.34

Table 45- Morse Reservoir Regression between Chl a Residuals and PC: Chl a Value, TDS, TSS and Turbidity

Morse Regression Statistics Chl a Squared Residuals					
R^2	0.679	Observations	24		
	Regression Coefficients	Standard Error	p-value	Lower 95%	Upper 95%
Intercept	20970.66	11687.2	0.09	-3805.11	45746.42
PC: Chl a Value	-463.01	425.61	0.29	-1365.26	439.25
TDS	-77649.3	43674.53	0.09	-170235.00	14936.54
Turbidity	-70.69	150.57	0.65	-389.88	248.50
TSS	52.79	57.45	0.37	-69.00	174.58

The Chl a regressions do not reveal that any of these parameters are affecting the performance of the reverse-best algorithms in Geist or Morse reservoirs. Therefore other factors such as atmospheric calibration or sampling errors may be causing the algorithms to predict erroneously. Similar regressions were performed for the prediction of PC in Geist and Morse reservoirs (Geist best algorithm: $R_{600-628}$, Morse: $R_{704/619}$) (Tables 46 and 47).

Table 46- Geist Reservoir Regression between PC Residuals and PC: Chl a Value, TDS, TSS and Turbidity

Geist Regression Statistics PC Squared Residuals					
R^2	0.679	Observations	24		
	Regression Coefficients	Standard Error	p-value	Lower 95%	Upper 95%
Intercept	-6885.81	5991.53	0.26	-19426.2	5654.60
PC: Chl a Value	339.22	874.65	0.70	-1491.45	2169.89
TDS	6143.10	14470.41	0.68	-24143.8	36430.02
Turbidity	541.36	236.44	0.03	46.48	1036.242
TSS	-11.06	115.30	0.92	-252.38	230.26

Table 47- Morse Reservoir Regression between PC Residuals and PC: Chl a Value, TDS, TSS and Turbidity

Morse Regression Statistics PC Squared Residuals					
R^2		Observations			
	Regression Coefficients	Standard Error	p-value	Lower 95%	Upper 95%
Intercept	-38781.93	24973.01	0.14	-91722.34	14158.48
PC: Chl a Value	282.02	909.44	0.76	-1645.91	2209.94
TDS	149382.94	93322.97	0.13	-48452.92	347218.79
Turbidity	-743.97	321.73	0.03	-1426.01	-1426.01
TSS	357.93	122.76	0.01	97.70	97.69526

As indicated by the regression of the best algorithm to predict PC for Morse Reservoir as applied to the Geist Reservoir data, turbidity has a statistically significant affect on how this algorithm predicts PC. The regression shows (due to the sign of the coefficient) that as turbidity increases, the error of estimation increases as well. For Morse Reservoir turbidity

and TSS affect the performance of the reverse-best algorithm. Indicating that as turbidity increases the error will decrease, and as TSS increases the error will increase.

The following tables show the correlations of parameters for each reservoir (Tables 48 and 49).

Table 48- Geist Reservoir Correlation Matrix

		Chl a	*PC*	*TDS*	*TSS*	*Turbidity*
Geist Reservoir	*Chl a*	1.00				
	PC	0.74	1.00			
	TDS	-0.71	-0.89	1.00		
	TSS	0.51	0.43	-0.43	1.00	
	Turbidity	0.25	-0.09	0.07	0.69	1.00

Only sites where all of the data was available were used for the correlations.

Table 49- Morse Reservoir Correlation Matrix

		Chl a	*PC*	*TDS*	*TSS*	*Turbidity*
Morse Reservoir	*Chl a*	1.00				
	PC	0.88	1.00			
	TDS	-0.05	-0.23	1.00		
	TSS	0.86	0.87	0.11	1.00	
	Turbidity	0.87	0.87	0.15	0.98	1.00

Only sites where all of the data was available were used for the correlations.

In Geist Reservoir the correlation between both pigments (Chl a and PC) and TSS and Turbidity are generally low (<0.51), indicating that quite a bit of non-algal particles are present in the reservoir. For Morse Reservoir, it is opposite. A much higher correlation exists between pigments and TSS/ turbidity, indicating that the particulate matter is dominated by algae. This is important to understanding the performance of the two PC algorithms, in each reservoir.

In Geist Reservoir the reverse best algorithm has error that is statistically significantly related to turbidity. This makes sense because at the time of ample collection in Geist Reservoir the turbidity was mostly non-algal and is of higher concentration than in Morse Reservoir. In Morse Reservoir there is less turbidity so it would seem that the

turbidity should not be correlated to the error of the $R_{600-628}$ algorithm. However, that coefficient is negative, indicating that a decrease in turbidity causes the error increase. This makes sense because the turbidity at the time of collection in Morse Reservoir is mostly algal, indicating that with less turbidity (less algae) there is less reflectance for the algorithm to predict from. One might also think that because TSS was higher in Geist reservoir, that it should not be related to the error of prediction in Morse Reservoir. This is likely caused by the fact that at the time of collection the TSS was highly correlated to PC concentration in Morse Reservoir, which is different than in Geist Reservoir. The correlation means that in Morse Reservoir, locations of high PC concentration also have high concentration of TSS. Therefore, TSS is present to cause prediction errors. It appears that the type (algal or non-algal) of turbidity and the correlation of TSS to the PC concentration affects the performance of the PC algorithms in each reservoir.

10.0 Conclusions and Future Work

Conclusions

The results of this study show that airborne hyperspectral reflectance are statistically significant ($p < 0.03$) in predicting Chl a or PC pigment concentration in all three reservoirs without the consideration of other parameters. This demonstrates that airborne hyperspectral imagery can be used to estimate pigment concentrations in these reservoirs.

In cases where ground truth data were available for the reservoir, i.e. Geist and Morse Reservoirs, the p-value for both pigments was much smaller, $p < 0.00001$, than for Eagle Creek Reservoir ($p < 0.03$)(where the atmospheric calibration factors were taken from Geist Reservoir). These results indicate that proper atmospheric calibration is a key component in predicting pigment concentration from AISA imagery. Furthermore, there is no consistency between reservoirs on whether one pigment is predicted more accurately than the other.

With Geist and Morse Reservoir, there are few significant variables from the regressions between the prediction error and other water quality constituents. The low p-values of the regression variables, for both Geist and Morse Reservoirs, indicate that the error in prediction is not caused by other optically active constituents (i.e. TDS, TSS and Turbidity) but by other sources mentioned in the error section. With Eagle Creek Reservoir, the situation is different, indicating that the PC: Chl a Value will cause errors in prediction for Chl a and TDS will cause errors in PC prediction.

The results of this study show that different algorithms explain the variation in pigment concentration most accurately for Geist and Morse even though the concept, i.e. the areas of the spectrum used, behind the algorithms is the same (due to the lack of ground truth data for Eagle Creek Reservoir, it was not considered). This may indicate that it will be difficult to create a single semi-empirical model to work in both reservoirs. This may also indicate that the reservoirs are fundamentally different, but more data are needed to

support this conclusion. Through regression analysis, it appears that the cause of the differing performance of the PC algorithms in Geist and Morse Reservoir type of turbidity (algal or non-algal) and the correlation of TSS to the PC concentration. This study was unable to determine the cause of differing algorithm performance for Chl a prediction between reservoirs. The fact that Morse Reservoir was dominated by algal turbidity on the day of sampling may also explain why, in general, pigment estimation algorithms performed better. The type of algal turbidity may also explain why the when the data were logged the algorithms for Geist Reservoir improved while the data for Morse Reservoir did not need that transformation.

The ratio of Chl a concentration to PC concentration, i.e. the type phytoplankton present or physiological state of the phytoplankton, has no effect on the prediction of the pigment concentration for Geist and Morse reservoirs. However, for Eagle Creek Reservoir it does affect the prediction of Chl a. This could indicate that Eagle Creek Reservoir has differing phytoplankton populations and, contrary to the study done by Schalles et al. (1998), the ratio of phytoplankton pigments is a problem for this algorithm to account for. Or this may be caused by the unique situation of the Eagle Creek Reservoir data.

Summary of Contributions

1) This study has shown that in central Indiana reservoirs, certain photosynthetic pigments (Chl a and PC), attributed to cyanobacteria, can be estimated from airborne hyperspectral imagery.
2) This work has also outlined the success of several different previously published algorithms as they are applied to each reservoir in the study.
3) Findings from the literature review indicate that this is the first study to use AISA hyperspectral airborne imagery to estimate PC concentration; and the first attempt

to quantify photosynthetic pigments in small, Case II waters from airborne imagery of central Indiana.

4) This study has allowed the creation of high resolution pigment concentration maps for the three reservoirs in the study, providing water resource managers with an important visual tool.
5) This study also shows that on the day of sample collection, the success of the algorithms to predict the concentration of PC was dependent upon turbidity and TSS in the reservoir.

Future Research

For future research, it would be interesting to see similar work done on the three reservoirs of this study. Companion studies which explored temporal variation, expanded constituent quantification (e.g. TSS or CDOM) or those that expanded to different study sites area would be particularly interesting.

Another route that might be interesting to explore would be to create a spectral catalogue of pseudoinvariant features surrounding the reservoirs. Thus, it would eliminate the need for concurrent field sampling to remove the effects of atmospheric path radiance of the image. This type of data would be useful for the calibration of both airborne and satellite imagery.

If this study were repeated, it is suggested to try different airborne platforms to gather the data. Possibly one with a higher signal to noise ratio to improve the data collected. It is also suggested to tune the bands of the collected imagery to phytoplankton pigments of interest, i.e. higher spectral resolution around key features of the spectrum. Another way to improve the ease of using airborne data would be to collect the entirety of a reservoir with fewer swaths, thus reducing the image processing needed. Furthermore, it

may be inadequate to calibrating an 8 million pixel image with only 27 sample sites, i.e. 250 pixels, especially when some of those sites are removed due to lab errors. It is suggested to do a study to determine the minimum number of image calibration points.

11.0 Appendix

Summary of Parameters by Reservoir

Geist Reservoir								
Sample Site	**Measured Chl a ug/L**	**Predicted Chl a ug/L**	**Measured PC ug/L**	**Predicted PC ug/L**	**PC: Chl a Value**	**TDS g/L**	**TSS mg/L**	**Turbidity NTU**
GR 236	118.90	86.94	155.56	173.62	1.12	0.301	22.4	11
GR 237	84.46	80.07	135.56	130.64	0.96	0.300	17.2	9.3
GR 238			118.94	123.22		0.300	19.6	9.5
GR 239	111.32	83.60	130.56	160.48	1.23	0.304	18.8	8.7
GR 240	107.73	90.93	185.06	120.75	0.65	0.301	23.2	11
GR 241	98.89	86.56	159.94	103.68	0.65	0.302	25.6	9.5
GR 242	59.98	78.98	98.69	107.75	1.09	0.301	18.8	9.6
GR 243	76.14	68.08	88.94	110.02	1.24	0.303	19.2	9.2
GR 244	92.04	80.69	102.06	79.26	0.78	0.300	17.2	9.5
GR 245	51.80	86.55	120.81	112.64	0.93	0.301	19.2	9.3
GR 246	68.63	87.45	136.31	106.60	0.78	0.300	26.4	11
GR 247			76.81	103.12	1.34	0.307	20	10
GR 248			84.31	96.23	1.14	0.305	24.8	11
GR 249	74.21	86.99	107.31	94.31	0.88	0.310	29.2	12
GR 250	100.55	84.87	119.56	90.76	0.76	0.308	24.4	12
GR 251	105.80	91.33	96.19	76.27	0.79	0.302	23.2	11
GR 252	62.11	79.15	110.81	85.51	0.77	0.307	24.8	10
GR 253	88.51	77.54	117.94	85.43	0.72	0.306	23.2	11
GR 254	58.72	79.54	75.56	120.97	1.60	0.343	16.8	9.5
GR 255	50.81	54.62	65.31	75.69	1.16	0.344	14.4	9.2
GR 256	55.73	57.61	46.31	60.66	1.31	0.358	18.8	13
GR 257	35.05	38.32	37.44	54.60	1.46	0.366	16	8.3
GR 258	45.49	40.36	53.20	38.50	0.72	0.361	15.2	7
GR 259	37.64	42.13	57.75	43.63	0.76	0.362	13.2	7.7
GR 260	51.07	44.02	30.81	39.58	1.28	0.364	18.8	11
GR 261	48.15	57.32	27.06	28.49	1.05	0.365	15.2	9
GR 262	72.22	88.45	25.20	26.09	1.04	0.369	28.4	18
n	24	24	27	27	26	27	27	27
Average	73.16	73.00	94.96	90.69	1.01	0.32	20.52	10.27
Standard Deviation	24.96	17.78	42.79	37.42	0.27	0.03	4.36	2.05
Minimum	35.05	38.32	25.20	26.09	0.65	0.30	13.20	7.00
Maximum	118.90	91.33	185.06	173.62	1.60	0.37	29.20	18.00

Blank cells indicate missing data, data in which the error between duplicates >30% or data with high studentized residuals

Predicted pigment values based on best algorithms

Morse Reservoir								
Sample Site	**Measured Chl a ug/L**	**Predicted Chl a ug/L**	**Measured PC ug/L**	**Predicted PC ug/L**	**PC: Chl a Value**	**TDS g/L**	**TSS mg/L**	**Turbidity NTU**
MR 271	32.92	30.87	2.97	10.94	0.09	0.270	12	5.6
MR 272	28.26	25.28				0.269	7.2	4
MR 273	22.68	21.43	2.45	12.70	0.11	0.268	4.4	2.9
MR 274	26.40	26.11	2.19	7.68	0.08	0.268	4.8	2.7
MR 275	28.46	26.99	7.15	13.95	0.25	0.268	5.2	2.3
MR 276	21.95	27.42	3.41	5.87	0.16	0.268	6	2.6
MR 277	25.47	27.41				0.268	5.6	2.3
MR 278	22.41	27.41	4.29	7.50	0.19	0.269	6.4	2.8
MR 279	28.66	25.97	6.91	12.98	0.24	0.268	4.8	3
MR 280	18.02	30.04	2.89	8.86	0.16	0.267	8.4	4.9
MR 281	26.13	37.51	8.22	2.26	0.31	0.268	7.2	2.8
MR 282	19.02	29.30	4.46	4.71	0.23	0.268	4.4	2.4
MR 283			38.06	6.42		0.267	4.8	2.3
MR 284	25.94	26.75	20.30	9.16	0.78	0.267	6	3.1
MR 285	54.46	22.05	44.45	22.29	0.82	0.264	10	3.8
MR 286	33.65	49.83	29.84	46.55	0.89	0.264	7.6	3.4
MR 287	45.95	52.18	58.45	64.19	1.27	0.263	9.6	4.8
MR 288	39.63	50.45	41.12	46.22	1.04	0.264	8.8	4.6
MR 289	70.16	56.01				0.263	14.4	6.4
MR 290	73.35	64.75	54.34	97.45	0.74	0.262	10	5.3
MR 291	70.69	87.55	73.24	54.06	1.04	0.260	11.2	5.5
MR 292	125.53	80.18	76.47	68.34	0.61	0.260	23.6	8.9
MR 293	88.38	78.11	124.69	94.05	1.41	0.265	26	9.1
MR 294	74.55	89.39	107.36	110.26	1.44	0.264	36.8	12
MR 295	111.70	125.99	112.16	87.70	1.00	0.265	44	18
MR 296	151.69	159.27	113.56	98.05	0.75	0.277	42.8	18
MR 297	168.58	145.60				0.281	53.2	19
MR 298	131.56	139.49				0.278	54.4	30
n	27	27	23	23	22	28	28	28
Average	58.01	57.90	40.82	38.79	0.62	0.27	15.70	6.88
Standard Deviation	44.28	41.79	41.81	37.38	0.46	0.00	15.64	6.70
Minimum	18.02	21.43	2.19	2.26	0.08	0.26	4.40	2.30
Maximum	168.58	159.27	124.69	110.26	1.44	0.28	54.40	30.00

Blank cells indicate missing data or data in which the error between duplicates >30%

Predicted pigment values based on best algorithms

Eagle Creek Reservoir								
Sample Site	**Measured Chl a ug/L**	**Predicted Chl a ug/L**	**Measured PC ug/L**	**Predicted PC ug/L**	**PC: Chl a Value**	**TDS g/L**	**TSS mg/L**	**Turbidity NTU**
ECR 200	50.27	48.08	72.71	66.18	1.45	0.245	11	5
ECR 201	49.81	48.77	126.44	70.71	2.54	0.244	12	4.3
ECR 202	28.20	47.18	72.94	82.11	2.59	0.245	10	4.8
ECR 203	32.85	48.12	80.81	77.44	2.46	0.245	11	4.7
ECR 204	58.39	46.44	98.35	91.53	1.68	0.245	12	5.6
ECR 205	32.98	47.62	79.19	93.07	2.40	0.244	12	5.5
ECR 206	63.84	48.64	71.56	89.56	1.12	0.245	15	6.4
ECR 207	98.95	52.20	83.31	73.98	0.84	0.244	15	7.8
ECR 208			130.46	87.61		0.244	9	4.7
ECR 209	33.45	45.71				0.244	11	4.4
ECR 210	42.76	47.58	92.44	88.11	2.16	0.246	11	4.8
ECR 211	28.40	46.74	95.37	101.97	3.36	0.245	8	4.4
ECR 212	38.77	46.74	83.30	106.68	2.15	0.246	9	3.9
ECR 213	38.64	48.04	75.81	78.39	1.96	0.245	8	4.3
ECR 214	55.53	49.90	107.71	77.58	1.94	0.244	10	4.8
ECR 215	43.69	47.25	89.16	89.69	2.04	0.244	10	4
ECR 216	69.83	46.84		92.45		0.244	11	5.1
ECR 217	45.95	47.24	93.10	86.46	2.03	0.245	9	3.9
ECR 218	86.52	48.68	109.72	73.50	1.27	0.243	10	4.7
ECR 219	60.18	48.99	60.20	76.38	1.00	0.243	7	4.3
ECR 220	38.30	64.91	50.06	50.00	1.31	0.245	12	5.5
ECR 221	30.32	63.22	35.06	50.98	1.16	0.242	10	4.8
ECR 222	48.41	47.70	44.94	72.99	0.93	0.244	7	3.6
ECR 223	32.12	54.59	47.81	54.52	1.49	0.255	10	5
ECR 224	27.93	50.68	24.56	63.16	0.88	0.255	8	4.4
ECR 225	35.11	54.20	54.42	57.02	1.55	0.255	11	5.5
ECR 226	33.45	59.39	39.29	49.85	1.17	0.257	10	5.3
ECR 227	94.70	52.75				0.256	15	8.6
ECR 228	48.28	51.14	84.06	67.44	1.74	0.259	12	6.7
ECR 229	76.28	53.91	83.94	63.75	1.10	0.257	16	9.7
ECR 230	106.20	66.60	93.06	49.89	0.88	0.260	19	11
ECR 231	107.07	102.50	81.94	71.96	0.77	0.28	24	15
n	31	31	29	30	28	32	32	32
Average	52.81	52.66	77.99	75.17	1.64	0.25	11.41	5.70
Standard Deviation	24.06	10.78	25.77	15.81	0.66	0.01	3.52	2.39
Minimum	27.93	45.71	24.56	49.85	0.77	0.24	7.00	3.60
Maximum	107.07	102.50	130.46	106.68	3.36	0.28	24.00	15.00

Blank cells indicate missing data or data in which the error between duplicates >30%

Predicted pigment values based on best algorithms

12.0 Works Cited

Adler-Golend, S. M., Matthew, M. W., Bernstein, L. S., Levine, R. Y., Berk, A., Richtsmeier, S., et al. (1999). Atmospheric correction for short-wave spectral imagery based on MODTRAN4. *Part of the SPIE Conference on Imaging Spectrometry V , 3753*, 61-69.

Backer, L. C. (2002). Cyanobacterial harmful algal blooms (CyanoHABs): developing a public health response. *Lake and Reservoir Management , 18*, 20-31.

Brando, V. E., & Dekker, A. G. (2003). Satellite hyperspectral remote sensing for estimating estuarine and coastal water quality. *IEEE Transactions on Geoscience and Remote Sensing , 41*, 1378-1387.

Bukata, R. P., Jermoe, J. H., Kondratyev, K. Y., & Pozdnyakov, D. V. (1995). *Optical Properties and Remotes Sensing of Inland and Coastal Waters.* Boca Raton: CRC Press.

Carmichael, W. W. (2001). Health effects of toxin-producing cyanobacteria: "The CyanoHABs". *Human and Ecological Risk Assesment , 7*, 1393-1407.

Carmichael, W. W. (1994). The toxins of cyanobacteria. *Scientific American* , 78-86.

Carmichael, W. W. (1988). Toxicity and partial structure of a hepatotoic peptide produced by the cyanobacterium Nodularia spumigena Mertens emend L575 from New Zealand. *American Society for Microbiology , 54*, 2257-2263.

Caselles, V., & Lopez Garcia, M. J. (1989). An alternative simple approach to estimate atmorpheric correction in multitemporal studies. *International Journal of Remote Sensing , 10*, 1127-1134.

Chorus, I., & Bartram, J. (1999). *Toxic Cyanobacteria in Water: A Guide to Their Public Health Consequences, Monitoring and Mangement.* London: E & FN Spoon.

Cohen, W. B., Maiersperger, T. K., Spies, T. A., & Oetter, D. R. (2001). Modelling forest cover attributes as continuous variables in a regional context with Thematic Mapper data. *International Journal of Remote Sensing , 22*, 2279-2310.

Coppin, P. R., & Bauer, M. E. (1994). Processing of multitemporal Landsat TM imagery to optimize extraction of forest cover change features. *IEEE Transactions on Geoscience and Remote Sensing , 32*, 918-927.

Dall'Olmo, G., Gitelson, A. A., Rundquist, D. C., Leavitt, B., Barrow, T., & Holz, J. C. (2005). Assessing the potential of SeaWiFS and MODIS for estimating chlorophyll concentration in turbid productive water using red and near-infrared bands. *Remote Sensing of Environment , 96*, 176-187.

Dekker, A. G. (1993). *Detection of Optical Water Quality Parameters for Eutrophic Waters by High Resolution Remote Sensing.* Vrije University Amsterdam.

Dekker, A. G., Malthus, T. J., Wijnen, M. M., & Seyhan, E. (1992). Remote sensing as a tool for assessing water quality in Loosdrecht lakes. *Hydrobiologia , 233*, 137-159.

Du, Y., Cihlar, J., Beaubien, J., & Latifovic, R. (2001). Radiometric normalization, compositing, and quality control for satellite high resolution image mosaics over large areas. *IEEE Transactions on Geoscience and Remote Sensing , 39*, 623-634.

Du, Y., Teillet, P. M., & Cihlar, J. (2002). Radiometric normalization of multitemporal high-resolution satellite images with quality conrtol for land cover change detection. *Remote Sensing of Environment , 82*, 123-134.

Eckhardt, D. W., Verdin, J. P., & Lyford, G. R. (1990). Automated update of an irrigated lands GIS using SPOT HRV imagery. *Photogrammetric Engineering & Remote Sensing , 56*, 1515-1522.

Elvidge, C. D., Yuan, D., Weerackoon, R. D., & Lunetta, S. R. (1995). Relative radiometric normalization of Landsat Multispectral Scanner (MSS) data using an automatic scattergram-controlled regression. *Photogrammetric Engineering & Remote Sensing , 61*, 1255-1260.

EPA. (1997). In virto determination of chlorophyll a and pheophytin a in marine and freshwater algae by fluorescence. *Method 445.0, Revision 1.2* . Cincinnati, Ohio: U. S. Environmental Protection Agency.

Fraser, R. N. (1998). Hyperspectral remote sensing of turbidity and chlorophyll a among Nebraska Sand Hills lakes. *International Journal of Remote Sensing , 19*, 1579-1589.

Giardino, C., Candiani, G., & Zilioli, E. (2005). Detecting chlorophyll-a in Lake Garda using TOA MERIS radiances. *Photogrammetric Engineering & Remote Sensing , 71*, 1045-1051.

Gitelson, A. A. (1993). Algorithms for remote sensing of phytoplankton pigments in inland waters. *Advances in Space Research , 13*, 197-201.

Gitelson, A. A. (1992). The peak near 700 nm on radiance spectra of algae and water: relationships of its magnitude and position with chlorophyll concentration. *International Journal of Remote Sensing , 13*, 3367-3373.

Gitelson, A. A., Laorawat, S., Keydan, G. P., & Vonshank, A. (1995). Optical properties of dense algal culture outdoors and their application to remote estimation of biomass and pigment concentration in Spirulina Platensis (Cyanobacteria). *Journal of Phycology , 31*, 828-834.

Gitelson, A. A., Mayo, M., Yacobi, Y. Z., Parparov, A., & Berman, T. (1994). The use of high-spectral resolution radiometer data for detection of low chlorophyll concentrations in Lake Kinneret. *Journal of Plankton Research , 16*, 993-1002.

Gitelson, A. A., Schalles, J. F., Rundquist, D. C., Schiebe, F. R., & Yacobi, Y. (1999). Comparative reflectance properties of algal cultures with manipulated densities. *Journal of Applied Phycology , 11*, 345-354.

Gitelson, A. A., Yacobi, Y. Z., Schalles, J. F., Rundquist, D. C., Han, L., Stark, R., et al. (2000). Remote estimation of phytoplankton density in productive waters. *Archiv fuer Hydrobiologie- Special Issues Advancements in Limnology , 55*, 121-136.

Gons, H. J. (1999). Optical teledetction of chlorophyll a in turbid inland water. *Environmental Science & Technology , 33*, 1127-1132.

Gons, H. J., Rijkeboer, M., & Ruddick, K. G. (2002). A chlorophyll-retrieval algorithm for satellite imagery (Medium Resolution Imaging Spectometer) of inland and coastal waters. *Journal of Plankton Research , 24*, 947-951.

Gordon, H. R., Brown, O. B., & Jacobs, M. M. (1975). Computed relationships between the inherent and apparent optical properties of a flat homogeneous ocean. *14*, 417-427.

Hakvoort, H., de Haan, J., Jordans, R., Vos, R., Peters, S., & Rijkeboer, M. (2002). Towards airborne remote sensing of water quality in the Netherlands-validation and error analysis. *ISPRS Journal of Photogrammetry & Remote Sensing , 57*, 171-183.

Hall, F. G., Strebel, D. E., Nickeson, J. E., & Goetz, S. J. (1991). Radiometric rectification: toward a common radiometric response among multidate multisensor images. *Remote Sensing of Environment , 35*, 11-27.

Hallegraeff, G. M. (1993). A review of harmful algal blooms and their apparent global increase. *Phycologia , 32*, 79-99.

Han, L., Rundquist, D. C., Liu, L. L., Fraser, R. N., & Schalles, J. F. (1994). The spectral responses of algal chlorophyll in water with varying levels of suspended sediment. *International Journal of Remote Sensing , 15*, 3707-3718.

Heo, J., & FitzHugh, T. W. (2000). A standardized radiometric normalization method for change detection using remotely sensed imagery. *Photogrammetric Engineering & Remote Sensing , 66*, 173-181.

Hoogenbloom, H. J., Dekker, A. G., & de Haan, J. F. (1998). Retrieval of chlorophyll and suspended matter from imaging spctrometry data by matrix inversion. *Canadian Journal of Remote Sensing , 24*, 144-152.

Indiana Department of Environmental Management. (2006). *Indiana Integrated Water Quality Monitoring and Assessment Report*. Retrieved March 6, 2007, from http://www.in.gov/idem/programs/water/303d/index.html

Indiana Department of Environmental Managment. (2004). *Indiana Integrated Water Quality Monitoring and Assessment Report*. Retrieved from http://www.in.gov/idem/programs/water/303d/index.html

Indiana Department of Environmental Managment. (2002). *Indiana Integrated Water Quality Monitoring and Assessment Report IDEM/34/02/004/2002*. Retrieved from http://www.in.gov/idem/programs/water/303d/index.html

ITT Visual Information Services. (2006). *FLAASH Module User's Guide, ENVI FLAASH Module Version 4.3.* ITT Visual Information Services.

ITT Visual Information Solutions. (2004). ENVI. *version 4.2* . Boulder, Colorado: ITT Visual Information Solutions.

Jensen, J. R. (1996). *Introductory Digital Image Processing* (2nd Edition ed.). Upper Saddle River: Prentice Hall.

Jupp, D. L., Kirk, J. T., & Harris, G. P. (1994). Detection, identification and mapping of cyanobacteria- using remote sensing to measure the optical quality of turbid inland waters. *Australian Journal of Marine and Freshwater Research , 45*, 801-828.

Kallio, K., Koponen, S., & Pullianinen, J. (2003). Feasibility of airborne imaging spectrometry for lake monitoring- a case study of spatial chlorophyll a distribution in two meso-eutropic lakes. *International Journal of Remote Sensing , 24*, 3771-3790.

Kallio, K., Kuster, T., Hannonen, T., Koponen, S., Pullianinen, J., Vepsalainen, J., et al. (2001). Retrieval of water quality from airborne imaging spectromentry of various lake types in differen season. *The Science of the Total Environment , 268*, 59-77.

Kirk, J. T. (1984). Dependence of the relationship between inherent and apparent optical properties of water on solar altitude. *Limnology and Oceanography , 29*, 350-356.

Kuster, T., Hannonen, T., Kallio, K., Koponen, S., Pulliainen, J., Pyhalahti, T., et al. (1998). Monitoring of turbid coastal and inland water by airborne imaging spectometer AISA. *Geoscience and Remote Sensing Symposium Proceedings , 5*, 2597-2599.

Lenth, R. V. (2001). Some practical guidelines for effective sample-size determination. *The American Statistician ,* 187-193.

Li, L., Pascual, D. L., Tedesco, L. P., Randolph, K. L., Sengpiel, R. E., Hall, B. E., et al. (2006). *Developing a survey tool for the rapid assessment of blue-green algae in central Indiana's reservoirs.* IUPUI. Indianapolis: Central Indiana Resources Partnership/ CEES.

Liu, Y., Islam, M. A., & Gao, J. (2003). Quantification of shallow water quality parameters by means of remote sensing. *Progress in Physical Geography , 27*, 24-43.

Makarewicz, J. C. (1993). Phytoplankton biomass and species composition in Lake Erie, 1970-1987. *Journal of Great Lakes Research , 19*, 258-274.

Markager, S., & Vincent, W. F. (2000). Spectral light attenuation and the absorption of UV and blue light in natural waters. *Limnology and Oceanography , 45*, 642-650.

Matthews, A. M., Duncan, A. G., & Davison, R. G. (2001). An assesment of validation techniques for estimating chlorophyll-a concentration from airborne multispectral imagery. *International Journal of Remote Sensing , 22*, 429-447.

Mertes, L. A., Dekker, A. G., Brakenridge, G. R., Birkett, C. M., & Letouneau, G. (2004). Rivers and lakes . In S. L. Ustin, *Remote sensing for natural resource managment and enivronmental monitoring* (pp. 345-400). New Jersey: John Wiley & Sons, Inc.

Millie, D. F., Baker, M. C., Tucker, C. S., Vinyard, B. T., & Dionigi, C. P. (1992). High-resolution airborne remote sensing of bloom-forming phytoplankton. *Journal of Phycology , 28*, 281-290.

Mittenzwey, K.-H., Gitelson, A. A., & Kondratiev, K. Y. (1992). Determination of chlorophyll a of inland waters on the basis of specral reflectance. *Limnology and Oceanography , 37*, 147-149.

Morel, A., & Gentili, B. (1991). Diffuse reflectance of oceanic waters: its dependence on sun angle as influence by the molecular scattering contribution. *Applied Optics , 30*, 4427-4438.

Morel, A., & Gordon, H. R. (1980). Report of the working group on water color. *Boundary-Layer Meteorology , 18*, 343-355.

Morel, A., & Prieur, L. (1977). Analysis of variations in ocean color. *Limnology and Oceanography , 22*, 709-722.

Olthof, I., Pouliot, D., Fernandes, R., & Latifovic, R. (2005). Landsat-7 ETM+ radiometric normalization comparison for northern mapping applications. *Remote Sensing of Environment , 95*, 388-398.

Pascual, D. L., Rafits, R., Filippelli, G., & Tedesco, L. P. (2006). Run-off and tile drainage versus internal recycling: three year mass balance approach to understand phophorous loading and productivity in a small, urban reservoir, Eagle Creek Reservoir, IN, USA. *North American Lake Managers Association International Symposium.* Indianapolis.

Perk, R., Gitelson, A., & Rundquist, D. (2006). Airborne AISA "Eagle" hyperspectral remote sensing. *North American Lake Managers Association International Symposium-Meeting Workshop "Remote Sensing Methods for Lake Assessment".* Indianapolis.

Pozdnyakov, D., Shuchman, R., Korosov, A., & Hatt, C. (2005). Operational algorithm for the retrieval of water quality in the Great Lakes. *Remote Sensing of Environment , 97*, 352-370.

Quibell, G. (1991). The effect of suspended sediment on reflectance from freshwater algae. *International Journal of Remote Sensing , 12*, 177-182.

Richardson, L. L. (1996). Remote Sensing of Algal Bloom Dynamics. *BioScience , 46*, 492-501.

Richardson, L. L., Buisson, D., Liu, C., & Ambrosia, V. (1994). The detection of algal photosynthetic accessory pigments using Airborne Visible-Infrared Imaging Spectrometer (AVIRIS) spectral data. *Marine Technology Society Journal , 28*, 10-21.

Rowan, K. S. (1989). *Photosynthetic Pigments of Algae.* Cambridge: Cambridge University Press.

Rundquist, D. C., Han, L., Schalles, J. F., & Peake, J. S. (1996). Remote measurement of algal chlorophyll in surface waters: the case for the first derivative of reflectance near 690 nm. *Photogrammetric Engineering & Remote Sensing , 62*, 195-200.

Sarada, R., Pillai, M. G., & Ravishankar, G. A. (1999). Phycocyanin from Spirulin sp: influence of processing of biomass on phycocyanin yield, analysis of efficacy of extraction methods and stability studies on phycocyanin. *Process Biochemistry , 34*, 795-801.

Schalles, J. F., & Yacobi, Y. Z. (2000). Remote detection and seasonal patterns of phycocynin, carotenoid and chlorophyll pigments in eutrophic waters. *Archiv fuer Hydrobiologie-Special Issues Advancements in Limnology , 55*, 153-168.

Schalles, J. F., Gitelson, A. A., Yacobi, Y. Z., & and Kroenke, A. E. (1998). Estimation of chlorophyll a from time series mesurements of high spectral resolution reflectance in an eutrophic lake. *Journal of Phycology , 34*, 383-390.

Schalles, J. F., Rundquist, D. C., & Schiebe, F. R. (2001). The influence of suspended clays on phtoplankton reflectance signature and the remote estimation of chlorophyll. *Verhandlungen Internationale Vereinigung für Theoretische und Angewandte Limnologie , 27*, 3619-3625.

Schott, J. R., Slavaggio, C., & Volchok, W. J. (1988). Radiometric scene normalization using pseudoinvariant features. *Remote Sensing of Environment , 26*, 1-16.

Shirai, M., Ohtake, A., Sano, T., Matsumoto, S., Sakamoto, T., Sato, A., et al. (1991). Toxicity and toxins of natural blooms and isolated strains of Microcystis spp. (Cyanobacteria) and improved procedure for purification of cultures. *Applied and Evironmental Microbiology , 57*, 1241-1245.

Simis, S. G., Peters, S. W., & Gons, H. (2005). Remote Sensing of the cyanobacterial pigment phycocyanin in turbid inland water. *Limnology and Oceanography , 50*, 237-245.

Simis, S. G., Ruiz-Verdu, A., Dominguez-Gomez, J. A., Pena-Marinez, R., Peters, S. W., & Gons, H. J. (2007). Influence of phtoplankton pigment composition on remote sensing of cynobacterial biomass. *Remote Sensing of Environment , 106*, 414-427.

Sturm, R. H., Gilbert, R. H., Brock, R. A., & Crooke, J. D. (1991). *Soil Survey of Marion County, Indiana.* Natural Resources Conservation Service- United States Department of Agriculture.

Tedesco, L. P., Atekwana, E. A., Filippelli, G., Licht, K., Schrake, L. K., Hall, B. E., et al. (2003). *Water quality and nutrient cycling in three Indiana watershes and their reservoirs: Eagle Creek/ Eagle Creek Reservior, Fall Creek/ Geist Resrvoir and Cicero Creek/ Morse Reservoir.* IUPUI. Indianapolis: Central Indiana Water Resources Partnership/ CEES.

Tedesco, L. P., Pascual, D. L., Shrake, L. K., Casey, L. R., Hall, B. E., Vidon, P. G., et al. (2005). *Eagle Creek watershed management plan: An integrated appraoch to improved water quality.* IUPUI. Indianapolis: Eagle Creek Watershed Alliance/ CEES.

Teillet, P. M., Markham, B., & Irish, R. R. (2006). Landsat cross-calibration based on near simultaneous imaging of common ground targets. *Remote Sensing of Environment , 102*, 264-270.

Vincent, R. K., Qin, X., McKay, R. M., Miner, J., Czajkowski, K., Savino, J., et al. (2004). Phcyocyanin detection from Landsat TM data for mapping cyanobacterial blooms in Lake Erie. *Remote Sensing of Environment , 89*, 381-392.

Vos, R. J., Hakvoort, J. H., Jordans, R. W., & Ibelings, B. W. (2003). Multiplatform optical monitoring of eutrophication in temporally and spatially variable lakes. *The Science of the Total Evironment , 312*, 221-243.

Wang, S., Yan, F., Zhou, Y., Zhu, L., Wang, L., & Jiao, Y. (2005). Water quality monitoring using hyperspectral remote sensing data in Taihu Lake China. *Geoscience and Remote Sensing Symposium , 7*, 4553-4556.

Whitton, B. A., & Potts, M. (2000). *The Ecology of Cyanobacteria: Their Diversity in Time and Space.* Netherlands: Kluwer Academic Publishers.

Yacobi, Y. Z., Gitelson, A., & Mayo, M. (1995). Remote sensing of chlorophyll in Lake Kinneret using high-spectral-resolution rediometer and Landsat TM: spectral features of reflectance and algorithm development. *Journal of Plankton Research , 17*, 2155-2173.

Yang, X., & Lo, C. P. (2000). Relative radiometric normalization performance for change detection from multi-dat satellite images. *Photogrammetric Engineering & Remote Sensing , 66*, 967-980.

Zimba, P. V., & Gitelson, A. (2006). Remote estimation of chlorophyll concentration in hyper-eutrophic aquatic systems: Model tuning and accuracy optimization. *Aquaculture , 256*, 272-286.

Curriculum Vitae

Rebecca Elizabeth Sengpiel

Education:

Indiana University Purdue University Indianapolis:

- Indiana University: Master of Science in Earth Sciences
- Graduated August, 2007
- GPA 3.9/4.0

University of the Pacific:

- Bachelor of Science in Geology
- Graduated May, 2004
- GPA 3.6/4.0

Honors, Awards, Fellowships:

- Arthur Mirsky Geology Fellowship (2006)- awarded to an outstanding master's student.
- William Christiansen Award (2004)- presented to an outstanding graduating senior majoring in the Geosciences.
- Delbert H. Brown Award (2002)- presented to a Freshman or Sophomore Geosciences student who shows exceptional promise.

Research Experience and Skills:

Software:

- ArcGIS
- Adobe Acrobat
- Adobe Illustrator
- Microsoft Office (Word, Excel, Powerpoint)
- RSI ENVI
- ERDAS Imagine
- SYSTAT

Lab Analyses:

- Total Suspended Sediment Content
- Loss on Ignition (organics) Content
- Chlorophyll a extraction and measurement
- Phycocyanin extraction and measurement

Equipment Experience:

- YSI Multi-parameter Probe
- Secchi Disk
- ASD Field Spectroradiometer
- Ocean Optics Field Spectroradiometer

Professional Experience:

Neil O. Anderson and Associates, Inc.: May 2004- June 2005

- Wrote Technical Reports- i.e. Soil Suitability Studies, Nitrate Loading Studies and Surface/Subsurface Contamination Reports
- Conducted Field Work- Site visits/reconnaissance, soil samples and soil column profiles, percolation tests, soil drilling
- Performed Research- Investigated county records for several areas including Contamination Reports, UST/LUST Lists etc.
- Assisted with Technical Reports- including Earthquake Hazard Reports and Phase I/ Phase II Reports

Sales Associate- Federated Stores Inc. (Macy's): Summer 2002- Spring 2004

- General Clerk Activities- assisted customers with purchases performed markdowns and maintained a clean and organized department
- Performed Yearly Inventories

Lab Teaching Assistant at University of the Pacific: Fall 2001- Spring 2004

- Aided Students- Answering lab and class related questions
- Maintained Lab- Responsible for space and equipment

Quester I.T.: Summer 2001

- Internet Software- Quester I.T. provided Internet classes; wrote program code to create internet accessible documents
- Edited, Tested and Repaired Website- Tested and fixed to ensure so functionality and user friendliness

Publications:

Sengpiel, R. E., L. Li, D. L. Pascual, L. P. Tedesco, and J. S. Wilson, 2007. Using hyperspectral remote sensing to estimate chlorophyll a and phycocyanin in a mesotrophic reservoir. International Journal of Remote Sensing, *submitted*.

Li L., D. L. Pascual, L. P. Tedesco, K. L. Randolph, **R. E. Sengpiel**, B. E. Hall, and J. S. Wilson, 2006. Developing a survey tool for the rapid assessment of blue-green algae in central Indiana's reservoirs. Reservoir. Central Indiana Water Resources Partnership, CEES Publication 2006-01, IUPUI, Indianapolis, IN, 49 p.

Abstracts:

Sengpiel, R., L. Li, L. Tedesco, J. Wilson, L. Pascual, and D. Moran, Mapping the concentration and spatial distribution of cyanobacteria using airborne hyperspectral remote sensing, CIWRP 2006 Fall Meeting, Dec. 5-6, 2006, Indianapolis, Indiana.

Li, L., D. L. Pascual, **R. Sengpiel**, K. Randolph, L. Tedesco, B. E. Hall, J. Wilson, D. Moran, and C. Mysore, Quantifying chlorophyll a and phycocyanin of drinking water reservoir using genetic algorithms (GA)-partial least square modeling and neural networks, CIWRP 2006 Fall Meeting, Dec. 5-6, 2006, Indianapolis, Indiana.

Sengpiel, R., L. Li, L. Tedesco, J. Wilson, L. Pascual, and D. Moran, Mapping the concentration and spatial distribution of cyanobacteria in Indianapolis reservoirs using airborne hyperspectral remote sensing, North American Lake Management Society (NALMS) 2006 International Symposium, Indianapolis, Indiana, Nov. 8-10, 2006.

Li, L., D. L. Pascual, **R. Sengpiel**, K. Randolph, L. Tedesco, B. E. Hall, J. Wilson, D. Moran, and C. Mysore, Quantifying chlorophyll a and phycocyanin of drinking water reservoirs through GA-PLS modeling of hyperspectral reflectance, North American Lake Management Society (NALMS) 2006 International Symposium, Indianapolis, Indiana, Nov. 8-10, 2006.

Sengpiel, R., L. Li, L. Tedesco, J. Wilson, and D. L. Pascual, Mapping concentration and spatial distribution of cyanobacteria in mesotrophic to eutrophic reservoirs using airborne hyperspectral remote sensing imagery, 27th Annual Indiana Water Resources Association Spring Meeting *"Energizing Indiana's Water Community"*, June 21-23, 2006, Purdue University, West Lafayette, Indiana.